UCGE Reports
Number 20228

Department of Geomatics Engineering

Triple Frequency Cascading Ambiguity Resolution for Modernized GPS and GALILEO

(URL: http://www.geomatics.ucalgary.ca/links/GradTheses.html)

by

Wentao Zhang

July 2005

ABSTRACT

Both modernized GPS and GALILEO will have three frequencies modulated with three signals, all of which will be accessible to all users in the near future.

This thesis starts with the investigations on the linear combinations (LC) rising from the triple frequencies of the two systems, some of which show potential benefits in carrier phase integer ambiguity resolution. For each system, a set of combinations with stepwise wavelengths (GPS: 0.190, 0.862 and 5.861 m; GALILEO: 0.190, 0.814 and 9.768 m) were fully studied, analyzed, and then selected in the development of a GPS/GALILEO triple frequency cascading ambiguity resolution (CAR) method involving the Least-squares Ambiguity Decorrelation Adjustment (LAMBDA).

The performance analysis of a basic CAR under error condition of measurement noise level was first conducted to set a baseline for the application of CAR. Further efforts were spent to the last step of the CAR to deal with the gradually increased residual measurement errors by integrating various models - such as geometry-free/based integer ambiguity model, ionosphere-free and stochastic ionospheric models, and etc.

Tests, analysis and comparison of the algorithms were made in simulated scenarios of the two systems under error conditions of typical multipath, troposphere, medium and high ionosphere over 1 to 70 km baselines, followed by final conclusions and suggestions for future work.

ACKNOWLEDGEMENTS

This thesis is the result of half on-campus and half off-campus work, whereby I have been supported by many people. It turns to be a pleasant part that I have now the opportunity to express my gratitude to all of them.

I am deeply indebted to my supervisor, Dr. Cannon who not only offered me the study chance and research environment, but also sets a vivid example of a researcher. Had it not been for her continuous, stimulating instructions, I would have never made this thesis in shape. Beyond research, what counts more is the light that her impressive personality shed on my professional career and life.

I also would like to thank my former colleagues and friends in PLAN group: Luiz P. S. Fortes, Mark Petovello, Glen MacGougan, Junjie Liu, Paul Alves, Olivier Julien and Yong-won Ann for their unselfish knowledge sharing, beneficial discussions, and suggestive comments on my work. Besides, Xiaoji Niu deserves my special thanks for his warm-hearted help. His printing and delivery work for my thesis played a significant part in smoothing out the difficulties and time lag caused by my off-campus status.

Finally my thanks would be given to my dear wife Tao Lin, whose love enabled this work.

TABLE OF CONTENTS

LIST OF TABLES

LIST OF FIGURES

LIST OF SYMBOLS AND ABBREVIATIONS

$\nabla\Delta$	Double difference (DD) operator
f_{LC}	Phase linear combination
f_i	Phase measurement on the i-th frequency in units of cycles (i =1 ~ 3)
Φ_i	Phase measurement on the i-th frequency in units of metres
e_{Φ_i}	Phase measurement noise in units of metres
N_i	Carrier phase ambiguity on the i-th frequency
N_{NWL}	Carrier phase ambiguity of the NWL linear combination
N_{WL}	Carrier phase ambiguity of the WL linear combination
N_{EWL}	Carrier phase ambiguity of the EWL linear combination
$\nabla\Delta N_{12}$	DD ambiguity of the linear combination using 1st and 2nd frequencies
$\nabla\Delta N_{23}$	DD ambiguity of the linear combination using 2nd and 3rd frequencies
$\nabla\Delta T_1$	DD tropospheric error in the measurement on the 1st frequency
$\nabla\Delta I_1$	DD ionospheric error in the measurement on the 1st frequency
$\nabla\Delta R$	DD geometry range
$\nabla\Delta dR$	DD orbital error
$\nabla\Delta G$	Sum of the DD geometry-related components
$\nabla\Delta r$	DD code measurement
l_i	Wavelength of the i-th frequency
l_{IF_1}	Wavelength of the first ionosphere-free linear combination

l_{LC}	Wavelength of specified phase linear combination
s_{LC}	Measurement noise of the specified phase linear combination

AR	Ambiguity Resolution
CIR	Cascading Integer Resolution
CAR	Cascading Ambiguity Resolution
DD	Double Difference
DLL	Delay Lock Loop
ESA	European Space Agency
EU	European Union
EWL	Extra Wide Line
FOM	Figures of Merit
GB	Geometry-based
GF	Geometry-free
GNSS	Global Navigation Satellite System
GPS	Global Positioning System
GPST	Global Positioning System Time
GST	GALILEO System Time
GTRF	GALILEO Terrestrial Reference Frame
IGS	International GPS Station
LAMBDA	Least-squares Ambiguity Decorrelation Adjustment
LC	Linear Combination
LSQ	Least-squares

ML	Medium Lane
MTTCF	Mean Time To Correct Fix
IF	Ionosphere-Free
IGEB	Interagency GPS Executive Board
ITRF	International Terrestrial Reference Frame
ITRS	International Terrestrial Reference System
PC	Percentage of correct ambiguity fixes
RMS	Root Mean Square
SA	Selective Availability
SPS	Standard Positioning Service
TCAR	Triple Frequency Cascading Ambiguity Resolution
TEC	Total Electron Content
TTF	Time To Fix
UERE	User Equivalent Range Error
UT	Universal Time
UTC	Universal Time Coordinated
VC	Variance-Covariance
WL	Wide-Lane

1 INTRODUCTION

1.1 BACKGROUND

Motivated by the United States Department of Defense (DoD), the current Global Positioning System (GPS) has experienced three decades' development. Although the original motivation was only for military purposes, GPS has been widely used in civilian applications during the past few decades. However, the integrity, availability, and accuracy still need further improvement, especially for aviation applications (Sandhoo et al., 2000). Therefore, a GPS modernization program was started in the late 1990's, in an attempt to upgrade GPS performance for both civilian and military applications. For civilian users, the first real step towards GPS modernization was the discontinuity of Selective Availability (SA) on May 1, 2000, which enabled the improvement of the Standard Positioning Service (SPS) from a horizontal accuracy of 75.0 to 22.5 m 95% of the time (Sandhoo et al., 2000). Subsequent GPS modernization steps for civil users consist of the broadcast of a second civil signal on L2 (L2C), and a third civil signal on an additional civil frequency L5. Therefore, future civilian GPS users will be able to receive three signals on L1, L2 and L5, which will improve the SPS accuracy to only a few metres (Bossche et al., 2004), and additionally will provide an improved anti-jam capability and higher integrity (McDonald, 2001; Miller, 2004). Currently, the GPS modernization program is moving forward, in which the number of working satellites in the current GPS constellation is 29, with gradual replenishment of modernized satellites

in the near future. The first GPS satellite with modernized signals (a new M code on L1, second civil signal on L2) will be launched soon (GPS World, 2005c).

In parallel, European community has been conceiving an independent and civilian satellite navigation system for several years, and has resulted in GALILEO, which has been jointly initiated by the European Commission (EC) and the European Space Agency (ESA). GALILEO will be a part of the Global Navigation Satellite System (GNSS) 2nd Generation. Although the system is designed for civilian use, special protection measures regarding security and safety have been stressed to prevent against threats to the system's operation and use for purposes contrary to the interests of EU and its member states (EU Transport Council, 2004). The GALILEO constellation will consist of 27 satellites evenly placed in three orbital planes, plus one in each plane for backup, for a total of 30 satellites, that is expected to become fully operational by 2008. In GALILEO's initial system design, both independence from, and compatibility to, the existing GNSS(s) comprised the most important considerations, which afterwards involves the interoperability with GPS as an additional and increasing concern. GALILEO users will be able to access three free-of-charge signals modulated on three frequencies E1, E5b and E5a through an Open Service (OS), which is expected to enable equivalent or even better positioning accuracy compared to modernized GPS (European Commission, 2003).

The modernization of GPS and the establishment of GALILEO will propel satellite-based positioning and navigation applications to such a level that the positioning reliability, integrity, availability, and accuracy will be improved tremendously. One significant

benefit to high precision positioning brought by modernized GPS and GALILEO is that carrier phase integer Ambiguity Resolution (AR) will be greatly facilitated by involving three carrier frequencies. In addition, for the purpose of interoperability, two of the GALILEO frequencies (E1 and E5a) overlap with GPS L1 and L5, which will not only help simplify the RF front-end design in a combined GPS/GALILEO receiver, but will also lead to some beneficial interoperable algorithms for multi-frequency applications.

During the past few years, a lot of research work has focused on algorithm studies for integer ambiguity resolution making use of three carrier frequencies. Early studies can be found in Hatch (1996), which introduced the idea of wide laning involving dual or triple frequencies, and he gave some theoretical analyses of the benefits with regards to ambiguity resolution. Forssell et al. (1997) first proposed the Three-Carrier Ambiguity Resolution (TCAR) method for the European GNSS-2 program. TCAR was further discussed and extended in Vollath et al. (1998) which showed promising results for fast AR when using triple frequencies for the European GNSS-2. Similar discussions were carried out in Bonillo-Martinez et al. (1999), Han et al. (1999) and Jung (1999) by considering a triple frequency GPS system (modernized GPS), which gave rise to expectations on likely equivalent AR performance for GPS and GALILEO. In Jung et al. (2000), a Cascading Integer Resolution (CIR) was defined for GPS triple frequency ambiguity resolution. Some other efforts aimed to apply the Least-squares Ambiguity Decorrelation Adjustment (LAMBDA) (Teunissen, 1993) to triple frequency ambiguity resolution (de Jong et al., 2001). A comparison among TCAR, CIR and LAMBDA

methods was made in Teunissen et al. (2002) with a thorough interpretation of the common ground and differences.

The advent of GALILEO and the modernization of GPS raised a lot of attention to the study of the compatibility and interoperability of the two systems. A number of performance analyses were conducted with respect to availability, reliability, accuracy, and integrity in different simulated scenarios (such as open sky and urban canyons) for the two systems individually and when integrated (O'Keefe, 2001; Sheridan et al., 2001; Verhagen, 2002; O'Donnell et al., 2002). The overall conclusions were that the global availability can be improved to a tremendous level when the two systems are combined. Compatibility and interoperability of GPS and GALILEO at different levels ranging from system architecture to user implementation have been fully discussed in the past a few years (e.g. Leonard, 2002; Fyfe et al., 2002), with a lot of problems identified and solutions proposed. Compatibility and interoperability still continue to be issues for discussion today.

In light of modernized GPS and GALILEO, it has become a concern as to how the aforementioned ambiguity resolution will benefit from the co-existence of the two systems. Eissfeller et al. (2001) investigated the performance of real-time kinematic (RTK) GPS/GALILEO positioning. Alves (2001) studied single and dual frequency ambiguity resolution for the individual and combined systems using the LAMBDA method, and showed promising benefits from the combination of both systems. The work was then extended in Julien et al. (2003) on triple frequency resolution, and a tight

coupling of the two systems was realized in terms of the signal characteristics of the two systems. In Julien et al. (2004), the study was moved on to the implementation of ionospheric modeling in the GPS/GALILEO triple frequency resolution algorithm. As a parallel effort to Julien et al. (2003), Zhang et al. (2003) combined the TCAR, CIR and LAMBDA in GPS/GALILEO triple frequency resolution and standardized the dual-system multi-frequency cascading ambiguity resolution (CAR) procedures. This thesis is a continuous effort that includes a summary of the research in Zhang et al. (2003), implementation and development of new models to improve the applicability of CAR, and a performance investigation of the developed methods in different scenarios.

1.2 OBJECTIVES

The main purposes of this research are to make best use of the two triple-frequency satellite navigation systems, and to study the achievable performance in ambiguity resolution using a cascading ambiguity resolution method. The specific objectives are as follows:

(1) Develop a standardized scheme for cascading ambiguity resolution for the two triple-frequency systems;

(2) Study the performance of modernized GPS only, GALILEO only and combined GPS/GALILEO for integer ambiguity resolution over baselines of short and medium lengths under different ionospheric and multipath error levels;

(3) Study the possibility of instantaneous ambiguity resolution using the two triple-frequency systems;

(4) Study the advantages of two triple-frequency systems over one dual-frequency system in terms of the ambiguity resolution performance.

1.3 THESIS OUTLINE

Chapter 2 gives an overview of modernized GPS and GALILEO system in terms of the system performance, signals in space, interoperability and benefits brought to ambiguity resolution by the two systems. Chapter 3 starts with a general discussion of the error sources in double differenced measurements, followed by a study of triple frequency linear combinations for both systems. In Chapter 4, by applying the linear combinations, the geometry-free cascading ambiguity rounding algorithm for both systems is first discussed in a united way, and then a geometry-based cascading ambiguity resolution method is studied. Chapter 5 consists of the efforts to further improve geometry-based cascading ambiguity resolution by implementing an ionosphere-free model and a stochastic ionospheric model in the last cascading step. Chapter 6 addresses some implementation issues in geometry-based cascading ambiguity resolution methods for both systems. Chapter 7 sets up a series of simulated tests over short and medium baselines for both the basic geometry-based cascading ambiguity method and the one augmented by ionospheric modeling, and presents the corresponding test results together

with analysis. Chapter 8 summaries both the advantages and disadvantages of the geometry-based cascading ambiguity resolution method, and also suggests some ideas for further improvements.

2 GPS MODERNIZATION AND GALILEO EVOLUTION

Global Navigation Satellite Systems (GNSS) are evolving to a new era due to the modernization of the current GPS and the upcoming GALILEO system. In this chapter, the background of the GPS modernization program and the status of GALILEO are introduced. A discussion on the compatibility and interoperability of the two systems is also included, and the expected benefits of the systems for improved ambiguity resolution are presented.

2.1 GPS MODERNIZATION AND GALILEO EVOLUTION

(1) GPS Modernization Program

The GPS modernization program is an effort to extend the great success achieved in the past three decades. The goals of the program are to protect the services for military users, prevent the adversary exploitation of the system, and preserve civil use with enhancements (Swider, 2001). The earliest action was taken in 1997 when the Interagency GPS Executive Board (IGEB) held the first meeting to discuss the need for an additional civil GPS signal and it was agreed to identify a second civil frequency within a year. In the year that followed, it was announced by the US government that a second civil signal would be broadcast at GPS L2; and a third civil signal specifically designed for safety-of-life services would be broadcast on the third frequency L5. In

March 1999, another announcement by the US government declared that the frequency of the third civil signal, L5 was selected to be 1176.45 MHz (Sielski, 2000). In December 2005, with the release of a new US presidential GPS policy, the IGEB has been replaced by a National Space-Based Positioning, Navigation, and Timing (PNT) Executive Committee, co-chaired by the Deputy Secretaries of the US Departments of Defense and Transportation (GPS World, 2005a). Meanwhile, the free, open use of current and future GPS civil signals and unrestricted access to the technical specifications were reaffirmed, and the GPS modernization program has been moving forward with the leadership of the US Department of Defense (DoD) and Department of Transportation (DoT) (GPS World, 2005a).

(2) GPS Modernization Schedules

The GPS modernization program started with the cancellation of SA in 2000. It will be followed by the addition of a new military signal (M-code) and a second civil code on L2 (L2C), then a third civil frequency L5. Further modernization consists of the assessment and design of a new generation of satellites to meet military and civil requirements through 2030. Table 2.1 includes a summary of the launch schedule of the modernized GPS satellites according to Miller (2004) and GPS World (2005c).

Table 2.1 Launch Schedule of Modernized GPS Satellites

GPS Blocks	First Launch
GPS IIR-M - C/A Codes on L1/L2 - M Codes on L1/L2	Expected in mid of 2005
GPS IIF - C/A Codes on L1/L2/L5 - M Codes on L1/L2	Expected in mid of 2006
GPS III	Expected in 2012

GPS Block IIR-M is the second part of Block IIR, with eight modernized satellites being built by Lockheed Martin. The IIR-M satellites will have a new civil signal on L2 and new M codes on L1/L2 at higher signal power than normal IIR satellites. The Boeing company has the contract for GPS Block IIF, with nine satellites in total, that are intended to provide improved anti-jam capability, increased accuracy, higher integrity, and secured operational M-codes. Additionally, a third civil code at a new frequency L5 will also be included. The purpose of the GPS III program is to deliver major improvements in accuracy, assured service, integrity, and flexibility for civil and military users. Currently led by both Lockheed Martin and Boeing both, the team of GPS III program has proposed the use of the same signal structure as GALILEO for its open signals and decided the year 2012 as the target date of the launch of first GPS III satellite (GPS World, 2005c).

(3) **Modernized GPS Signals**

The modernized GPS signals are depicted in Figure 2.1, and specifications of the frequencies and chipping rates of the modulated signals are listed in Table 2.2. At the

moment, only one civil signal modulated on L1 is accessible to civilian users. When the GPS modernization program is fully implemented, another two civil signals on L2 and L5 are expected to be available. However, the second civil signal L2 is not sufficient to allow its use for civil aviation safety-of-life applications because of potential interference from existing ground radars that broadcast in and near GPS L2 band (Fontana et al., 2001). The third civil signal on L5 has more anti-jam capability, since the signal power is designed to be 6 dB higher than the L1 signal. The code length will be longer than the C/A codes on L1 and L2 to reduce system self-interference caused by CDMA cross-correlation (ARINC Inc., 2001).

For stand alone real-time GPS users, the addition of second and third civil GPS signals is expected to provide more signal redundancy, improved positioning accuracy by eliminating the ionospheric error, improved signal availability and integrity, improved continuity of service, and improved resistance to radio frequency (RF) interference.

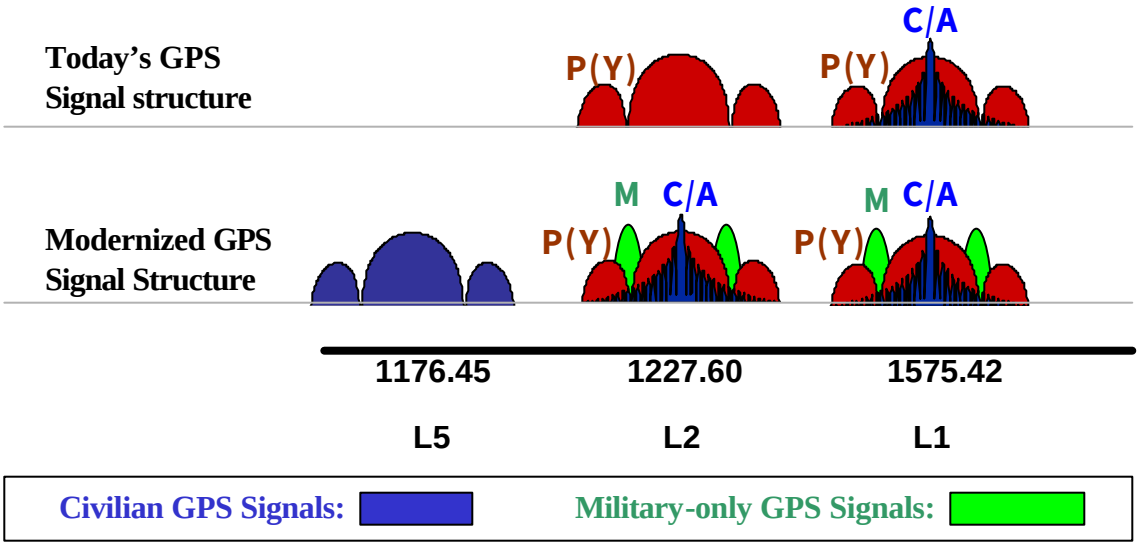

Figure 2.1 Evolution of Modernized GPS Signals (US DoT, 2003)

For differential applications, the addition of a third frequency is expected to enable better estimation of the spatially uncorrelated ionospheric components seen over a baseline. With the third frequency available, more linear combinations will be possible using the three available frequencies, which will definitely benefit integer ambiguity resolution. The need for GPS modernization and the principal driving factors are detailed in McDonald (2001).

(4) Expected Performance

Each modernization step leads to a system performance improvement. The ceasing of SA gives an SPS stand-alone horizontal accuracy of 22.5 m (95%) (Sandhoo et al., 2000). When another civil signal becomes available, the ionospheric errors can be directly estimated, so that the User Equivalent Range Error (UERE) can be reduced to about 2 m, which will enable the SPS stand-alone horizontal accuracy to be improved to 3 ~ 8 m 95% of the time (McDonald, 2002). The New and Improved Clock and Ephemeris (NICE) will further reduce the GPS satellite clock and ephemeris errors to approximately 1.2 m, so that the SPS horizontal accuracy will be further improved to 2 ~ 5 m (Perz, 2004; Rodriguez et al., 2004). With the technology advancement in the reduction of code noise and code multipath, there is still further potential for SPS.

2.2 EUROPEAN SATELLITE NAVIGATION SYSTEM – GALILEO

GALILEO is a European GNSS currently under development that will provide a highly accurate and guaranteed global positioning service.

(1) Background of GALILEO Project

Both the US GPS and Russian GLONASS are under military control, whereas GALILEO was originated from the desire of civilian service. In the early 1990s, the EU began to conceive its own global satellite navigation system for better and guaranteed coverage over northern Europe. The EC assumes political responsibility for GALILEO and ESA leads the program development. In 1998, a series of studies were formally commissioned by ESA aimed at the design of an independent, civil satellite navigation service. Three years later, a tentative GALILEO frequency and signal plan (Hein et al., 2001) was published, which is regarded as the baseline for the development of Europe's satellite navigation system. In 2002, the development phases of GALILEO were finally decided in a meeting of the Transport Council of the EU. Taking into account the compatibility and interoperability with GPS, the GALILEO frequencies and signals were refined in the same year, and another frequency and signal plan was published (Hein et al., 2002). In the mid of 2004, a few more important changes were carried out in the waveforms on L1 and E6 as a consequence of the agreement made between the US and EU in the same year (Rodriguez et al., 2004). In addition, the orbit selection for the GALILEO constellation was finalized in Zandbergen et al. (2004).

After some delay, the EU Transport Council has declared the final deployment of the GALILEO constellation in December 2004. At the same time, five distinct services of GALILEO were confirmed that include: an open service, which is free of charge for all users (OS); a value-added commercial service (CS); safety of life (SoL); search and rescue services (SAR) and a public regulated service (PRS) (GPS World, 2005b). Moreover, concerns regarding security issues were raised. While keeping the GALILEO system's civil nature, efforts are being spent on controlling access to the encrypted PRS and establishing security agencies to detect and prevent unauthorized or hostile use of the system (GPS World, 2005b).

(2) Phases of the GALILEO Program

The development of the GALILEO system consists of three phases. During the first phase (2001 to present), the mission requirements were consolidated, the satellites and ground-based components were under developed, and the overall in-orbit-validation (IVO) of GALILEO was started. IVO includes the delivery of the first four satellites in the GALILEO constellation of 30, along with a number of ground control and monitoring stations. The first launch of GALILEO satellites is expected by the end of 2005 (GPS World, 2005b). Now it is on the very edge to the second phase – deployment phase (before 2008), which covers the entire network of ground infrastructure and the launch of the remaining 26 satellites; then in the third phase starting from 2008, the whole system will become commercially operational. The GALILEO Joint Undertaking (GJU), set up

by ESA and the EU to select a concessionaire to operate GALILEO, is still trying to choose between two competing teams (GPS World, 2005d).

(3) Frequencies and Signals Modulation

In Figure 2.2, the selection of GALILEO frequencies and signals according to European Commission (2002) and Hein et al. (2002) are presented. As shown, 10 navigation signals in the frequency ranges of 1164 ~ 1215 MHz (E5a and E5b), 1215 ~ 1300 MHz (E6) and 1559 ~ 1592 MHz (E2-L1-E1[1]) are selected. Among those signals, six are accessible to all GALILEO users on E5a, E5b and L1 as an OS and a SoL; two signals on E6 with encrypted ranging codes are only accessible to CS users, and the remaining two (one in the E6 band and one in the E2-L1-E1 band) with encrypted ranging codes and data are accessible to authorized users of the Public Regulated Service (PRS).

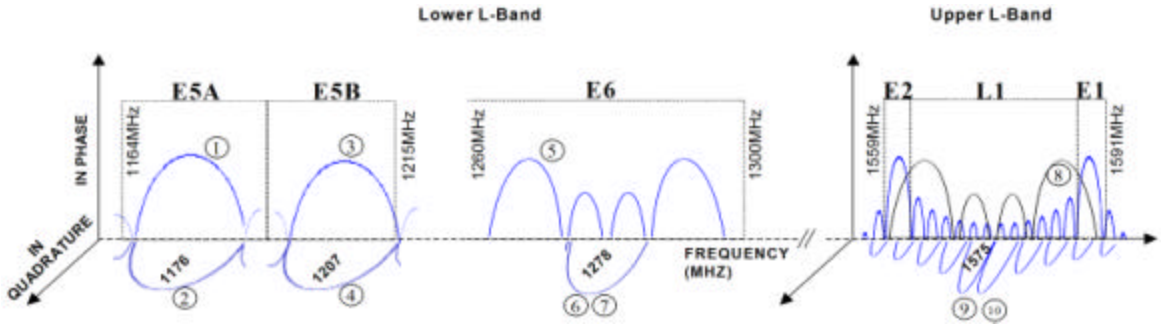

Figure 2.2 GALILEO Frequencies and Signals (European Commission, 2002)

(4) Expected Performance in Positioning Accuracy

GALILEO has been designed to have competitive system performance compared to GPS. The GALILEO OS horizontal and vertical accuracy are expected to be 4 m and 8 m respectively, with global availability, 99.8% of the time (European Commission, 2003)

2.3 SYSTEM COMPATIBILITY AND INTEROPERABILITY

As a new member of the GNSS, the compatibility and interoperability of GALILEO with the existing GPS has been an important issue. Compatibility is the minimum requirement for the co-existing GNSSs – if there is no mutual benefit, at least there is no mutual interference that might cause performance degradation. However, interoperability is at a higher level, which not only ensures no mutual interference, but also requires mutual benefits. Issues regarding the compatibility and interoperability of GALILEO and GPS from the system architecture design level to the user application level have been deeply discussed in Dellago et al. (2003), Fyfe et al. (2002), Ganguly et al. (2004), Leonard et al. (2002), Lortie (2000), Miller et al. (2004) and Spiller et al. (2001). Agreement has been finally signed between US and EC in June 2004 to ensure the compatibility of GPS and GALILEO, which covers the signal structure to avoid interference, as well as time and geodetic standards to facilitate the joint use of the two systems (GPS World, 2004a).

---

[1] The frequency band E2-L1-E1 is sometimes denoted as L1 for convenience.

(1) GPS and GALILEO Constellations

As shown in Figure 2.3, the proposed GALILEO constellation is very similar to GPS. The GPS system adopts a 24/6/1 Walker constellation, whereas the GALILEO system adopts a 27/3/1 Walker constellation, plus three additional satellites as backups (one active spare per plane). The GALILEO orbital inclination is designed to be 56 degrees, slightly larger than the GPS orbital inclination (55 degrees), so as to provide better coverage over northern Europe. During phase B of the GAILEO project, two different orbital altitude choices have been provided for system studies. One choice that has been widely adopted for the GALILEO orbital altitude is 23616 km, which leads to a revolution of GALILEO satellite in orbit every 14 hours 21 minutes, slightly longer than the GPS orbital period of 11 hours 56 minutes. A lot of GALLEO system performance analyses have been published in the past a few years, some of which are based on the above constellation configurations, such as Salgado et al. (2001) and Fyfe et al. (2002), and some are based on a constellation which is a little different from the above configurations, e.g. O'Keefe (2001). According to Zandbergen (2004), the GALILEO orbital altitude has been finally decided to the other choice at the end of GALILEO project phase C0, which is approximately 23230 km, leading to an orbit period of about 14 hours and 5 minutes. Since the research of this thesis has started before the GALILEO orbital altitude was finally decided, the same GALILEO constellation as configured in references Salgado et al. (2001) and Fyfe et al. (2002) is used.

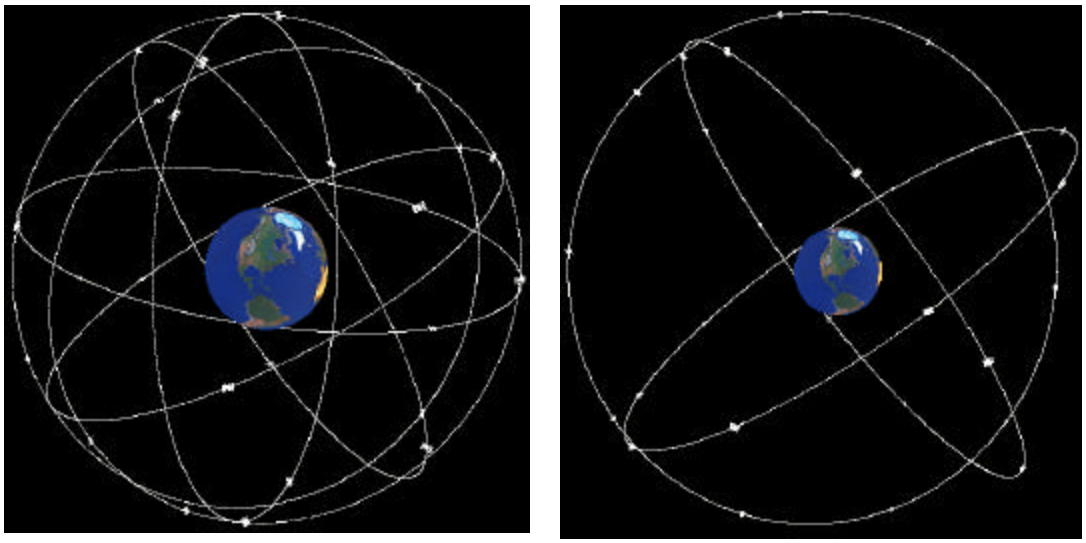

(1) GPS (2) GALILEO

Figure 2.3 GPS and GALILEO Constellations[2]

(2) Time Reference Frames

GPS Time is steered to a real-time representation of International Atomic Time (TAI) produced at the US Naval Observatory (USNO). GALILEO System Time (GST) will be generated at a GALILEO Precise Timing Facility (PTF), which is independent from GPS Time, but at the same time is kept close to GPS Time. The offset between GPS Time and GST is an important issue for interoperability of the two navigation systems. Bossche et al. (2004) show that the GPS-GALILEO time offset (GGTO) will be in the order of tens of nanoseconds, which will cause a slowly changing bias between GPS and GALILEO measurements in a combined navigation receiver. However, the GGTO will be monitored by the PTF and a correction at the precision of 5 ns (95% of time) is planned to be

[2] To have a clear view of the two constellations in one frame, they are plot using one same self-developed tool instead of using figures from different references.

broadcast in the navigation messages of both GPS and GALILEO (Bossche et al., 2004; Miller, 2004), and in addition, Bossche et al. (2004) proposes another approach for users to cope with the GGTO by introducing an additional unknown into the position solution. In the research of this thesis, for the purpose of simplicity, the simulation of GPS and GALILEO measurements is based on the assumption that the GST is precisely synchronized to GPS time.

(3) Coordinate Reference Frames

GPS uses the World Geodetic System 84 (WGS84) as its coordinate reference frame, which is a practical realization of the International Terrestrial Reference Frame (ITRF). For independence reasons, GALILEO will adopt a different realization of ITRF as its coordinate reference frame, which is referred to as the GALILEO Terrestrial Reference Frame (GTRF) (Hein et al., 2002). However, the difference between GTRF and WGS84 will be limited to only about 2 cm, a small systematic difference that is not a major concern for most users (Miller, 2004), and the transformation parameters between the two reference frames will be provided by a GALILEO external Geodetic Reference Service Provider (Hein et al., 2002). For simplification purposes, the simulations of both GPS and GALILEO measurements in this thesis were performed in WGS84 thereby neglecting the difference between the two coordinate reference frames.

(4) Signals-in-Space

The frequencies and civilian signals of modernized GPS and the frequencies and signals for the GALILEO Open Service (Hein et al., 2002) are summarized in Table 2.2. As it is shown, the GPS and GALILEO signals at L1/E1 and L5/E5a have identical carrier frequencies, but different signal structures and code sequences. The partial frequency overlap of GPS and GALILEO brings convenience to the interoperability of the two systems, considering that the RF front-end design of the dual-system receiver can be drastically simplified and the reception of the signals can be greatly facilitated (Leonard et al., 2002). However, the use of common centre frequencies for the navigation signals also gives rise to concerns of the mutual interference of the two systems. Although the agreement made between US and EC in June 2004 has ensured no interference between modernized GPS and GALILEO, the mutual interference between the two systems has been, and is still being, intensely investigated (Fyfe at el., 2002; Soualle at el., 2003; Ganguly at el., 2004). In Chapter 3, the frequency overlapping of L1/E1 and L5/E5a will be further discussed.

Table 2.2 Frequencies and Civilian Signals of Modernized GPS and GALILEO Open-Service Frequencies and Signals

		Frequency (MHz)	Wavelength (m)	Chipping Rate (Mc/s)
Modernized GPS	L1	1575.42	0.190 m	1.023
	L2	1227.60	0.244 m	1.023
	L5	1176.45	0.254 m	10.23
GALILEO	E1	1575.42	0.190 m	2.046
	E5b	1207.14	0.248 m	10.23
	E5a	1176.45	0.254 m	10.23

The chipping rate of a pseudorandom code directly reflects the noise level of the code measurement obtained through a delay lock loop (DLL). For the chipping rate listed in Table 2.2, if the received codes can be matched to the locally generated codes at the precision of 1/100 width of a chip, the measurement noise of the L1 and E1 codes would be around 3 and 1.5 m respectively (most commercial receivers on the market are actually better). Therefore, the noise reduction in code measurements primarily relies on advancements in receiver technology, and the chipping rate is one key factor when making noise assumptions to simulate the GPS and GALILEO measurements.

(5) Availability

One of the most important benefits of simultaneously using GPS and GALILEO is the improvement in availability, especially in urban areas. A lot of geometry and availability analysis, including the potential for both GPS and GALILEO in high mask angle environments, was shown in O'Keefe (2001), Merino (2001) and O' Donnell (2002). The results indicate that GALILEO has a slightly better availability than GPS over Europe, but neither system alone is able to provide sufficiently reliable visibility of satellites in an urban environment. However, the combination of GPS and GALILEO in that case is able to increase the service availability from around 50% with GPS only to near 95% (Merino et al., 2001; Spiller et al., 2001), namely for 95% of the time users in urban areas will see more than four satellites in view. From another point of view, the potential of GPS and GALILEO to work as mutual backups, is able to improve the reliability when either system is under some type of failure.

(6) Positioning Accuracy Improvement

Bossche et al. (2004) investigated the GALILEO only and GPS/GALILEO combined positioning accuracies for users uniformly distributed at a global $3^\circ \times 5^\circ$ grid through a 3-day simulation test. The results are considered representative and therefore included in Table 2.3, which covers the global average and the worst horizontal positioning errors (HPE) and vertical positioning errors (VPE) 95% of the time. The HPE and VPE in both the average and the worst cases are significantly improved when GPS and GALILEO are combined in the solutions.

Table 2.3 GALILEO and Combined GPS/GALILEO Stand-Alone Accuracy (Bossche et al., 2004)

	Average, 95%		**Worst, 95%**	
	HPE	**VPE**	**HPE**	**VPE**
GALILEO	2.1 m	3.7 m	3.3 m	6.6 m
GPS/GALILEO	1.6 m	2.8 m	2.8 m	5.4 m

2.4 BENEFITS OF GPS MODERNIZATION AND GALILEO IN AMBIGUITY RESOLUTION

The main focus of this thesis is how modernized GPS and GALILEO can benefit the application of carrier phase integer ambiguity resolution. In summary, the main benefits are as follows:

(1) Improved User Equivalent Range Error (UERE)

As introduced in Section 2.1, the improvement in UERE will lead to an improvement in the SPS stand-alone accuracy and will enable a better initial receiver position to perform ambiguity resolution. Both the accuracy of the initial receiver position and the UERE will impact the estimation of float ambiguities. A better estimation of float ambiguities will bring more ease in the integer ambiguity fixing. In later chapters of this thesis, when a cascading approach is used for ambiguity resolution, there will be a clear view of how the magnitude of the UERE directly affects the success of ambiguity fixing.

(2) Better Constellation Geometry

Poor geometry might lead to a degradation in the stand-alone positioning accuracy, given a certain magnitude of UERE. A large offset in the initial position might result in slow ambiguity fixing or even incorrect fixing if the position converges to an incorrect place due to the poor geometry. When both GPS and GALILEO are simultaneously in operation, compared to the case of GPS only, there would be a global improvement in the constellation geometry since at least 51 (simulated constellations in Figure 2.3) satellites will be available (Section 2.3). In this regard, there will also be a corresponding global improvement in ambiguity resolution.

(3) More Measurement Combinations

Ambiguity resolution directly on L1/E1 is very difficult since the wavelengths are so short that the measurements of L1/E1 are susceptible to ionospheric errors and other errors. However, the proper combination of the phases on the two carrier frequencies might have benefits of a longer wavelength and lower vulnerability to ionospheric errors or other errors, so the ambiguity may be easier to fix than for L1/E1 ambiguities. Once three frequencies are available, more combinations among the phases of different carrier frequencies are possible.

A lot of research has been done on the code/phase measurement combinations, or phase linear combination (Hatch 1996; Han et al., 1999; Bonillo-Martinez et al., 1999) even before the frequencies and signals of modernized GPS and GALILEO were clearly specified. Since two frequencies are overlapped between modernized GPS and GALILEO, and two of the frequencies are very close to each other whereas the third is much further away, these characteristics should provide the ability to develop special combinations that are further studied in the next chapter.

3 MEASUREMENTS AND LINEAR COMBINATIONS

This chapter includes discussions on the main error sources in double differenced (DD) GNSS measurements. A general form of a triple-frequency phase linear combination is developed and the features of a variety of specific phase linear combinations are studied and compared.

3.1 ERROR SOURCES IN DD CODE AND PHASE MEASUREMENTS

For precise carrier phase positioning, usually DD phase observations are adopted. This eliminates or reduces several error sources and aids integer ambiguity resolution. As the basis of further discussion in this thesis, the DD phase observation function is summarized as follows:

$$\nabla\Delta f_i = \frac{1}{l_i}\nabla\Delta R + \frac{1}{l_i}\nabla\Delta dR - \frac{l_i}{l_1^2}\nabla\Delta I_1 + \frac{1}{l_i}\nabla\Delta T - \nabla\Delta N_i + \frac{1}{l_i}\nabla\Delta e_{\Phi_i} \qquad (3.1)$$

where

$\nabla\Delta$ is the DD operator;

f_i is the phase observation on the i-th carrier frequency, in cycles (i = 1, 2, 3);

l_i is the wavelength of the i-th carrier frequency;

R is the geometric range (metres);

dR is the orbital error (metres);

I_1 is the ionospheric delay (metres) on the 1st carrier frequency (L1 for GPS, and E1 for GALILEO);

T is the troposheric delay (metres);

N_i is the phase ambiguity (cycles) of the i-th carrier frequency, and

e_{Φ_i} is the phase noise (including receiver noise and multipath).

3.1.1 Multipath and Receiver Noise

Multipath errors are caused by reflected satellite signals from surfaces near the receiver that shift the correlation peak, and corrupt the correlation envelope between the locally generated signals and the received signals. The magnitude of multipath is environment-dependent, and the resulting errors in code can range from a few centimetres to several tens of metres, and the error in L1 phase is limited to a quarter of a wavelength (Bonillo-Martinez, 1999). Receiver noise is the error the receiver makes in measuring the signal transit time by matching the local signals to the received signals, which is primarily affected by thermal noise of the receiver.

Both multipath and receiver noise cannot be eliminated through differential techniques. Usual ways to decrease multipath are cautious site selecting and using multipath mitigation devices. Receiver noise is highly dependent on the technology incorporated in a particular receiver so that the decrease of receiver noise mainly relies on the development of receiver technology. Through GPS modernization and the GALILEO

design, great efforts have been spent on technology developments for both low thermal noise and low code multipath (Hein, 2002; Weill, 2002).

3.1.2 Satellite Orbital Errors

Satellite orbital errors consist of radial, tangential and a cross track components. The effective error on a range is line-of-sight dependent, so the capability of differential techniques to compensate for the orbital errors will depend on the position of users relative to the reference station. Bauersima (1983) estimates the baseline error Δr as a function of the orbital error ΔR and baseline length l as:

$$|\Delta r| = \frac{l}{r} \cdot |\Delta R| \tag{3.2}$$

where r is the distance between the satellite and the user. The accuracy of the current GPS broadcast ephemeris is around 2.6 m, and it will be further reduced to 1.25 m through GPS modernization (IGS, 2005). So for short and medium baselines, orbital errors are of no concern, and even the broadcast ephemeris can be adopted for high precision applications.

3.1.3 Ionospheric Delay Errors

The ionospheric group delay, $\Delta t_{ion}(f)$, is usually approximated at the first order of the carrier frequency, f, as:

$$\Delta t_{ion}(f) = \frac{40.3}{f^2} TEC \tag{3.3}$$

where TEC is the total electron content in a 1 m^2 cross-sectional tube along the path of transmission through the ionosphere. Second order approximation of the ionospheric delay is addressed in Hoffmann-Wellenhof et al. (1994).

For single frequency applications, differencing is the main technique to reduce the ionospheric effect, since the broadcast ionospheric model can only compensate for about 50% of the delay (ARINC Inc., 1993), and even ionospheric corrections using the Global Ionosphere Maps (GIM) can only correct the ionospheric delay to several decimetres (CODE, 2005). Considering that TEC is not only temporally and spatially varying, but also path dependent, the compensation for ionopsheric errors using a differential technique will depend on the user-to-reference station baseline vector.

For dual or triple frequency applications, there are two options for ionospheric compensation. One is to take advantage of the fact that the atmospheric delay is frequency dependent to estimate and remove the error due to ionospheric delay (Hatch, 1996). The other involves further reduction in ionospheric errors by a differencing technique. A general discussion of ionospheric estimation with two pseudorange or phase measurements (assuming no cycle ambiguities) from the same satellite at two different frequencies is as follows:

$$\begin{cases} r_i = G + \dfrac{f_1^2}{f_i^2} I_1 + e_{r_i} \\ r_j = G + \dfrac{f_1^2}{f_j^2} I_1 + e_{r_j} \end{cases} \tag{3.4}$$

Where r_i and r_j are the measurements (metres) at frequencies f_i and f_j; G is the geometrical part, including the calculated range, tropospheric errors, and orbital errors; I_1 is the ionospheric errors in code or phase on the frequency L1 or E1; e_{r_i} and e_{r_i} are the measurement noise values (including multipath). Using this equation and solving for I_1 gives:

$$I_1 = \frac{f_i^2 f_j^2}{f_j^2 - f_i^2} \cdot \frac{1}{f_1^2} \cdot (r_i - r_j) \tag{3.5}$$

with a standard deviation of:

$$s_{I_1} = \frac{f_i^2 f_j^2}{\left| f_j^2 - f_i^2 \right|} \cdot \frac{1}{f_1^2} \cdot \sqrt{(s_{r_i}^2 + s_{r_j}^2)} \tag{3.6}$$

Table 3.1 gives a numerical accuracy analysis of the above ionospheric estimation using the measurements for both modernized GPS and GALILEO, based on the noise assumption of 0.003 cycles for all single phase measurements, 0.36 m for L1 code (which is pessimistic for future receiver technologies), 0.04 for L5 code, 0.10 m for E1 code, and 0.045 m for E5a code measurements.

The results shown in Table 3.1 indicate that the accuracy of ionospheric estimation is a function of two factors: (1) the noise level of the measurements on f_i and f_j; (2) the

frequency spacing between them. Larger frequency spacing leads to better ionospheric estimation. Therefore, ionospheric estimation with code measurements is not accurate enough for high precision application since the code noise is too large with respect to an L1 cycle. With phase measurements, ionospheric error estimation is at the 1 cm level (except using L2/L5, and E5b/E5a pairs), but the magnitude will be doubled when DD phase measurements are in use.

Table 3.1 Accuracy of Ionospheric Error Estimation with Two Single Code or Phase Measurements

	f_i	f_j	s_{r_i} (m)	s_{r_j} (m)	s_{I_1} (m)
Code	L1	L2	0.50	0.240	0.8573
		L5		0.180	0.6699
	L2	L5	0.240	0.180	2.0502
	E1	E5b	0.240	0.185	0.4309
		E5a		0.185	0.3820
	E5b	E5a	0.185	0.185	2.9062
Phase	L1	L2	0.0053	0.0068	0.0134
		L5		0.0071	0.0112
	L2	L5	0.0068	0.0071	0.0675
	E1	E5b	0.0053	0.0069	0.0125
		E5a		0.0071	0.0112
	E5b	E5a	0.0069	0.0071	0.1107

3.1.4 Tropospheric Delay Errors

Tropospheric delay of satellite signals is caused by the index of refraction along the signal path in the neutral atmosphere layer ranging from 0 to 10 km. The delay is frequency-independent, and is only related to the meteorological parameters (atmospheric pressure, temperature and relative humidity), the magnitude of which amounts to about 2.3 m in the zenith direction and over 25 m for an elevation of 5**0**(Rothacher, 2002), and

over 90% can be compensated through the Hopfield, Saastamoinen, or Niell model for example (Parkinson et al., 1996). The compensation for the remaining errors has to resort to differential techniques again, although a residual error will remain.

3.2 PHASE LINEAR COMBINATIONS

The imminent triple frequency systems will enable more linear combinations of the carrier phase observations. The study here is in an attempt to seek proper candidates with good features for better ambiguity resolution performance. Detailed analysis can be also found in Richert (2005) in the same field, but from a different perspective.

3.2.1 General Form of Triple-frequency Linear Combinations

The linear combination of the phase observations between carrier frequencies plays a very important role in the field of ambiguity resolution. As both GALILEO and modernized GPS will provide civil users with three frequencies, more linear combinations will be available. Equation (3.7) gives a general form for the triple frequency linear combination:

$$f_{LC} = k_1 \cdot f_1 + k_2 \cdot f_2 + k_3 \cdot f_3 \tag{3.7}$$

where f_1, f_2 and f_3 represent the phase observations on L1, L2 and L5 for the GPS system, or on E1, E5b and E5a for GALILEO in cycles. k_1, k_2 and k_3 are the

coefficients and f_{LC} is the linearly combined phase. The corresponding ambiguity linear combination is:

$$N_{LC} = k_1 \cdot N_1 + k_2 \cdot N_2 + k_3 \cdot N_3 \tag{3.8}$$

where N_1, N_2 and N_3 are the carrier phase ambiguities. For integer coefficients, the resulting ambiguity N_{LC} is also an integer, so this kind of combination can be referred to as integer linear combination. However, for real-valued coefficients, N_{LC} is no longer an integer, but a kind of float ambiguity. Usually, interest is focused on the integer linear combination since the integerness of N_1, N_2 and N_3 is preserved in N_{LC}. In the following sections, some excellent properties of the float linear combination are also studied.

3.2.2 Linear Combination of DD Phase Observations

Since DD measurements are of interest in this thesis, the linear combination of the DD measurements is directly discussed. Based on Equations (3.1) and (3.7), the triple-frequency linear combination can be formed as:

$$\begin{aligned} \nabla\Delta f_{LC} = &(\frac{k_1}{l_1} + \frac{k_2}{l_2} + \frac{k_3}{l_3})(\nabla\Delta R + \nabla\Delta dR + \nabla\Delta T) \\ &-(k_1 \frac{1}{l_1} + k_2 \frac{l_2}{l_1^2} + k_3 \frac{l_3}{l_1^2})\nabla\Delta I_1 \\ &-\nabla\Delta N_{LC} + (\frac{k_1}{l_1} + \frac{k_2}{l_2} + \frac{k_3}{l_3})\nabla\Delta e_{\Phi_{LC}} \end{aligned} \tag{3.9}$$

where $\nabla\Delta f_{LC}$ represents the DD phase linear combination in cycles. As in Equation (3.4), the three items of geometrical errors ($\nabla\Delta R$, $\nabla\Delta dR$ and $\nabla\Delta T$) can be denoted as $\nabla\Delta G$ for the purpose of simplification.

When selecting different coefficients to form a linear combination through Equation (3.9), the wavelength of the linear combination can be derived as:

$$l_{LC} = \frac{1}{\frac{k_1}{l_1} + \frac{k_2}{l_2} + \frac{k_3}{l_3}} \tag{3.10}$$

where a basic requirement to be met is that $(\frac{k_1}{l_1} + \frac{k_2}{l_2} + \frac{k_3}{l_3}) > 0$. Using the above equation, the wavelength of each linear combination can be calculated.

3.2.3 Measurement Noise

Assuming that the measurement noise of a single phase observation is $a\%$ of the wavelength, namely:

$$s_i = a\% \cdot l_i \tag{3.11}$$

The noise of the DD phase in metres would be:

$$\nabla\Delta s_i = 2a\% \cdot l_i \tag{3.12}$$

Applying variance propagation to Equation (3.7), the noise of the DD phase linear combination in metres can be derived as:

$$\nabla\Delta s_{LC} = \sqrt{k_1^2 + k_2^2 + k_3^2} \cdot 2a\% \cdot l_{LC} \tag{3.13}$$

When the measurement noise of the phase linear combination exceeds a certain threshold, correct ambiguity resolution becomes difficult or highly unlikely. However, in practice it is hard to determine the noise threshold for the linear combination candidates since the amounts of other residual errors are unknown and also lead to difficulties in ambiguity resolution. In need of correct rounding, Jung (2000) set a basic criterion for an ideal phase linear by limiting the measurement noise to within half a cycle. Therefore the noise of an acceptable linear combination should at least meet:

$$\nabla\Delta s_{LC} < \frac{1}{2} l_{LC} \tag{3.14}$$

Substituting Equation (3.13) into (3.14) leads to a limiting condition for the coefficients of an acceptable linear combination as follows:

$$(k_1^2 + k_2^2 + k_3^2) < (\frac{1}{4a\%})^2 \tag{3.15}$$

In the following analysis, the measurement noise of a single carrier-phase observation is assumed to be 2.8% (a sum of the multipath and noise listed in Section 7.2.3) of the wavelength. According to Equation (3.15) with $a\%$ being 2.8%, the coefficients of any acceptable linear combination should meet the requirement $(k_1^2 + k_2^2 + k_3^2) < 80$.

3.2.4 DD Ionospheric Errors

The ionospheric errors of the DD linear combination in metres can also be derived through Equation (3.9) as:

$$\nabla\Delta I_{\Phi_{LC}} = a_I \cdot \nabla\Delta I_1 \text{ (metres)} \tag{3.16}$$

where

$$a_I = (k_1 \frac{1}{l_1} + k_2 \frac{l_2}{l_1^2} + k_3 \frac{l_3}{l_1^2}) \cdot l_{LC} \tag{3.17}$$

and the ionospheric errors in cycles:

$$\nabla\Delta I_{f_{LC}} = b_I \cdot \frac{\nabla\Delta I_1}{l_1} \text{ (cycles)} \tag{3.18}$$

where

$$b_I = (k_1 + k_2 \frac{l_2}{l_1} + k_3 \frac{l_3}{l_1}) \tag{3.19}$$

In the above equations, the ionospheric errors of the DD linear combination expressed in both units are compared to the DD ionospheric influence on the 1st carrier frequency (E1 for GALILEO and L1 for modernized GPS), with both a_I and b_I being unitless indices, 'Φ' and 'f' associated to quantities expressed in metres and in cycles respectively. The coefficient a_I reflects the DD range errors due to the ionospheric delay compared to those for the L1/E1 ranges, which also indirectly reflects the positioning accuracy using that linear combination. The coefficient b_I indicates the ionospheric influence level on the linear combination in cycles compared to that on the L1/E1, which also indirectly reflects the difficulty for ambiguity resolution using that linear combination. So ideally,

the corresponding a_I and b_I should be as small as possible from the perspectives of both an ambiguity resolution and a positioning accuracy. Radovanovic (2001) also presented similar criteria for the selection of optimized GPS L1/L2 carrier phase combinations, but in a different way.

An extreme case for Equations (3.16) and (3.18) assures that the combined DD ionospheric error $\nabla\Delta I_{LC}$ equals to zero when $(k_1 \frac{1}{l_1} + k_2 \frac{l_2}{l_1^2} + k_3 \frac{l_3}{l_1^2}) = 0$. Under such a condition, the linear combination is immune to ionospheric influence and therefore is referred to as an ionosphere-free (IF) linear combination.

3.2.5 DD Geometrical Errors

According to Equation (3.9), the DD geometric errors of the phase linear combination in units of cycles are:

$$\begin{aligned} \nabla\Delta G_{f_{LC}} &= (\frac{k_1}{l_1} + \frac{k_2}{l_2} + \frac{k_3}{l_3}) \cdot (\nabla\Delta R + \nabla\Delta dR + \nabla\Delta T) \\ &= l_1 (\frac{k_1}{l_1} + \frac{k_2}{l_2} + \frac{k_3}{l_3}) \cdot \frac{1}{l_1} (\nabla\Delta R + \nabla\Delta dR + \nabla\Delta T) \qquad \text{(cycles)} \qquad (3.20) \\ &= b_G \cdot \frac{1}{l_1} (\nabla\Delta R + \nabla\Delta dR + \nabla\Delta T) \end{aligned}$$

In the above equation, b_G indicates the influence of the geometrical errors on the linear combination (cycles) with respect to that on the L1/E1. In the case that $(\frac{k_1}{l_1} + \frac{k_2}{l_2} + \frac{k_3}{l_3}) > 0$, b_G is equal to $\frac{l_1}{l_{LC}}$, which indicates that when the wavelength of

the linear combination is greater than l_1, the influence of the geometrical errors (cycles) with respect to L1/E1 (cycles) can be decreased. In the case that $(\frac{k_1}{l_1}+\frac{k_2}{l_2}+\frac{k_3}{l_3})=0$, namely the wavelength of the linear combination is infinitely long, the influence of the geometrical errors on the linear combination in cycles no longer exists, so this linear combination is referred to as a geometry-free (GF) linear combination in this thesis.

3.2.6 Integer Linear Combination

(1) Measurement Noise

For linear combinations with integer coefficients, the measurement noise is

$$\nabla\Delta s_{LC}=\sqrt{k_1^2+k_2^2+k_3^2}\cdot 2a\%\cdot l_{LC}>=2a\%\cdot l_{LC} \tag{3.21}$$

where all the coefficients cannot be zero simultaneously. Therefore, the noise of DD linear combinations is at least two times the noise of a single-phase measurement in cycles.

(2) Possibility of Integer Ionosphere-Free Combinations

Collins (2000) discussed an integer ionosphere-free linear combination with two frequencies, corresponding to the linear combination (77, -60, 0), which is too noisy to be applicable, and also too noisy to pass the threshold in Equation (3.15). A further investigation on possible integer ionosphere-free linear combination involving three

frequencies, based on Equations (3.10), (3.15) and (3.19) for both modernized GPS and GALILEO is given below whereby, following inequalities should be met:

$$\begin{cases} (\frac{k_1}{l_1}+\frac{k_2}{l_2}+\frac{k_3}{l_3})>0 \\ (k_1^2+k_2^2+k_3^2)<80 \\ (k_1+k_2\frac{77}{60}+k_3\frac{154}{115})=0 \end{cases} \text{(GPS)} \quad \begin{cases} (\frac{k_1}{l_1}+\frac{k_2}{l_2}+\frac{k_3}{l_3})>0 \\ (k_1^2+k_2^2+k_3^2)<80 \\ (k_1+k_2\frac{77}{59}+k_3\frac{154}{115})=0 \end{cases} \text{(GALILEO)} \quad (3.22)$$

For a linear combination meeting Equation (3.22), the relationship among k_1, k_2 and k_3 is shown in Figure 3.1. For given integer-valued k_2 and k_3, to get an ionosphere-free measurement ($b_I = 0$), several values for k_1 can be obtained through Equation (3.22). In the left column of Figure 3.1, $[k_1]$ represents the rounding of k_1, so the vertical axes ($z = k_1 - [k_1]$) represent the differences between k_1 and the nearest integer of k_1, where z should be zero if an integer k_1 exists enabling an ionosphere-free measurement. Around 55 LCs with the smallest absolute values of z are chosen from the left column of Figure 3.1 and plotted in the right column of Figure 3.1. Each of the LCs is sorted by the absolute value of its z (namely $|z|$), with the horizontal axes representing the sort numbers, and the vertical axes representing $|z|$. Unfortunately, when going through all candidates, **,** even the smallest $|z|$ (shown in the right column of Figure 3.1) for both GPS and GALILEO are not equal to zero, which indicates that no integer k_1 exists and an integer ionosphere-free linear combination meeting the pre-defined noise condition for both the GPS and GALILEO cases remains impossible. However, a series of ionosphere-free combination sets (k_1, k_2, k_3) with real-valued k_1 that are very close to integers can be obtained (as shown in the right column of Figure 3.1), such as: (1.0043, -6, 5),

(2.9014, 4, -6), (3.9058, -2, -1), (3.9616, -1, -2), (5.0217, -6, 2), (5.0775, -5, 1) for modernized GPS, (3.9493, -2, -1), (3.9833, -1, -2), (7.9326, -3, -3) for GALILEO. When the real-valued k_1 are rounded to the nearest integers, the resulting combinations can be obtained with the features as listed in Table 3.2.

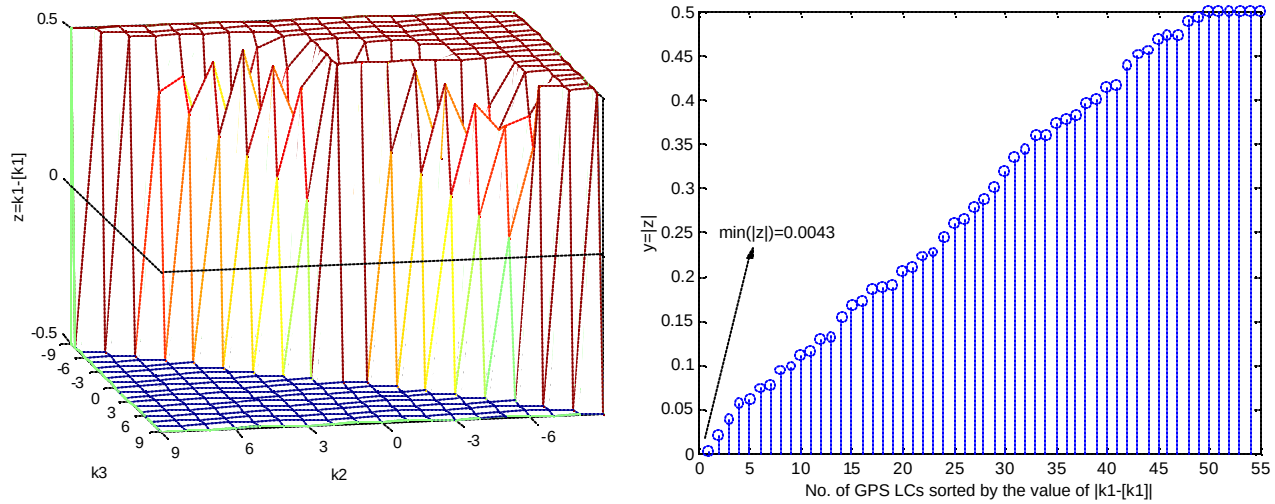

(1) GPS

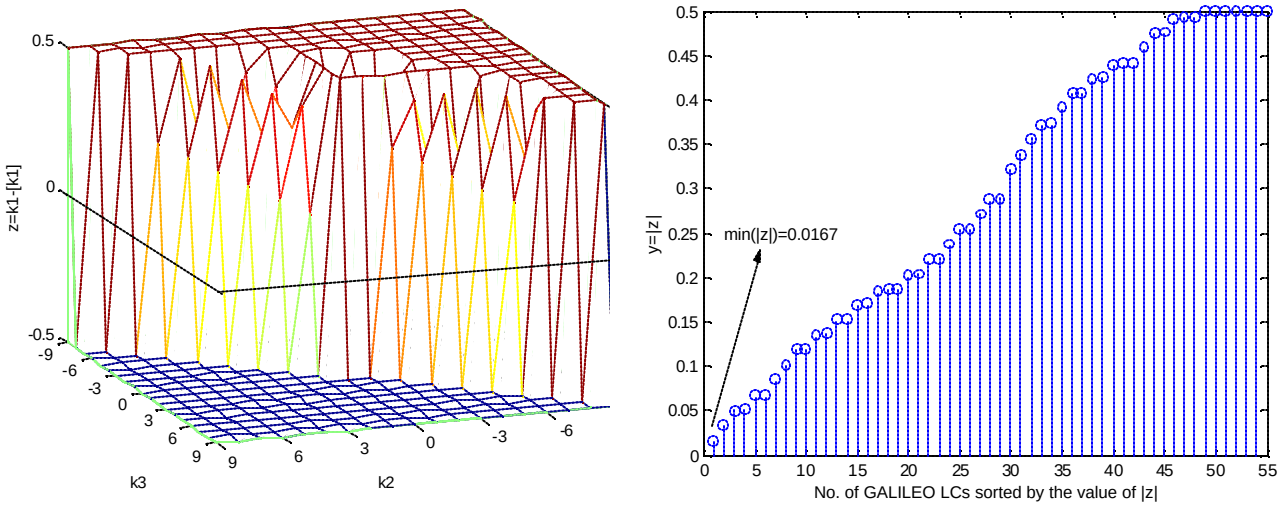

(2) GALILEO

Figure 3.1 Selection of Integer IF Linear Combination

Compared to the ionospheric errors existing in the L1/E1 carrier phase, the ionospheric errors (a_I and b_I) in the above integer combinations are one to two order(s) smaller, which can be almost neglected. However, the noise of these combinations is 4 ~ 10 times larger than that of the DD L1/E1 carrier phase ($2 \times 2.8\%$ cycles). In addition, the wavelengths of all the above combinations are shorter than L1/E1 except the combination (1, -6, 5), therefore exacerbating the influence of geometrical errors in cycles. The combination (1, -6, 5) is desirable in terms of both ionospheric and geometrical influence in cycles, but the significant weakness is that the noise occurs as almost half a cycle leading to problems when applying the linear combination to ambiguity resolution.

Table 3.2 Approximately Ionosphere-free Triple-frequency Integer Linear Combinations

System	Coefficients			l_{LC}	$\nabla\Delta s_i$		Error Level		
	k_1	k_2	k_3	(m)	(m)	(Cycle)	a_I	b_I	b_G
GPS	1	-6	5	3.256	1.435	0.440	-0.074	-0.004	0.058
	3	4	-6	0.116	0.050	0.437	0.060	0.098	1.636
	4	-2	-1	0.112	0.028	0.256	0.055	0.094	1.694
	4	-1	-2	0.110	0.028	0.256	0.022	0.038	1.726
	5	-6	2	0.104	0.047	0.451	-0.012	-0.021	1.817
	5	-5	1	0.102	0.041	0.399	-0.041	-0.077	1.851
GALILEO	4	-2	-1	0.110	0.028	0.256	0.029	0.050	1.720
	4	-1	-2	0.109	0.028	0.256	0.009	0.016	1.741
	8	-3	-3	0.055	0.027	0.507	0.019	0.067	3.459

(2) Some Useful Integer Linear Combinations

In the study of integer linear combinations, most literature pays attention to the measurement noise in the search for ideal combinations (Ericson, 1999; Jung, 2000). To get practical linear combinations, all the integer linear combinations in Equation (3.22)

were strictly filtered under the conditions that the DD noise is below 0.2 cycles, and that the ionosphere index, b_I, is no larger than 1.0. Therefore, the triple-frequency integer linear combinations in the following table are obtained.

Table 3.3 Triple-frequency Integer Linear Combinations

System	Coefficients			l_{LC}	$\nabla\Delta s_i$		Error Level		
	k_1	k_2	k_3	(m)	(m)	(cycles)	a_I	b_I	b_G
GPS	0	1	-1	5.861	0.464	0.079	-1.719	-0.056	0.032
	1	-2	1	1.011	0.138	0.137	-1.208	-0.228	0.188
	1	-1	0	0.862	0.079	0.079	-1.283	-0.283	0.221
	1	0	-1	0.751	0.059	0.079	-1.339	-0.339	0.253
	1	0	0	0.190	0.010	0.056	1	1	1
	1	1	-2	0.666	0.091	0.137	-1.382	-0.395	0.286
	1	1	-1	0.184	0.017	0.097	0.915	0.944	1.032
	1	2	-2	0.179	0.030	0.168	0.834	0.888	1.065
	2	-2	1	0.160	0.026	0.168	0.650	0.772	1.188
	2	-1	-1	0.401	0.055	0.137	-1.313	-0.622	0.474
	2	-1	0	0.156	0.019	0.125	0.587	0.717	1.221
	2	0	-1	0.152	0.019	0.125	0.527	0.661	1.253
	2	1	-2	0.148	0.024	0.168	0.471	0.605	1.286
	3	-1	-1	0.129	0.024	0.185	0.256	0.378	1.474
GALILEO	0	1	-1	9.768	0.773	0.079	-1.748	-0.034	0.019
	1	-2	1	0.888	0.121	0.137	-1.265	-0.271	0.214
	1	-1	0	0.814	0.064	0.079	-1.305	-0.305	0.234
	1	0	-1	0.751	0.059	0.079	-1.339	-0.339	0.253
	1	0	0	0.190	0.010	0.056	1	1	1
	1	1	-2	0.698	0.095	0.137	-1.368	-0.373	0.273
	1	1	-1	0.187	0.018	0.097	0.947	0.966	1.019
	1	2	-2	0.183	0.030	0.168	0.897	0.932	1.039
	2	-2	1	0.157	0.026	0.168	0.600	0.729	1.214
	2	-1	-1	0.391	0.053	0.137	-1.323	-0.644	0.487
	2	-1	0	0.154	0.019	0.125	0.563	0.695	1.234
	2	0	-1	0.152	0.019	0.125	0.527	0.661	1.253
	2	1	-2	0.150	0.025	0.168	0.493	0.627	1.273
	3	-1	-1	0.128	0.023	0.185	0.239	0.356	1.487

For each linear combination, the degree to which it can be possibly and successfully applied in ambiguity resolution, is directly represented by the wavelength, the noise level in cycles, together with the error levels (the smaller the b_I and b_G, the higher the possibility they can be applied). In the above table, the shaded rows highlight linear combinations with small noise (in cycles). For both the modernized GPS and GALILEO cases, the linear combination (0, 1, -1) come out to be an excellent choice for efficient ambiguity resolution due to small amounts of all errors (in cycles), and the sole weakness is that measurement noise (in metres) limits the positioning precision which could be obtained using this linear combination.

The linear combinations (1, -1, 0) and (1, 0, -1) enable better positioning precision with smaller measurement noise (in metres), with the ionospheric and geometrical errors (b_I and b_G) at acceptable levels. For other linear combinations with comparable wavelengths, (1, -2, 1) has better features in terms of the ionospheric and geometrical errors, but worse in the measurement noise; (1, 1, -2) and (2, -1, -1) are worse in both measurement noise and errors.

The linear combination (1, 0, 0) actually represents L1/E1, since it is the most precise measurement, the ambiguity of which is always the target of efforts. For other linear combinations with a comparable wavelength, all of them have much larger measurement noise although some have less ionospheric influence (b_I). The combinations (0, 1, 0) and (0, 0, 1), namely L2/E5b and L5/E5a, are not regarded as practical linear combinations

although they have as small noise as (1, 0, 0), since the ionospheric influence (b_I) is over 1.28 times larger as shown in Equation (3.19).

The shaded integer linear combinations in Table 3.3 are extracted and summarized in Table 3.4 since they are frequently cited in the research of this thesis.

Table 3.4 Practical Triple-frequency Integer Linear Combinations

System	LC	Coefficients			l_{LC}	$\nabla\Delta s_i$ (m)	Ionospheric Level	
		k_1	k_2	k_3			a_I	b_I
GPS	EWL	0	1	-1	$\frac{l_2 l_3}{l_3 - l_2}$	0.464	$-\frac{l_2 l_3}{l_1^2}$	$-\frac{l_3 - l_2}{l_1}$
	WL	1	-1	0	$\frac{l_1 l_2}{l_2 - l_1}$	0.079	$-\frac{l_2}{l_1}$	$-\frac{l_2 - l_1}{l_1}$
	ML	1	0	-1	$\frac{l_1 l_3}{l_3 - l_1}$	0.059	$-\frac{l_3}{l_1}$	$-\frac{l_3 - l_1}{l_1}$
	L1	1	0	0	l_1	0.010	1.0	1.0
GALILEO	EWL	0	1	-1	$\frac{l_2 l_3}{l_3 - l_2}$	0.773	$-\frac{l_2 l_3}{l_1^2}$	$-\frac{l_3 - l_2}{l_1}$
	WL	1	-1	0	$\frac{l_1 l_2}{l_2 - l_1}$	0.064	$-\frac{l_2}{l_1}$	$-\frac{l_2 - l_1}{l_1}$
	ML	1	0	-1	$\frac{l_1 l_3}{l_3 - l_1}$	0.059	$-\frac{l_3}{l_1}$	$-\frac{l_3 - l_1}{l_1}$
	E1	1	0	0	l_1	0.010	1.0	1.0

In the above table, EWL, WL and ML represent the Extra-Wide-Lane, Wide-Lane and Medium-Lane correspondingly. In this thesis, EWL always stands for the linear combination (0, 1, -1), WL stands for (1, -1, 0) and ML represents (1, 0, -1) for both modernized GPS and GALILEO. In light of Table 3.4, significant features of the two sets of linear combinations EWL/WL/ML/L1 and EWL/WL/ML/E1 can be found:

- Cascading wavelengths

The two sets of linear combinations are with similar cascading wavelengths starting from 5.86 m (9.77 m), then decreasing to 0.86 m (0.81 m), and then to 0.75 m (0.75 m), finally arriving at 0.19 m (0.19 m). It indicates that a stepwise improvement in positioning accuracy remains possible using either of the linear combination sets.

- Cascading measurement noises in metres

For the GPS case, the DD measurements of the two sets of linear combinations have similar cascading noise values starting from 0.464 m (GALILEO: 0.773 m), then decreasing to 0.079 m (GALILEO: 0.064 m), and then to 0.059 m (GALILEO: 0.059 m), finally arriving at 0.010 m (GALILEO: 0.010 m). It reconfirms the possibility of a stepwise improvement in positioning accuracy using either of the linear combination sets.

- Same measurement noises in units of cycles (except L1/E1)

All the DD measurements of the linear combinations are at the same noise level of 0.079 cycles, except for L1/E1 at 0.056 cycles. It indicates that the measurement noise of all the linear combinations affects ambiguity resolution at a low level.

- Small ionospheric and geometrical influence in cycles (except L1/E1)

Although b_I and b_G rise with the drop in wavelengths from EWL to ML, b_I and b_G are always small, so that ambiguity resolution of EWL/WL/ML should be promising.

Due to the above features, the two sets of linear combinations EWL/WL/L1 and EWL/WL/E1 are used in GPS and GALILEO ambiguity resolution in subsequent chapters. As an extension of Table 3.1, the accuracy of ionospheric estimation using the above linear combinations (assuming ambiguity free) is presented in Table 3.5, which indicates that ionospheric errors cannot be accurately estimated at the centimetre level until L1/E1 are used.

Table 3.5 Accuracy of Ionospheric Estimation with Two DD Phase Measurements

Phase	f_i	f_j	$\nabla\Delta s_{r_i}$ (m)	$\nabla\Delta s_{r_j}$ (m)	$\nabla\Delta s_{I_1}$ (m)
GPS	L1	EWL	0.0076	0.3316	0.1221
		WL		0.0488	0.0218
	WL	EWL	0.0488	0.3316	0.9964
GALILEO	E1	EWL	0.0076	0.5526	0.2012
		WL		0.0460	0.0204
	WL	EWL	0.0460	0.5526	1.6395

3.2.7 Float Linear Combinations

Two kinds of float linear combinations, the geometry-free (GF) and the ionosphere-free (IF) that remove the geometrical and ionospheric effects in Equation (3.9) respectively, are of great importance and are discussed below.

(1) GF Linear Combinations

Table 3.6 gives some typical GF linear combinations using triple frequency for both GALILEO and modernized GPS.

Table 3.6 Triple Frequency Geometry-Free (GF) Linear Combinations

System	LC	Coefficients			l_{LC}	$\nabla\Delta s_i$ (cycles)	b_I
		k_1	k_2	k_3			
GPS	GF_{12}	l_1	$-l_2$	0	N/A	$11.48 \cdot a$ %	2.28
	GF_{13}	l_1	0	$-l_3$	N/A	$9.86 \cdot a$ %	2.34
	GF_{23}	0	l_2	$-l_3$	N/A	$66.48 \cdot a$ %	2.62
GALILEO	GF_{12}	l_1	$-l_2$	0	N/A	$10.78 \cdot a$ %	2.31
	GF_{13}	l_1	0	$-l_3$	N/A	$9.86 \cdot a$ %	2.34
	GF_{23}	0	l_2	$-l_3$	N/A	$109.84 \cdot a$ %	2.64

The coefficients for each GF linear combination are actually the wavelengths of the carrier frequencies. The measurement noise and ionospheric influences in Table 3.6 will be further explained and discussed in Chapter 5.

(2) IF Linear Combinations

With the criteria introduced in Section 3.2.3, some triple frequency IF linear combinations are formed and listed in Table 3.7.

Table 3.7 Triple Frequency Ionosphere-Free (IF) Linear Combinations

System	LC	Coefficients			l_{LC}	$\nabla\Delta s_i$ (m)	a_I & b_I
		k_1	k_2	k_3			
GPS	IF_{12}	1	$-\frac{l_1}{l_2}$	0	$\frac{l_1 l_2^2}{l_2^2 - l_1^2} = 0.4844$	0.0246	0
	IF_{13}	1	0	$-\frac{l_1}{l_3}$	$\frac{l_1 l_3^2}{l_3^2 - l_1^2} = 0.4302$	0.0215	0
	IF_{23}	0	1	$-\frac{l_2}{l_3}$	$\frac{l_2 l_3^2}{l_3^2 - l_2^2} = 2.9929$	0.1658	0
GALILEO	IF_{12}	1	$-\frac{l_1}{l_2}$	0	$\frac{l_1 l_2^2}{l_2^2 - l_1^2} = 0.4609$	0.0232	0

	IF_{13}	1	0	$-\frac{l_1}{l_3}$	$\frac{l_1 l_3^2}{l_3^2 - l_1^2} = 0.4302$	0.0215	0
	IF_{23}	0	1	$-\frac{l_2}{l_3}$	$\frac{l_2 l_3^2}{l_3^2 - l_2^2} = 4.9471$	0.2763	0

For both modernized GPS and GALILEO, although three IF linear combinations are available, only two of them are linearly independent. The third IF linear combination IF_{23} for both GPS and GALILEO is too noisy, so only the first two will be used later. In the later chapters, the ionosphere-free combinations, IF_{12} and IF_{13} for both GPS and GALILEO, are referred to as IF_1 and IF_2 respectively.

4 TRIPLE-FREQUENCY CASCADING AMBIGUITY RESOLUTION

4.1 CASCADING AMBIGUITY RESOLUTION METHODS

In the case of a large quantity of ambiguities on multiple frequencies, a conventional method of fixing the ambiguities is to directly include the ambiguities on all frequencies in one filter and to follow the procedures of the LAMBDA method (Teunissen, 1993) to fix all carrier phase ambiguities simultaneously (de Jong et al., 2001; Julien et al., 2003). Another approach involves the cascading ambiguity resolution (CAR) method, which aims to seek some wide lane phase linear combinations with cascading wavelengths and to fix the ambiguities in several steps in order of the length of the lanes from the longest to the shortest, until all are fixed. In this method, the ambiguities on each frequency are finally derived through the ambiguities fixed for the various wide lanes. Since the longer the wavelength, the easier it is to fix the ambiguities, it is a wise decision to deal with wider lanes instead of directly resolving the ambiguities on each frequency. The phase linear combinations studied in Table 3.4 are of a cascading nature (EWL/WL/L1 and EWL/WL/E1), which make it feasible to perform cascading ambiguity resolution.

In earlier studies of GALILEO carrier phase ambiguity resolution, Three-Carrier Ambiguity Resolution (TCAR) was proposed (Forssell et al., 1997) by means of a cascading method, which was further extended in Vollath et al. (1998). Afterwards, with the release of the GPS modernization plan, a similar method called Cascading Integer

Resolution (CIR) was suggested for GPS (Jung et al., 2000; Hatch et al., 2000).

A detailed comparison of TCAR, CIR and LAMBDA was conducted in Teunissen (2002). Although proposed for different systems, TCAR and CIR are in principle the same. They are both based on geometry-free models for instantaneous integer ambiguity resolution by using integer rounding. Meanwhile, they both originated from the idea of wide laning to take advantage of the stepwise improved precision in phase ranges from the longest wavelength (EWL) to the shortest one (L1/E1). Moreover, both TCAR and CIR are designed in such a way that once the three cascading ambiguities (EWL/WL/L1 or EWL/WL/E1) are fixed, the ambiguities at any of the three frequencies (L1/L2/L5 or E1/E5b/E5a) can be derived from the fixed ones. Although TCAR and CIR are dependent on the carrier frequency allocation of the systems, and with the evolution of GALILEO frequencies the practical linear combinations according to the final frequency selection are different from those studied in Vollath et al. (1997) and Bonillo-Martinez (1999), very similar cascading wavelengths are provided.

4.2 GEOMETRY-FREE CASCADING AMBIGUITY RESOLUTION

This section is a summary of the aforementioned cascading ambiguity resolution methods for both GPS and GALILEO.

4.2.1 Cascading Ambiguity Resolution Procedures

The cascading ambiguity resolution for both GPS and GALILEO consists of three steps as shown in Figure 4.1.

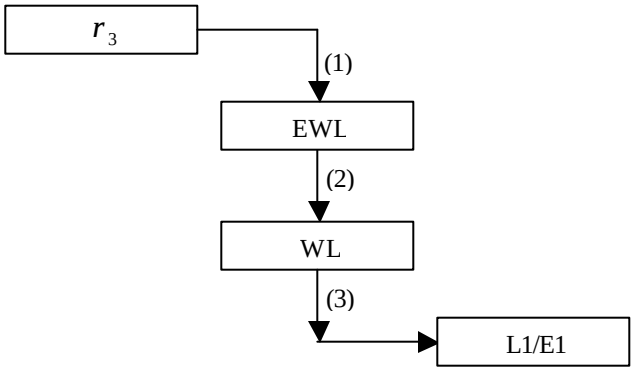

Figure 4.1 Procedures of Cascading Ambiguity Resolution Methods

In the first step, the EWL ambiguities are resolved using r_3, which represents the most precise code ranges. Then in the second step, the fixed EWL ranges are used to resolve the WL ambiguities. Finally, the fixed WL ranges serve to resolve the L1/E1 ambiguities. In each step, the geometry-related components in the observation equations are cancelled, so the entire procedure is geometry-free.

- **First Step**

The DD observation equation of the most precise code measurement is:

$$\nabla\Delta r_3 = \nabla\Delta R + \nabla\Delta dR + \nabla\Delta I_{r_3} + \nabla\Delta T + \nabla\Delta e_{r_3} \tag{4.1}$$

where

r_3 is the most precise DD code observable;

I_{r_3} is the DD ionospheric error on the code, and

e_{r_3} is the measurement noise of the DD code observable.

The other terms were defined in Equation (3.1). The interpretation of $\nabla\Delta r_3$ is the DD code observable on the third frequency of GALILEO or modernized GPS. According to Table 2.2, the code measurement on the third frequency of GALILEO (E5a) has the best precision due to the highest chipping rate (10.23 Mchip/s). For modernized GPS, the most precise civil code will be available on the third frequency (L5) at the same chipping rate as the E5a code.

The DD observation equation of the EWL phase measurement is:

$$\begin{aligned}(\nabla\Delta f_{EWL} + \nabla\Delta N_{EWL}) \cdot l_{EWL} \\ = \nabla\Delta R + \nabla\Delta dR + \nabla\Delta I_{EWL} + \nabla\Delta T + \nabla\Delta e_{\Phi_{EWL}}\end{aligned} \tag{4.2}$$

where

f_{EWL} is the EWL phase measurement in units of cycles;

N_{EWL} is the EWL ambiguity;

l_{EWL} is the wavelength of the EWL;

I_{EWL} is the ionospheric error in the EWL measurement, and

$e_{\Phi_{EWL}}$ is the EWL phase noise in units of metres.

Since the geometry-related components in Equations (4.1) and (4.2) are identical, by neglecting the residual ionospheric errors, the float EWL ambiguity $\nabla\Delta\tilde{N}_{EWL}$ can be

estimated through the subtraction of the two equations as:

$$\nabla\Delta\tilde{N}_{EWL} = \frac{\nabla\Delta r}{l_{EWL}} - \nabla\Delta f_{EWL} \tag{4.3}$$

As the EWL wavelengths for GPS and GALILEO are 5.861 m and 9.768 m respectively, the influence of neglected residual ionospheric errors and the measurement noise on EWL ambiguity estimation in Equation (4.3) should be limited, so the integer EWL ambiguity can be obtained:

$$\nabla\Delta N_{EWL} = round\left[\nabla\Delta\tilde{N}_{EWL}\right] \tag{4.4}$$

where $round[x]$ indicates the nearest integer to x.

Once the EWL ambiguity is resolved, the fixed EWL range becomes the most precise range and therefore can be used to resolve the WL ambiguity.

- **Second Step**

The DD observation equation of the WL phase measurement is:

$$\begin{aligned}(\nabla\Delta f_{WL} + \nabla\Delta N_{WL}) \cdot l_{WL} \\ = \nabla\Delta R + \nabla\Delta dR + \nabla\Delta I_{WL} + \nabla\Delta T + \nabla\Delta e_{\Phi_{WL}}\end{aligned} \tag{4.5}$$

where

f_{WL} is the WL phase measurement (cycles);

N_{WL} is the WL ambiguity;

l_{WL} is wavelength of the WL;

I_{WL} is the ionospheric error in the WL measurement, and

$e_{\Phi_{WL}}$ is the WL phase noise (metres).

Since the geometry-related components in Equations (4.2) and (4.5) are identical, the float WL ambiguity $\nabla\Delta\tilde{N}_{WL}$ can be estimated in a similar way as in the previous step by neglecting the residual ionospheric errors:

$$\nabla\Delta\tilde{N}_{WL} = (\nabla\Delta f_{EWL} + \nabla\Delta N_{EWL}) \cdot \frac{l_{EWL}}{l_{WL}} - \nabla\Delta f_{WL} \tag{4.6}$$

Under the condition that the sum of the neglected ionospheric errors and the measurement noise in Equation (4.6) is within a half of the WL wavelength, the integer WL ambiguity can be successfully obtained by rounding the float ambiguity to the nearest integer:

$$\nabla\Delta N_{WL} = round\left[\nabla\Delta\tilde{N}_{WL}\right] \tag{4.7}$$

After the WL ambiguity is fixed, the WL range becomes the most precise range and therefore can be used in the estimation of the L1/E1 ambiguity.

- **Third Step**

The DD observation equation of the L1/E1 phase measurement is:

$$\begin{aligned}(\nabla\Delta f_1 + \nabla\Delta N_1) \cdot l_1 \\ = \nabla\Delta R + \nabla\Delta dR + \nabla\Delta I_1 + \nabla\Delta T + \nabla\Delta e_{\Phi_1}\end{aligned} \tag{4.8}$$

where

f_1 is the L1/E1 phase measurement (cycles);

N_1 is the L1/E1 ambiguity;

l_1 is the wavelength of the L1/E1;

I_1 is the ionospheric error in the L1/E1 measurement, and

e_{Φ_1} is the L1/E1 phase noise (metres).

Again, the geometry-related components in Equations (4.5) and (4.8) are identical, so the float L1/E1 ambiguity $\nabla\Delta\tilde{N}_1$ can be estimated by neglecting the residual ionospheric errors:

$$\nabla\Delta\tilde{N}_1 = (\nabla\Delta f_{WL} + \nabla\Delta N_{WL}) \cdot \frac{l_{WL}}{l_1} - \nabla\Delta f_1 \tag{4.9}$$

The integer L1/E1 ambiguity can be obtained in Equation (4.10) assuming that the sum of the neglected ionospheric errors and measurement noise in Equation (4.9) does not exceed half of an L1/E1 cycle.

$$\nabla\Delta N_1 = round\left[\nabla\Delta\tilde{N}_1\right] \tag{4.10}$$

Once $\nabla\Delta N_{EWL}$, $\nabla\Delta N_{WL}$ and $\nabla\Delta N_1$ are fixed, the L2/E5b ambiguity ($\nabla\Delta N_2$) and L5/E5 ambiguity ($\nabla\Delta N_3$) can be derived as:

$$\nabla\Delta N_2 = \nabla\Delta N_1 - \nabla\Delta N_{WL} \tag{4.11}$$

$$\nabla\Delta N_3 = \nabla\Delta N_1 - \nabla\Delta N_{WL} - \nabla\Delta N_{EWL} \tag{4.12}$$

In the other chapters of this thesis, sometimes $\nabla\Delta N_{WL}$ is also represented as $\nabla\Delta N_{12}$ since the latter can clearly indicate how the combination is formed, and $\nabla\Delta N_{EWL}$ is represented as $\nabla\Delta N_{23}$.

4.2.2 Error Analysis

Since all geometry-related errors are removed in geometry-free models, the efficiency of

TCAR/CIR in each step is mainly susceptible to two error sources:

(1) The error caused by ignoring ionospheric effects;

(2) The measurement noise (multipath included).

As the first error source, the ignored ionospheric errors in Equations (4.3), (4.6) and (4.9) are:

$$\begin{aligned}\nabla\Delta I_{r_3} - \nabla\Delta I_{EWL} &= -\frac{l_3^2}{l_1^2}\nabla\Delta I_1 - (-\frac{l_2 l_3}{l_1^2}\nabla\Delta I_1) \\ &= -\frac{l_3(l_3 - l_2)}{l_1^2}\nabla\Delta I_1\end{aligned} \tag{4.13}$$

$$\begin{aligned}\nabla\Delta I_{EWL} - \nabla\Delta I_{WL} &= -\frac{l_2 l_3}{l_1^2}\nabla\Delta I_1 - (-\frac{l_2}{l_1}\nabla\Delta I_1) \\ &= -\frac{l_2(l_2 - l_1)}{l_1^2}\nabla\Delta I_1\end{aligned} \tag{4.14}$$

$$\begin{aligned}\nabla\Delta I_{WL} - \nabla\Delta I_1 &= -\frac{l_2}{l_1}\nabla\Delta I_1 - \nabla\Delta I_1 \\ &= -\frac{l_1 + l_2}{l_1}\nabla\Delta I_1\end{aligned} \tag{4.15}$$

where l_2 and l_3 represent the L2/E5b and L5/E5a phase wavelengths respectively. The above neglected ionospheric errors are expressed in metres, and to directly reflect their influence on ambiguity estimation in each cascading step, the errors are further turned into the following:

$$\frac{\nabla\Delta I_{r_3} - \nabla\Delta I_{EWL}}{l_{EWL}} = -\frac{(l_3 - l_2)^2}{l_1 l_2} \cdot \frac{\nabla\Delta I_1}{l_1} \tag{4.16}$$

$$\frac{\nabla\Delta I_{EWL} - \nabla\Delta I_{WL}}{l_{WL}} = -\frac{(l_2 - l_1)^2}{l_1^2} \cdot \frac{\nabla\Delta I_1}{l_1} \tag{4.17}$$

$$\frac{\nabla\Delta I_{WL} - \nabla\Delta I_1}{l_1} = -\frac{l_1 + l_2}{l_1} \cdot \frac{\nabla\Delta I_1}{l_1} \tag{4.18}$$

For both modernized GPS and GALILEO, the ionospheric influences on each cascading step using Equations (4.13) to (4.18) are given in Table 4.1.

Table 4.1 Influence of Ionospheric Errors on Each Step of the Cascading Ambiguity Resolution using Geometry-free Model

Cascading Step	Ionospheric Influence	Modernized GPS	GALILEO
1	in metres	$-0.07\nabla\Delta I_1$	$-0.04\nabla\Delta I_1$
2		$-0.36\nabla\Delta I_1$	$-0.39\nabla\Delta I_1$
3		$-2.28\nabla\Delta I_1$	$-2.31\nabla\Delta I_1$
1	in cycles	$-0.0024\frac{\nabla\Delta I_1}{l_1}$	$-0.0009\frac{\nabla\Delta I_1}{l_1}$
2		$-0.0803\frac{\nabla\Delta I_1}{l_1}$	$-0.0931\frac{\nabla\Delta I_1}{l_1}$
3		$-2.2833\frac{\nabla\Delta I_1}{l_1}$	$-2.3051\frac{\nabla\Delta I_1}{l_1}$

According to the above table, the ionospheric influence on EWL ambiguity estimation in the first step is almost negligible. In the second step, the ionospheric influence on WL ambiguity estimation increases significantly, but still no more than 0.1 times for both GPS and GALILEO. However, compared to the ionospheric error in the L1/E1 measurement (Equation (4.8)), the ionospheric errors in L1/E1 ambiguity estimation in the third step is magnified over two times. So from an ionospheric error point of view, it is the most difficult to get a correct $\nabla\Delta N_1$ through Equation (4.10) in the third cascading

step, and the most probable to get correct $\nabla\Delta N_{EWL}$ in the first step.

Over short baselines, ionospheric errors can be effectively cancelled by double differencing. So the ambiguity estimation is mainly subject to measurement noise. With an increase in baseline length, the residual ionospheric errors increase gradually. So even if the impact of measurement noise is negligible, the residual ionospheric errors may lead to failures of integer rounding with an increase in baseline length. Therefore, instantaneous ambiguity resolution using TCAR/CIR is generally possible over very short baselines (Ericson, 1999; Jung, 1999).

4.2.2.1 Influence of Measurement Noise on Each Cascading Step

As the second error source, the measurement noise affects the ambiguity estimation as shown in Equations (4.3), (4.6) and (4.9). By applying the error propagation law, the variances of the estimated ambiguities in Equations (4.3), (4.6) and (4.9) can be derived as:

$$s_{\nabla\Delta\tilde{N}_{EWL}} = \sqrt{\frac{s^2_{\nabla\Delta r_3}}{l^2_{EWL}} + s^2_{\nabla\Delta f_{EWL}}} \tag{4.19}$$

$$s_{\nabla\Delta\tilde{N}_{WL}} = \sqrt{\frac{l^2_{EWL}}{l^2_{WL}} s^2_{\nabla\Delta f_{EWL}} + s^2_{\nabla\Delta f_{WL}}} \tag{4.20}$$

$$s_{\nabla\Delta\tilde{N}_{1}} = \sqrt{\frac{l^2_{WL}}{l^2_{1}} s^2_{\nabla\Delta f_{WL}} + s^2_{\nabla\Delta f_{1}}} \tag{4.21}$$

where $s^2_{\nabla\Delta r_3}$ is the variance of the DD code on L5/E5a, which is usually assumed to be 0.36 m^2, $s^2_{\nabla\Delta f_{EWL}}$, $s^2_{\nabla\Delta f_{WL}}$ and $s^2_{\nabla\Delta f_1}$ are the variances of the DD EWL, WL and L1/E1 phase due to measurement noise respectively, which are assumed to be $(0.028 \text{ cycles})^2$ in this thesis. Equation (4.20) is derived under the assumption that $\nabla\Delta N_{EWL}$ obtained through Equation (4.4) is correct; and Equation (4.21) is derived by assuming that $\nabla\Delta N_{WL}$ obtained through Equation (4.7) is correct. Based on the measurement noise assumed above, a quantitative analysis of the ambiguity variances is included in Table 4.2.

Table 4.2 Variance Analysis of the Ambiguity Estimation in Each Cascading Step using a Geometry-free Model

	Modernized GPS (cycles)	GALILEO (cycles)
$s_{\nabla\Delta\tilde{N}_{EWL}}$	0.0675	0.0471
$s_{\nabla\Delta\tilde{N}_{WL}}$	0.1924	0.3372
$s_{\nabla\Delta\tilde{N}_1}$	0.1301	0.1232

The likelihood of correct rounding for the ambiguities in Equations (4.4), (4.7) and (4.10) decreases with an increase in the estimation variances. So from a measurement noise point of view, the correct rounding of $\nabla\Delta\tilde{N}_{WL}$ in the second step is the most difficult, even more difficult than $\nabla\Delta\tilde{N}_1$; and the correct rounding of $\nabla\Delta\tilde{N}_{EWL}$ still remains the most probable. In addition, it is more difficult to get correct rounding for GALILEO than GPS in the second step.

4.3 GEOMETRY-BASED CASCADING AMBIGUITY RESOLUTION

Although all the geometric errors are gone in the geometry-free models introduced in Section 4.1, the influence of ionospheric errors on the third step is magnified. In this section, a geometry-based cascading ambiguity resolution scheme is developed, through which the influence of measurement noise on each step, and the ionospheric influences on the third step, are no longer enlarged. In addition, instead of integer rounding, ambiguity searching is adopted in each step to achieve fast, and more reliable ambiguity resolution.

4.3.1 Functional Models

The geometry-based cascading ambiguity resolution scheme also consists of three steps and follows the same procedure as shown in Section 4.1 except that the geometric components are full used, namely when the ambiguities in each step are estimated, the coordinate components are also estimated. The general form of the functional model is:

$$\mathbf{l} + \mathbf{r} = \mathbf{AX} \tag{4.23}$$

where $\mathbf{r}$ is the observation misclosure. In each cascading step, a different observation vector, $\mathbf{l}$, state vector, $\mathbf{X}$, and design matrix, $\mathbf{A}$, are assigned. The steps are detailed as follows:

- **First Step**

In this step, the observation vector consists of the DD EWL measurements and the DD precise code measurements:

$$\mathbf{l} = \begin{bmatrix} \nabla\Delta\mathbf{F}_{EWL} \\ \nabla\Delta\mathbf{?}_3 \end{bmatrix} \tag{4.24}$$

where $\nabla\Delta\mathbf{F}_{EWL}$ is a vector of the DD EWL phase measurements expressed in metres, and $\nabla\Delta\mathbf{?}_3$ is a vector of the DD code measurements on L5/E5a.

The design matrix in this step is:

$$\mathbf{A} = \begin{bmatrix} \frac{\partial f^i}{\partial X} & \frac{\partial f^i}{\partial Y} & \frac{\partial f^i}{\partial Z} & l_{EWL} & 0 & \cdots \\ \frac{\partial f^j}{\partial X} & \frac{\partial f^j}{\partial Y} & \frac{\partial f^j}{\partial Z} & 0 & l_{EWL} & \cdots \\ \cdots & \cdots & \cdots & \cdots & \cdots & \cdots \\ \frac{\partial f^i}{\partial X} & \frac{\partial f^i}{\partial Y} & \frac{\partial f^i}{\partial Z} & 0 & 0 & \cdots \\ \frac{\partial f^j}{\partial X} & \frac{\partial f^j}{\partial Y} & \frac{\partial f^j}{\partial Z} & 0 & 0 & \cdots \\ \cdots & \cdots & \cdots & \cdots & \cdots & \cdots \end{bmatrix} \tag{4.25}$$

where $(\frac{\partial f^i}{\partial X}, \frac{\partial f^i}{\partial Y}, \frac{\partial f^i}{\partial Z})$ are the partial derivative terms, and the superscripts 'i' and 'j' represent different satellites. The state vector consists of the three coordinate components and EWL ambiguities as follows:

$$\mathbf{X} = \begin{bmatrix} dX & dY & dZ & d(\nabla\Delta N_{EWL}) & \cdots \end{bmatrix}^T \tag{4.26}$$

where,

$$\begin{cases} dX = X - X_0 \\ dY = Y - Y_0 \\ dZ = Z - Z_0 \\ d(\nabla\Delta N_{EWL}) = \nabla\Delta N_{EWL} - \nabla\Delta N_{EWL_0} \end{cases} \tag{4.27}$$

with (X, Y, Z) referring to the final receiver position, and (X_0, Y_0, Z_0) to the initial position; $\nabla\Delta N_{EWL}$ to the actual ambiguity, and $\nabla\Delta N_{EWL_0}$ to the initial ambiguity estimate. The subscript '0' represents the initial, or previous state. The initial EWL ambiguities are estimated through Equation (4.3). Float EWL ambiguities can be estimated through a sequential least-squares filter as follows:

$$\mathbf{Q}_x = (\mathbf{A}^T \mathbf{Q}_l^{-1} \mathbf{A} + \mathbf{Q}_{x0}^{-1})^{-1} \tag{4.28}$$

$$\mathbf{X} = -\mathbf{Q}_x \mathbf{A}^T \mathbf{Q}_l^{-1} (\mathbf{l} - \mathbf{A}\mathbf{X}_0) \tag{4.29}$$

where $\mathbf{Q}_l$ is the measurement variance-covariance (VC) matrix that will be further detailed later in this chapter, $\mathbf{Q}_x$ is the state VC matrix. At the same time of the estimate of float ambiguities, the user position is also updated. Then the float EWL ambiguities and the VC matrix (a sub-matrix of $\mathbf{Q}_x$) are submitted to the ambiguity decorrelation and search algorithm – LAMBDA. If the EWL ambiguities cannot be fixed at the current epoch then the processing proceeds to the next epoch and reiterates the ambiguity estimation and search. When the EWL ambiguities are resolved then the algorithm goes to the second cascading step.

- **Second Step**

In this step, the observation vector consists of the DD fixed EWL ranges and the DD WL phase measurements (similar to Equation (4.24)). The state vector is the same as in Equation (4.26) except that $d(\nabla\Delta N_{EWL})$ is replaced by $d(\nabla\Delta N_{WL})$.

The design matrix also has the same form as Equation (4.25), except that l_{WL} takes the

place of l_{EWL}. The initial WL ambiguities are estimated through Equation (4.6). Similar to the preceding step, float WL ambiguities are first obtained from recursive least squares (Equation (4.29)) and then passed to the ambiguity searching routines, after which the user position is updated. The processing in this step is repeated until all the WL ambiguities are fixed. With the fixed WL ranges, the cascading ambiguity resolution is bridged to the final step.

- **Third Step**

As the final step, the observation vector consists of fixed DD WL ranges and DD L1/E1 phase measurements (similar to Equation (4.24)). The state vector is the same as Equation (4,26) except that $d(\nabla\Delta N_{EWL})$ is replaced by $d(\nabla\Delta N_1)$.

The design matrix can be obtained by replacing l_{EWL} in Equation (4.25) with l_1. The initial L1/E1 ambiguities are estimated through Equation (4.9). Ambiguity searching takes place after the float ambiguities are obtained from Equation (4.29). Again, processing reiteration is conducted until all L1/E1 ambiguities are fixed. Once fixed, the L1/E1, WL and EWL ambiguities are used to derive the L2/E5b and L5/E5a ambiguities through Equations (4.11) and (4.12).

At this point all the ambiguities are fixed. The time from the beginning of EWL ambiguity resolution to the current epoch is referred to as Time-To-Fix ambiguities (TTF).

4.3.2 Stochastic Models

(1) Stochastic Model of Linearly Combined Phase Measurements

Assume that the three DD phase observations on L1/E1 ($\nabla\Delta f_1$), L2/E5b ($\nabla\Delta f_2$) and L5/E5a ($\nabla\Delta f_3$) expressed in units of cycles are uncorrelated, and let:

$$\mathbf{f}^{i} = \begin{bmatrix} \nabla\Delta f_1 \\ \nabla\Delta f_2 \\ \nabla\Delta f_3 \end{bmatrix} \tag{4.30}$$

The VC matrix is:

$$\mathbf{Q}_{\mathbf{f}^{i}} = \begin{bmatrix} s^{2}_{\nabla\Delta f_1} & 0 & 0 \\ 0 & s^{2}_{\nabla\Delta f_2} & 0 \\ 0 & 0 & s^{2}_{\nabla\Delta f_3} \end{bmatrix} \tag{4.31}$$

where the superscript '*i*' stands for an arbitrary satellite, and the measurements of different satellites are regarded uncorrelated.

Equation (4.30) can be used to linearly form the following observation vector:

$$\mathbf{F}^{i}_{LC} = \begin{bmatrix} \nabla\Delta\Phi_1 \\ \nabla\Delta\Phi_{WL} \\ \nabla\Delta\Phi_{EWL} \end{bmatrix} \tag{4.32}$$

where Φ represents phase measurements expressed in metres. The relationship between Equations (4.32) and (4.30) is:

$$\mathbf{F}_{LC}^{i} = \mathbf{B} \cdot \mathbf{f}^{i} \tag{4.33}$$

where

$$\mathbf{B} = \begin{bmatrix} l_1 & 0 & 0 \\ l_{WL} & -l_{WL} & 0 \\ 0 & l_{EWL} & -l_{EWL} \end{bmatrix} \tag{4.34}$$

The corresponding VC matrix of $\mathbf{F}_{LC}$ can be derived through covariance propagation as follows:

$$\begin{aligned} \mathbf{Q}_{\mathbf{F}_{LC}^{i}} &= \mathbf{B} \cdot \mathbf{Q}_{\mathbf{f}^{i}} \cdot \mathbf{B}^{T} \\ &= \begin{bmatrix} Q^{i}_{\Phi_1} & Q^{i}_{\Phi_1\Phi_{WL}} & Q^{i}_{\Phi_1\Phi_{EWL}} \\ Q^{i}_{\Phi_{WL}\Phi_1} & Q^{i}_{\Phi_{WL}} & Q^{i}_{\Phi_{WL}\Phi_{EWL}} \\ Q^{i}_{\Phi_{EWL}\Phi_1} & Q^{i}_{\Phi_{EWL}\Phi_{WL}} & Q^{i}_{\Phi_{EWL}} \end{bmatrix} \\ &= \begin{bmatrix} l_1^2 s^2_{\nabla\Delta f_1} & l_1 l_{WL} s^2_{\nabla\Delta f_1} & 0 \\ l_1 l_{WL} s^2_{\nabla\Delta f_1} & l_{WL}^2 (s^2_{\nabla\Delta f_1} + s^2_{\nabla\Delta f_2}) & -l_{WL} l_{EWL} s^2_{\nabla\Delta f_2} \\ 0 & -l_{WL} l_{EWL} s^2_{\nabla\Delta f_2} & l_{EWL}^2 (s^2_{\nabla\Delta f_2} + s^2_{\nabla\Delta f_3}) \end{bmatrix} \end{aligned} \tag{4.35}$$

Equation (4.35) provides a basis for the stochastic model of the measurements in each cascading step.

(2) Stochastic Model of the Measurements in each Cascading Step

In the first step, the EWL phase measurements and the code measurements are assumed uncorrelated, so the VC matrix of the measurements for this step is:

$$\mathbf{Q}_{l} = \begin{bmatrix} \mathbf{Q}_{\mathbf{F}_{EWL}} & 0 \\ 0 & \mathbf{Q}_{?_3} \end{bmatrix} \tag{4.36}$$

where $\mathbf{Q}_{\mathbf{F}_{EWL}}$ and $\mathbf{Q}_{?_3}$ stand for the VC matrices of DD EWL and code measurements

respectively. The detailed form of $\mathbf{Q}_{\mathbf{F}_{EWL}}$ is:

$$\mathbf{Q}_{\mathbf{F}_{EWL}} = \begin{bmatrix} s^2_{\nabla\Delta\Phi_{EWL}} & \frac{1}{2}s^2_{\nabla\Delta\Phi_{EWL}} & \cdots & \frac{1}{2}s^2_{\nabla\Delta\Phi_{EWL}} \\ \frac{1}{2}s^2_{\nabla\Delta\Phi_{EWL}} & s^2_{\nabla\Delta\Phi_{EWL}} & \cdots & \frac{1}{2}s^2_{\nabla\Delta\Phi_{EWL}} \\ \cdots & \cdots & \cdots & \cdots \\ \frac{1}{2}s^2_{\nabla\Delta\Phi_{EWL}} & \frac{1}{2}s^2_{\nabla\Delta\Phi_{EWL}} & \cdots & s^2_{\nabla\Delta\Phi_{EWL}} \end{bmatrix} \tag{4.37}$$

The correlation between every two DD EWL measurements in Equation (4.37) originates from the common reference satellite when forming the DD measurements. Therefore, the matrix $\mathbf{Q}_{?_3}$ can be obtained only by replacing $s^2_{\nabla\Delta\Phi_{EWL}}$ with $s^2_{\nabla\Delta r}$ in Equation (4.37).

In the second step, the VC matrix of the DD WL and EWL phase measurements is:

$$\mathbf{Q}_l = \begin{bmatrix} \mathbf{Q}_{\Phi_{WL}} & \mathbf{Q}_{\Phi_{WL}\Phi_{EWL}} \\ \mathbf{Q}_{\Phi_{EWL}\Phi_{WL}} & \mathbf{Q}_{\Phi_{EWL}} \end{bmatrix} \tag{4.38}$$

where $\mathbf{Q}_{\Phi_{WL}}$ is the VC matrix of WL measurements in a similar form as Equation (4.37), and $\mathbf{Q}_{\Phi_{WL}\Phi_{EWL}}$ represents the covariance matrix between the EWL and WL measurements, which can be computed using Equation (4.35).

In the final step, the VC matrix of DD WL and L1/E1 measurements is:

$$\mathbf{Q}_l = \begin{bmatrix} \mathbf{Q}_{\Phi_1} & \mathbf{Q}_{\Phi_{WL}\Phi_1} \\ \mathbf{Q}_{\Phi_1\Phi_{WL}} & \mathbf{Q}_{\Phi_{WL}} \end{bmatrix} \tag{4.39}$$

where $\mathbf{Q}_{\Phi_1}$ is the VC matrix of L1/E1 measurements in a similar form as Equation (4.37), and $\mathbf{Q}_{\Phi_{WL}\Phi_1}$ represents the covariance matrix between WL and L1/E1 measurements that can be derived from Equation (4.35) as well.

5 EXTENDED CASCADING AMBIGUITY RESOLUTION

In this chapter, the triple-frequency cascading ambiguity resolution scheme is further analyzed in an attempt to identify and illustrate the limitations; then some extended techniques based on the cascading ambiguity resolution are studied to overcome these limitations.

5.1 LIMITATIONS OF THE CASCADING AMBIGUITY RESOLUTION METHOD

For the purpose of convenience, the geometry-free cascading ambiguity resolution method as discussed in Section 4.2 is adopted as the starting point. Given the float ambiguity $\nabla\Delta\tilde{N}_{EWL}$ and the corresponding correct integer ambiguity, $\nabla\Delta N_{EWL}$, of each cascading step, the difference is:

$$x = \nabla\Delta\tilde{N}_{EWL} - \nabla\Delta N_{EWL} \tag{5.1}$$

This difference follows a normal distribution, namely:

$$x \sim f(x \mid m_x, s_x) = \frac{1}{\sqrt{2p}\, s_x} \exp\left[-\frac{x^2}{2s_x^2}\right] \tag{5.2}$$

where m_x is the mean value of x, and s_x is the standard deviation, which is mainly related to two components as follows:

$$s_x = \sqrt{s_I^2 + s_\Phi^2} \tag{5.3}$$

where s_I^2 is the variance of the residual ionospheric errors, and s_Φ^2 is the variance of the measurement noise, which are listed in Table 4.1 and Table 4.2. The probability that $\nabla\Delta\tilde{N}_{EWL}$ can be correctly fixed through rounding is:

$$h_{EWL} = \int_{-0.5}^{0.5} f(x \mid m_x, s_x)dx \tag{5.4}$$

Similarly,

$$y = \nabla\Delta\tilde{N}_{WL} - \nabla\Delta N_{WL} \tag{5.5}$$

$$z = \nabla\Delta\tilde{N}_1 - \nabla\Delta N_1 \tag{5.6}$$

and the probability to correctly fix $\nabla\Delta\tilde{N}_{WL}$ and $\nabla\Delta\tilde{N}_1$ through rounding is:

$$h_{WL} = \int_{-0.5}^{0.5} f(x \mid m_x, s_x)dx \int_{-0.5}^{0.5} f(y \mid m_y, s_y)dy \tag{5.7}$$

$$h_1 = \int_{-0.5}^{0.5} f(x \mid m_x, s_x)dx \int_{-0.5}^{0.5} f(y \mid m_y, s_y)dy \int_{-0.5}^{0.5} f(z \mid m_z, s_z)dz \tag{5.8}$$

Based on the derived ionospheric errors in Table 4.1 and measurement noise in Table 4.2, for both modernized GPS and GALILEO, Figure 5.1 gives a visual representation of the trend of h_{EWL}, h_{WL} and h_1 along with the increase of the residual ionospheric errors, assuming zero means for x, y and z.

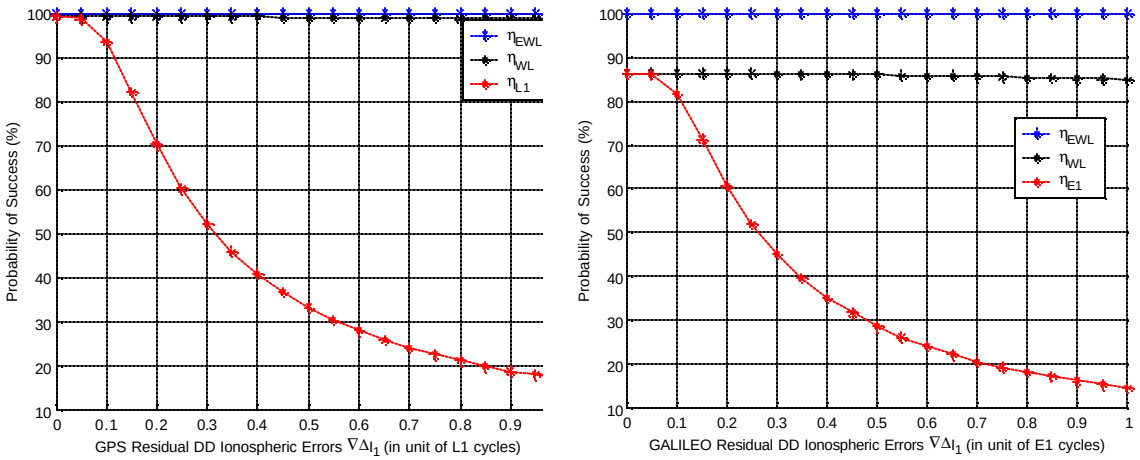

Figure 5.1 Success Rate of Rounding of EWL, WL and L1/E1 Ambiguities for both modernized GPS and GALILEO using the Cascading Ambiguity Resolution Method

Figure 5.1 (b) shows a pessimistic view for GALILEO WL rounding due to the impact of measurement noise (shown in Table 4.2). However in practice, the probabilities of success is supposed to rise to a considerable level due to the conservative nature of this thesis by using 2.8% of the wavelength as the noise level, which is actually much larger than real ones especially considering technology advancements in the future. With the growth of the ionospheric level from 0 to 1 L1/E1 cycle in Figure 5.1, the probabilities of correct rounding for EWL and WL ambiguities do not decrease much, but that of the L1/E1 drops fast to a very low level, which indicates that L1 is very sensitive to the growth of ionospheric errors, whereas the EWL and WL are much less susceptible.

More quantitative results are present in Section 7.3 that further indicate that the L1/E1 ambiguity resolution is a weak point, which may obstruct the successful application of cascading ambiguity resolution in the presence of increased residual ionospheric errors.

So improving techniques in dealing with the ionospheric impact on L1/E1 ambiguity resolution is an all-important consideration.

5.2 CASCADING AMBIGUITY RESOLUTION INVOLVING IONOSPHERE-FREE INTEGER AMBIGUITY MODEL

The first effort aims to improve the geometry-based cascading ambiguity resolution by implementing the ionosphere-free integer ambiguity model in the L1/E1 ambiguity resolution step.

5.2.1 Derivation of Ionosphere-free L1/E1 Integer Ambiguity Model

By using the phase measurements on the L1/E1 and L2/E5b, and Equation (4.11), the ionosphere-free phase combination can be formed and derived as follows:

$$\begin{aligned}\left(\nabla\Delta f_1 - \frac{l_1}{l_2}\nabla\Delta f_2\right) &= -\nabla\Delta N_1 + \frac{l_1}{l_2}\nabla\Delta N_2 + (\frac{1}{l_1} - \frac{l_1}{l_2^2})\nabla\Delta G \\ &= -\nabla\Delta N_1 + \frac{l_1}{l_2}(\nabla\Delta N_1 - \nabla\Delta N_{12}) + \frac{1}{l_1 l_2^2/(l_2^2 - l_1^2)}\nabla\Delta G \\ &= -\frac{l_2 - l_1}{l_2}\nabla\Delta N_1 - \frac{l_1}{l_2}\nabla\Delta N_{12} + \frac{1}{l_{IF_{12}}}\nabla\Delta G\end{aligned} \tag{5.9}$$

where $\nabla\Delta N_{12}$ is already fixed in the second cascading step, and $l_{IF_{12}}$ is the wavelength of the L1/E1 and L2/E5b ionosphere-free phase combination as listed in Table 3.7.

In a similar way, the following equation can be derived using the phase measurements on L1/E1 and L5/E5a:

$$\begin{aligned}\left(\nabla\Delta f_1-\frac{l_1}{l_3}\nabla\Delta f_3\right)&=-\nabla\Delta N_1+\frac{l_1}{l_3}\nabla\Delta N_3+(\frac{1}{l_1}-\frac{l_1}{l_3^2})\nabla\Delta G\\&=-\nabla\Delta N_1+\frac{l_1}{l_3}(\nabla\Delta N_1-\nabla\Delta N_{12}-\nabla\Delta N_{23})+\frac{1}{l_1 l_3^2/(l_3^2-l_1^2)}\nabla\Delta G\\&=-\frac{l_3-l_1}{l_3}\nabla\Delta N_1-\frac{l_1}{l_3}(\nabla\Delta N_{12}+\nabla\Delta N_{23})+\frac{1}{l_{IF_{13}}}\nabla\Delta G\end{aligned} \tag{5.10}$$

where $\nabla\Delta N_{12}$ and $\nabla\Delta N_{23}$ are fixed in the first and second cascading steps, and $l_{IF_{13}}$ is the wavelength of L1/E1 and L5/E5a ionosphere-free combination as listed in Table 3.7.

5.2.2 Functional Model in the last step

In order to analyze the influence of each component on $\nabla\Delta N_1$, Equations (5.9) and (5.10) are further expressed comparatively in the following form:

$$\begin{cases}\left(\nabla\Delta f_1-\frac{l_1}{l_2}\nabla\Delta f_2\right)\cdot\frac{l_2}{l_2-l_1}\\\qquad=-\nabla\Delta N_1-\frac{l_1}{l_2-l_1}\nabla\Delta N_{12}+\frac{l_2}{l_2-l_1}\frac{1}{l_{IF_{12}}}\nabla\Delta G\end{cases}\ \text{(cycles)} \tag{5.11}$$

$$\begin{cases}\left(\nabla\Delta f_1-\frac{l_1}{l_3}\nabla\Delta f_3\right)\cdot\frac{l_3}{l_3-l_1}\\\qquad=-\nabla\Delta N_1-\frac{l_1}{l_3-l_1}(\nabla\Delta N_{12}+\nabla\Delta N_{23})+\frac{l_3}{l_3-l_1}\frac{1}{l_{IF_{13}}}\nabla\Delta G\end{cases}\ \text{(cycles)} \tag{5.12}$$

Therefore the influence of measurement noise on $\nabla\Delta N_1$ estimation in Equation (5.11) is:

$$s_{f_1} = \frac{l_2}{l_2 - l_1}\sqrt{1+\frac{l_1^2}{l_2^2}}\cdot a\% \tag{5.13}$$

where $a\%$ is the assumed measurement noise of DD phase observation in cycles. Similarly in Equation (5.12), the measurement noise is:

$$s_{f_2} = \frac{l_3}{l_3 - l_1}\sqrt{1+\frac{l_1^2}{l_3^2}}\cdot a\% \tag{5.14}$$

Both the measurement noise and geometrical errors (tropospheric and orbital) are quantitatively analyzed in Table 5.1.

Table 5.1 Influence of Measurement Noise and Geometrical Errors on the Ionosphere-free L1/E1 Integer Ambiguity Resolution

System	Equation	Measurement Noise (cycles)	Geometrical Errors (cycles)
GPS	(5.11)	$5.74\cdot a\%$	$1.78\cdot \nabla\Delta G/l_1$
	(5.12)	$4.93\cdot a\%$	$1.75\cdot \nabla\Delta G/l_1$
GALILEO	(5.11)	$5.38\cdot a\%$	$1.65\cdot \nabla\Delta G/l_1$
	(5.12)	$4.93\cdot a\%$	$1.75\cdot \nabla\Delta G/l_1$

Table 5.1 indicates that the measurement noise achieves approximately the same amplification rates for both GPS and GALILEO compared to Equation (4.8) (5.74 or 5.38 for Equation (5.11) and 4.93 for Equation (5.12)), and that the influence of geometrical errors are also amplified by 1.65 ~ 1.78 times for both systems. However, the residual ionospheric errors are removed. So only when the influence of the residual ionospheric errors exceeds to great extent the sum of the measurement noise and tropospheric errors, it is necessary to implement Equations (5.11) and (5.12).

In implementation, the following equations are used:

$$\begin{cases} \nabla\Delta\Phi_1^{'} = \nabla\Delta G - l_1^{'}\nabla\Delta N_1 \\ \nabla\Delta\Phi_2^{'} = \nabla\Delta G - l_2^{'}\nabla\Delta N_1 \end{cases} \tag{5.15}$$

where

$$\nabla\Delta\Phi_1^{'} = \left(\nabla\Delta f_1 - \frac{l_1}{l_2}\nabla\Delta f_2 \right) \cdot l_{IF_{12}} + \frac{l_1}{l_2} l_{IF_{12}} \nabla\Delta N_{12}$$

$$\nabla\Delta\Phi_2^{'} = \left(\nabla\Delta f_1 - \frac{l_1}{l_3}\nabla\Delta f_3 \right) \cdot l_{IF_{13}} + \frac{l_1}{l_3} l_{IF_{13}} (\nabla\Delta N_{12} + \nabla\Delta N_{23})$$

$$l_1^{'} = \frac{l_2 - l_1}{l_2} l_{IF_{12}}$$

$$l_2^{'} = \frac{l_3 - l_1}{l_3} l_{IF_{13}}$$

The above ionosphere-free L1/E1 integer ambiguity model is implemented in the final step of the cascading ambiguity resolution technique to help resolve the L1/E1 ambiguities from previously fixed WL and EWL ranges. Here, $l_1^{'}$ and $l_2^{'}$ are referred to as the nominal wavelengths of $\nabla\Delta N_1$ in Equation (5.15) which are detailed in Table 5.2.

Table 5.2 Nominal Wavelengths of the Ionosphere-free Integer L1/E1 Ambiguity Model

System	Nominal Wavelengths	
GPS	$l_1^{'}$	0.106 m
	$l_2^{'}$	0.108 m
GALILEO	$l_1^{'}$	0.107 m
	$l_2^{'}$	0.108 m

Compared to the L1/E1 wavelengths (0.190 m), the above nominal wavelengths are much shorter. Therefore, the influence of measurement noise and geometrical errors on $\nabla\Delta N_1$

in Equation (5.15) is far larger than that on $\nabla\Delta N_1$ in Equation (4.8). Table 5.2 gives an extension of the analysis in Table 5.1, which further presents the trade off among eliminated ionospheric residual and amplified measurement noise and geometrical errors from the perspective of nominal wavelengths.

5.2.3 Stochastic Model

The stochastic model of Equation (5.15) is of the following form:

$$\mathbf{Q} = \begin{bmatrix} \mathbf{Q}_{\Phi'_1} & \mathbf{Q}_{\Phi'_1\Phi'_2} \\ \mathbf{Q}_{\Phi'_2\Phi'_1} & \mathbf{Q}_{\Phi'_2} \end{bmatrix} \tag{5.16}$$

where:

$$\mathbf{Q}_{\Phi'_1} = \begin{bmatrix} l_{IF_{12}}^2 (s_{f_1}^2 + \frac{l_1^2}{l_2^2} s_{f_2}^2) & & 0 \\ & \cdots & \\ 0 & & l_{IF_{12}}^2 (s_{f_1}^2 + \frac{l_1^2}{l_2^2} s_{f_2}^2) \end{bmatrix}$$

$$\mathbf{Q}_{\Phi'_2} = \begin{bmatrix} l_{IF_{13}}^2 (s_{f_1}^2 + \frac{l_1^2}{l_3^2} s_{f_3}^2) & & 0 \\ & \cdots & \\ 0 & & l_{IF_{13}}^2 (s_{f_1}^2 + \frac{l_1^2}{l_3^2} s_{f_3}^2) \end{bmatrix}$$

$$\mathbf{Q}_{\Phi'_2\Phi'_1} = \begin{bmatrix} l_{IF_{12}} l_{IF_{13}} s_{f_1}^2 & & 0 \\ & \cdots & \\ 0 & & l_{IF_{12}} l_{IF_{13}} s_{f_1}^2 \end{bmatrix}$$

$$\mathbf{Q}_{\Phi'_1\Phi'_2} = \mathbf{Q}_{\Phi'_2\Phi'_1}$$

5.3 CASCADING AMBIGUITY RESOLUTION INVOLVING STOCHASTIC IONOSPHERIC MODELING

This is an extension of the work by Odijk (2000), Liu (2001, 2002) and Julien et al. (2004). The stochastic ionosphere method was implemented in Odijk (2000) and Liu (2001, 2002) to handle the residual ionospheric errors in dual frequency ambiguity resolution for GPS. In the study of integrated GPS/GALILEO it was implemented in Julien et al. (2004) to improve triple frequency ambiguity resolution. This section involves applying the stochastic ionosphere modeling method in the last step of the cascading ambiguity resolution scheme.

5.3.1 Derivation of Phase Observation Equations

In the last step of cascading ambiguity resolution, the phase measurement on L1/E1 is:

$$\nabla\Delta f_1 \cdot l_1 = \nabla\Delta G - l_1\nabla\Delta N_1 + \nabla\Delta I_1 \tag{5.17}$$

where $\nabla\Delta N_1$ is the ambiguity to be resolved in this step. Since EWL and WL ambiguities are already fixed in the first two cascading steps, by using Equation (4.11), the phase measurement on L2/E5b can be derived as follows:

$$\begin{aligned}\nabla\Delta f_2 \cdot l_2 &= \nabla\Delta G - l_2\nabla\Delta N_2 + \nabla\Delta I_2 \\ &= \nabla\Delta G - l_2(\nabla\Delta N_1 - \nabla\Delta N_{12}) + \frac{l_2^2}{l_1^2}\nabla\Delta I_1 \\ &= \nabla\Delta G - l_2\nabla\Delta N_1 + l_2\nabla\Delta N_{12} + \frac{l_2^2}{l_1^2}\nabla\Delta I_1\end{aligned} \tag{5.18}$$

By using Equation (4.12), the phase measurement on L5/E5a can be derived in a similar manner:

$$\begin{aligned}\nabla\Delta f_3 \cdot l_3 &= \nabla\Delta G - l_3\nabla\Delta N_3 + \nabla\Delta I_3 \\ &= \nabla\Delta G - l_3(\nabla\Delta N_1 - \nabla\Delta N_{12} - \nabla\Delta N_{23}) + \frac{l_3^2}{l_1^2}\nabla\Delta I_1 \\ &= \nabla\Delta G - l_3\nabla\Delta N_1 + l_3\nabla\Delta N_{12} + l_3\nabla\Delta N_{23} + \frac{l_3^2}{l_1^2}\nabla\Delta I_1\end{aligned} \tag{5.19}$$

5.3.2 Functional Model

In implementation, Equations (5.17) to (5.19) are slightly modified and turned into the following forms:

$$\begin{cases} \nabla\Delta\Phi_1^{'} = \nabla\Delta G - l_1\nabla\Delta N_1 + \nabla\Delta I_1 \\ \nabla\Delta\Phi_2^{'} = \nabla\Delta G - l_2\nabla\Delta N_1 + \dfrac{l_2^2}{l_1^2}\cdot\nabla\Delta I_1 \\ \nabla\Delta\Phi_3^{'} = \nabla\Delta G - l_3\nabla\Delta N_1 + \dfrac{l_3^2}{l_1^2}\cdot\nabla\Delta I_1 \end{cases} \tag{5.20}$$

where:

$$\nabla\Delta\Phi_1^{'} = \nabla\Delta f_1 \cdot l_1$$

$$\nabla\Delta\Phi_2^{'} = (\nabla\Delta f_2 - \nabla\Delta N_{12}) \cdot l_2$$

$$\nabla\Delta\Phi_3^{'} = (\nabla\Delta f_3 - \nabla\Delta N_{12} - \nabla\Delta N_{23}) \cdot l_3$$

So in a matrix form, the functional model is:

$$\begin{bmatrix} \nabla\Delta\mathbf{F}'_1 \\ \nabla\Delta\mathbf{F}'_2 \\ \nabla\Delta\mathbf{F}'_3 \\ \nabla\Delta\mathbf{I}_p \end{bmatrix} = \begin{bmatrix} \mathbf{B} & \mathbf{A}_1 & \mathbf{E} \\ \mathbf{B} & \mathbf{A}_2 & \mathbf{C}_2 \\ \mathbf{B} & \mathbf{A}_3 & \mathbf{C}_3 \\ \mathbf{0} & \mathbf{0} & \mathbf{E} \end{bmatrix} \cdot \begin{bmatrix} \mathbf{b} \\ \mathbf{a} \\ \mathbf{I} \end{bmatrix} + \mathbf{e} \tag{5.21}$$

where:

$\mathbf{F}'_i$ is the vector of phase measurements (i=1, 2, 3);

$\mathbf{I}_p$ is the vector of pseudo ionospheric observable (on L1/E1);

b is the vector of coordinate components;

a is the vector of L1/E1 ambiguity unknowns;

I is the vector of L1/E1 ionosphere unknowns;

e is the vector of measurement noise, and

E is an identity matrix.

The details of Equation (5.21) are as follows:

$$\mathbf{b} = \begin{bmatrix} dX \\ dY \\ dZ \end{bmatrix},\ \mathbf{a} = \begin{bmatrix} \nabla\Delta N_1^1 \\ \nabla\Delta N_1^2 \\ \cdots \\ \nabla\Delta N_1^m \end{bmatrix},\ \mathbf{B} = \begin{bmatrix} \dfrac{\partial f}{\partial X^1} & \dfrac{\partial f}{\partial Y^1} & \dfrac{\partial f}{\partial Z^1} \\ \ldots & & \ldots \\ \dfrac{\partial f}{\partial X^m} & \dfrac{\partial f}{\partial Y^m} & \dfrac{\partial f}{\partial Z^m} \end{bmatrix},\ \mathbf{I} = \begin{bmatrix} \nabla\Delta I_1^1 \\ \nabla\Delta I_1^2 \\ \cdots \\ \nabla\Delta I_1^m \end{bmatrix},$$

$$\mathbf{A}_i = \begin{bmatrix} -l_i & & \\ & \ldots & \\ & & -l_i \end{bmatrix} (i = 1 \sim 3), \qquad \mathbf{C}_i = \begin{bmatrix} l_i^2 / l_1^2 & & \\ & \ldots & \\ & & l_i^2 / l_1^2 \end{bmatrix} (i = 2 \sim 3).$$

where the superscripts ‘1’ to ‘m’ represent satellite numbers.

5.3.3 Stochastic Model

The VC matrix of the measurements in Equation (5.21) is:

$$\mathbf{Q} = \begin{bmatrix} \mathbf{Q}_{\Phi_1'} & 0 & 0 & 0 \\ 0 & \mathbf{Q}_{\Phi_2'} & 0 & 0 \\ 0 & 0 & \mathbf{Q}_{\Phi_3'} & 0 \\ 0 & 0 & 0 & \mathbf{Q}_{I_p} \end{bmatrix} \tag{5.22}$$

where:

$$\mathbf{Q}_{\Phi_1'} = \begin{bmatrix} s^2_{\nabla\Delta\Phi_1} & & \frac{1}{2}s^2_{\nabla\Delta\Phi_1} \\ & \cdots & \\ \frac{1}{2}s^2_{\nabla\Delta\Phi_1} & & s^2_{\nabla\Delta\Phi_1} \end{bmatrix}$$

$$\mathbf{Q}_{\Phi_2'} = \begin{bmatrix} s^2_{\nabla\Delta\Phi_2} & & \frac{1}{2}s^2_{\nabla\Delta\Phi_2} \\ & \cdots & \\ \frac{1}{2}s^2_{\nabla\Delta\Phi_2} & & s^2_{\nabla\Delta\Phi_2} \end{bmatrix}$$

$$\mathbf{Q}_{\Phi_3'} = \begin{bmatrix} s^2_{\nabla\Delta\Phi_3} & & \frac{1}{2}s^2_{\nabla\Delta\Phi_3} \\ & \cdots & \\ \frac{1}{2}s^2_{\nabla\Delta\Phi_3} & & s^2_{\nabla\Delta\Phi_3} \end{bmatrix}$$

$$\mathbf{Q}_{I_p} = \begin{bmatrix} s^2_{I_p} & & \\ & \cdots & \\ & & s^2_{I_p} \end{bmatrix}$$

The performance of ambiguity resolution using Equation (5.21) is sensitive to two factors regarding the ionospheric pseudo-observables: one is the initial value, and the other is the variance. In implementation, the ionospheric pseudo-observables, $\nabla\Delta I_p$, are initialized with zero values and assumed uncorrelated among each other. By assigning different

variances, Q_{I_p}, for the pseudo-observables, different forms of Equation (5.21) can be derived.

When the variance is set to be infinite, i.e. $Q_{I_p} \to \infty$, the ionospheric effects are regarded as completely uncorrelated and unknown at both ends of the baseline. In this case, without the use of a priori knowledge of the ionospheric effects, no constraints are applied to the ionospheric pseudo-observables and the residual ionospheric errors are directly estimated with the L1 phase measurements and the fixed EWL and WL ranges. In implementation, infinity is not achievable for Q_{I_p}, instead sufficiently large variance (say $(10^8\ m)^2$) should be chosen to avoid biasing the estimated carrier ambiguities by an amount that may result in a wrong integer ambiguity (de Jong et al., 2001). This model is referred to as *Ionosphere Float*.

When the variances are set to zero, i.e. $Q_{I_p} \to 0$, the ionospheric pseudo-observables are so tightly constrained that the residual ionospheric errors are regarded as absent or known and can be compensated with external ionosphere values. In implementation, Q_{I_p} cannot be set to zero. Instead, a very small quantity (say $(10^{-8}\ m)^2$) can be assigned. This model is referred to as *Ionosphere Fixed*.

The above two models are extreme cases. In practice, sometimes the baselines are too long to regard the residual ionospheric errors in the double differenced measurements as cancelled, or too short to consider the ionospheric errors at both ends as uncorrelated. So

the key issue is to assign realistic VC information to the ionospheric pseudo-observables correctly reflecting the ionospheric magnitude and correlation, which introduces the third form of Equation (5.21) – *Ionosphere Weighted*.

Special care needs to be given to weighing the residual ionospheric errors, namely assigning proper VC information to the residual ionospheric errors. The variance of the ionospheric pseudo-observation can have a large effect on the filter's performance (Alves et al., 2002). In the weighing of the ionospheric pseudo-observations, although a lot of factors might exist, such as elevation dependency, temporal correlation and spatial correlation, the weight model is simplified to be only distance-dependent herein (similarly to Julien et al. (2003)). In addition, all ionospheric pseudo-observations are assumed to have the same variances that are obtained through $(k \times L)^2$ m^2, where k is the ionospheric level in ppm, and L is the baseline length in metres.

5.4 OTHER ISSUES IN THE LAST STEP OF CASCADING AMBIGUITY RESOLUTION

This section involves a discussion of two additional efforts in the final step of the cascading ambiguity resolution scheme.

5.4.1 Geometry-free Integer Ambiguity Model

The geometry-free model that will be introduced here is different from that adopted in Section 4.2. By using the phase measurements on L1/E1 and L2/E5b, and Equation (4.11), the geometry-free phase combination can be formed and the following equation can be derived:

$$\begin{aligned} l_2\nabla\Delta f_2 - l_1\nabla\Delta f_1 &= -l_2\nabla\Delta N_2 + l_1\nabla\Delta N_1 + (\frac{l_2^2}{l_1^2} - 1)\nabla\Delta I_1 \\ &= -(l_2 - l_1)\nabla\Delta N_1 + l_2\nabla\Delta N_{12} + \frac{l_2^2 - l_1^2}{l_1^2}\nabla\Delta I_1 \end{aligned} \tag{5.23}$$

In units of cycles, the above equation can be further expressed as:

$$\frac{1}{l_2 - l_1}(l_2\nabla\Delta f_2 - l_1\nabla\Delta f_1) = -\nabla\Delta N_1 + \frac{l_2}{l_2 - l_1}\nabla\Delta N_{12} + \frac{l_2 + l_1}{l_1^2}\nabla\Delta I_1 \tag{5.24}$$

Similarly, the following equation can be derived using the phase measurements on L1/E1 and L5/E5a:

$$\frac{1}{l_3 - l_1}(l_3\nabla\Delta f_3 - l_1\nabla\Delta f_1) = -\nabla\Delta N_1 + \frac{l_3}{l_3 - l_1}(\nabla\Delta N_{12} + \nabla\Delta N_{23}) + \frac{l_3 + l_1}{l_1^2}\nabla\Delta I_1 \tag{5.25}$$

In Equations (5.24) and (5.25), $\nabla\Delta N_{12}$ and $\nabla\Delta N_{23}$ are fixed in the previous cascading steps, and are assumed correct. Then the measurement noise value in Equations (5.24) and (5.25) is:

$$\frac{1}{l_i - l_1}\sqrt{l_1^2 + l_i^2}\cdot a\,\% \quad (\text{i} = 2, 3) \tag{5.26}$$

Table 5.3 lists the influences of both the measurement noise and residual ionospheric errors on the geometry-free L1/E1 ambiguity resolution.

Table 5.3 Influences of Measurement Noise and Ionospheric Errors on the Geometry-free L1/E1 Ambiguity Resolution

System	Equation	Measurement Noise (cycles)	Ionospheric Errors (cycles)
GPS	(5.24)	$5.74 \cdot a\,\%$	$2.28 \cdot \nabla\Delta I_1 / l_1$
	(5.25)	$4.93 \cdot a\,\%$	$2.34 \cdot \nabla\Delta I_1 / l_1$
GALILEO	(5.24)	$5.38 \cdot a\,\%$	$2.31 \cdot \nabla\Delta I_1 / l_1$
	(5.25)	$4.93 \cdot a\,\%$	$2.34 \cdot \nabla\Delta I_1 / l_1$

As shown in Table 5.3, the geometry-free measurement noise is identical to the ionosphere-free measurement noise (Table 5.1), and the ionospheric errors are at equivalent levels as shown in Table 4.1. Although the geometrical errors do not exist, according to Table 5.3 and Table 4.1, the geometry-free model introduced here indicates no advantage over the model described in Equation (4.9).

5.4.2 Ionosphere-free and Geometry-free Models

According to Sections 5.1 and 5.4.1, neither the ionosphere-free model nor the geometry-free model is perfect. In the ionosphere-free model, although the ionospheric influence is eliminated, the influence of geometrical errors is enlarged (Table 5.1). In the geometry-free model, although the geometrical errors are cancelled, the influence of residual ionospheric errors is amplified (Table 5.3). With phase measurements on triple frequencies, since two linearly independent ionosphere-free measurements can be formed (Equations (5.9) and (5.10)), it may be possible to further form a geometry-free measurement using the two ionosphere-free measurements.

Through Equations (5.9) and (5.10), the following two equations can be obtained:

$$\left(\nabla\Delta f_1 - \frac{l_1}{l_2}\nabla\Delta f_2\right)\cdot l_{IF_1} = -\frac{l_2 - l_1}{l_2} l_{IF_1}\nabla\Delta N_1 - \frac{l_1}{l_2} l_{IF_1}\nabla\Delta N_{12} + \nabla\Delta G \tag{5.27}$$

$$\left(\nabla\Delta f_1 - \frac{l_1}{l_3}\nabla\Delta f_3\right)\cdot l_{IF_2} = -\frac{l_3 - l_1}{l_3} l_{IF_2}\nabla\Delta N_1 - \frac{l_1}{l_3} l_{IF_2}\nabla\Delta N_{12} - \frac{l_1}{l_3} l_{IF_2}\nabla\Delta N_{23} + \nabla\Delta G \tag{5.28}$$

By subtracting Equation (5.27) from Equation (5.28), Equation (5.29) can be derived:

$$\left[(l_{IF_1} - l_{IF_2})\nabla\Delta f_1 - \frac{l_1}{l_2} l_{IF_1}\nabla\Delta f_2 + \frac{l_1}{l_3} l_{IF_2}\nabla\Delta f_3\right]\cdot\frac{1}{\frac{l_1 l_2}{l_1 + l_2} - \frac{l_1 l_3}{l_1 + l_3}} = -\nabla\Delta N_1 - [...]\cdot\nabla\Delta N_{12} + [...]\cdot\nabla\Delta N_{23} \tag{5.29}$$

where the coefficients of components $\nabla\Delta N_{12}$ and $\nabla\Delta N_{23}$ are too complicated and therefore are simplied as $[...]$.

On the right hand side of Equation (5.29), both residual ionospheric errors and geometrical errors are cancelled. At first glance, Equation (5.29) seems to be a perfect model since it is both ionosphere-free and geometry-free. However, a further analysis in Equation (5.30) indicates that the measurement noise of Equation (5.29) is too large to be practical.

$$\frac{1}{\frac{l_1 l_2}{l_1 + l_2} - \frac{l_1 l_3}{l_1 + l_3}}\sqrt{(l_{IF_1} - l_{IF_2})^2 + (\frac{l_1}{l_2} l_{IF_1})^2 + (\frac{l_1}{l_3} l_{IF_2})^2}\cdot a \approx 250.82\cdot a\,\% \tag{5.30}$$

6 COMBINATION OF GPS AND GALILEO IN CASCADING AMBIGUITY RESOLUTION

In previous chapters, the discussion of the cascading ambiguity resolution approach uses either modernized GPS or GALILEO. This section addresses the issues that arise in combing the two systems.

6.1 COMBINATION MODES

6.1.1 Loose Coupling Mode

If the coincidence of the frequencies between GPS and GALILEO is not taken into account then each of the systems will use its own independent base satellites and none of the DD observations will be formed across the two systems. However, the systems are still related through the mutually estimated position in the geometry-based approach, therefore the systems are not truly independently processed. In the geometry-free approach the observations between the two systems are not related through estimated parameters or mathematical correlation and, as a result, the addition of a second GNSS will not affect ambiguity resolution performance.

The combination of the two systems in the way described above is referred to as a *Loose Coupling Mode*. In this case, different base satellites are selected for GALILEO and

Modernized GPS, respectively, to form double differences. In each step, both the GPS and GALILEO measurements are assembled in the same observation vector as shown:

$$\mathbf{l}_1 = \begin{bmatrix} \nabla\Delta\Phi_{EWL}^{GPS} & \nabla\Delta\Phi_{EWL}^{GAL} & \nabla\Delta r^{GPS} & \nabla\Delta r^{GAL} \end{bmatrix}^T \tag{6.1}$$

$$\mathbf{l}_2 = \begin{bmatrix} \nabla\Delta\Phi_{WL}^{GPS} & \nabla\Delta\Phi_{WL}^{GAL} & \nabla\Delta r_{EWL}^{GPS} & \nabla\Delta r_{EWL}^{GAL} \end{bmatrix}^T \tag{6.2}$$

$$\mathbf{l}_3 = \begin{bmatrix} \nabla\Delta\Phi_{1}^{GPS} & \nabla\Delta\Phi_{1}^{GAL} & \nabla\Delta r_{WL}^{GPS} & \nabla\Delta r_{WL}^{GAL} \end{bmatrix}^T \tag{6.3}$$

where $\nabla\Delta r_{WL}$ and $\nabla\Delta r_{EWL}$ are the WL and EWL fixed ambiguities and carrier phase ranges respectively, and the subscripts '1', '2', and '3' represent the various stages in the three step cascading method. The corresponding VC matrices are:

$$\mathbf{Q}_{\mathbf{l}_1} = \begin{bmatrix} \mathbf{Q}_{\Phi_{EWL}}^{GPS} & 0 & 0 & 0 \\ 0 & \mathbf{Q}_{\Phi_{EWL}}^{GAL} & 0 & 0 \\ 0 & 0 & \mathbf{Q}_{r}^{GPS} & 0 \\ 0 & 0 & 0 & \mathbf{Q}_{r}^{GAL} \end{bmatrix} \tag{6.4}$$

$$\mathbf{Q}_{\mathbf{l}_2} = \begin{bmatrix} \mathbf{Q}_{\Phi_{WL}}^{GPS} & 0 & \mathbf{Q}_{\Phi_{WL}\Phi_{EWL}}^{GPS} & 0 \\ 0 & \mathbf{Q}_{\Phi_{WL}}^{GAL} & 0 & \mathbf{Q}_{\Phi_{WL}\Phi_{EWL}}^{GAL} \\ \mathbf{Q}_{\Phi_{WL}f_{EWL}}^{GPS} & 0 & \mathbf{Q}_{\Phi_{EWL}}^{GPS} & 0 \\ 0 & \mathbf{Q}_{\Phi_{WL}\Phi_{EWL}}^{GAL} & 0 & \mathbf{Q}_{\Phi_{EWL}}^{GAL} \end{bmatrix} \tag{6.5}$$

$$\mathbf{Q}_{\mathbf{l}_3} = \begin{bmatrix} \mathbf{Q}_{\Phi_1}^{GPS} & 0 & \mathbf{Q}_{\Phi_1\Phi_{WL}}^{GPS} & 0 \\ 0 & \mathbf{Q}_{\Phi_1}^{GAL} & 0 & \mathbf{Q}_{\Phi_1\Phi_{WL}}^{GAL} \\ \mathbf{Q}_{\Phi_1\Phi_{WL}}^{GPS} & 0 & \mathbf{Q}_{\Phi_{WL}}^{GPS} & 0 \\ 0 & \mathbf{Q}_{\Phi_1\Phi_{WL}}^{GAL} & 0 & \mathbf{Q}_{\Phi_{WL}}^{GAL} \end{bmatrix} \tag{6.6}$$

6.1.2 Tight Coupling Mode

When the coincident system frequencies are considered, another mode of combination is possible, which is referred to as a *Tight Coupling Mode* in Julien et al. (2003). Both modernized GPS and GALILEO possess the common L1/E1 and L5/E5a frequencies. With E1 and E5a, an ML combination can be formed. In the same way, another ML combination can be formed with L1 and L5. Since L1/E1 and L5/E5a overlap, the two ML combinations are identical so that it is possible to form double differenced ML measurements between GPS and GALILEO signals. Moreover, since the GALILEO E1 equals to GPS L1, it is also possible to form double differenced L1/E1 measurements between the two systems on these frequencies. In this case, the measurements of modernized GPS and GALILEO can be combined in a tight way. The corresponding cascading ambiguity resolution technique follows almost the same procedure as in the case of the Loose Coupling Mode.

Two weaknesses exist in the tight coupling approach: one is the difficulty in transition from the EWL ambiguity resolution to the ML ambiguity resolution because the ambiguity estimation noise of ML ($s_{\nabla\Delta N_{ML}}$) is larger than that of WL ($s_{\nabla\Delta N_{WL}}$) according to Equation (4.20) considering that the ML wavelength is shorter than WL (Table 3.3). The other lies in the estimation of the initial estimate of the ML ambiguities between the systems because the GPS EWL differs from GALILEO EWL. As a result, $\nabla\Delta N_{ML}^{G-G}$ must be estimated directly from precise code measurements, similar to Equation (4.2).

Due to these drawbacks, the *Tight Coupling Mode* is not expected to excel the *Loose Coupling Mode*. Therefore, in later chapters only the loosely coupled results will be used to compare the advantages of three-frequency GPS and GALILEO integration.

6.2 FILTERING APPROACH

6.2.1 Three Filter Approaches

The algorithm of geometry-based CAR, and the extended forms as introduced in Chapters 4 and 5, were implemented and applied to GPS only, GALILEO only and combined GPS/GALILEO cases, the flow chart of which is depicted in Figure 6.1. For each baseline (Table 7.1), the corresponding time limit (Table 7.2) is specified before starting CAR. An epoch counter is used to record the time to fix L1/E1 ambiguities since the start or each reset of CAR. If the epoch counter has reached the time limit with L1/E1 ambiguities still unfixed, CAR would be reset. This case is referred to as filter timing out. Those that fail to fix L1/E1 ambiguities before filter timing out are regarded as failures of ambiguity fixing.

The flow chart in Figure 6.1 consists of three sequential least-squares filters. In the first filter, both the L5/E5 code measurements and EWL phase measurements are used, through which the user position is updated and the resulting float EWL ambiguities are submitted to LAMBDA searching. This filter is run sequentially until either the EWL

ambiguities are fixed in the LAMBDA searching or the filter times out. During each run, the epoch counter is incremented by one.

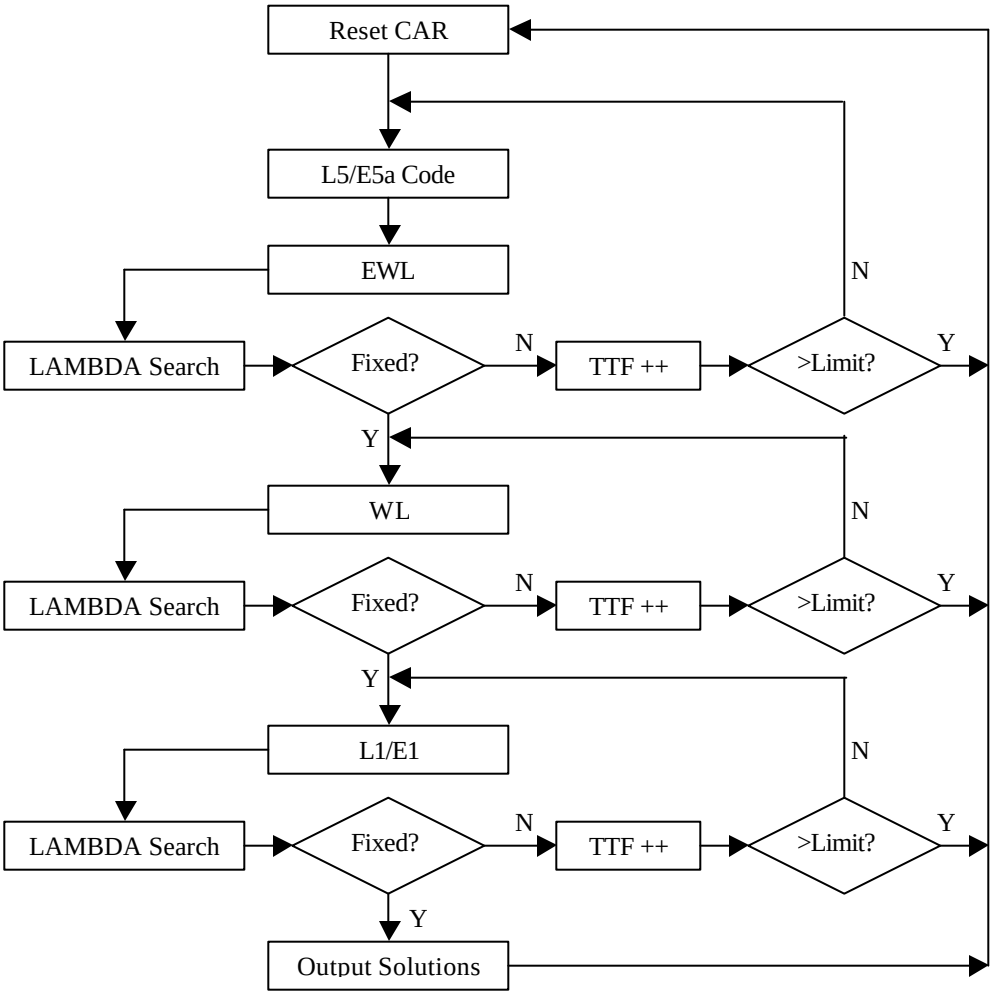

Figure 6.1 Flow Chart of the CAR Algorithm

If the EWL ambiguities are successfully fixed before timing out, the process moves on to the second filter, in which the estimation of float WL ambiguities is conducted based on the fixed EWL ranges and WL phase measurements. As a by-product, the user position is further updated. The LAMBDA method is then applied again to search the best integer WL ambiguity set. Similar to the first filter, the second filter is run sequentially until

either the WL ambiguities are fixed or this filter times out. The epoch counter keeps counting the times this filter runs.

Once the WL ambiguities are fixed, the third filter is activated with the fixed WL ranges and L1/E1 phase measurements. Similar to the previous two filters, the user position is further updated and the estimated float L1/E1 ambiguities are forwarded to the LAMBDA searching scheme. If the L1/E1 ambiguities are fixed in the sequential process, the integer L1/E1 ambiguities and the user position are output as the final solutions, and the content of the epoch counter represents the time to fix the L1/E1 ambiguities since the start of the first filter. If the third filter times out, this trial of ambiguity fixing is concluded to have failed and the CAR is reset thereafter.

The above three filters perform in similar ways, with the outputs of the preceding filter fed as the inputs to the succeeding filter. The accuracy of the fixed ranges is stepwisely improved, so does the accuracy of the user position. Although consisting of three filters and seeming complicated, the implementation of the CAR algorithm as depicted in Figure 6.1 is greatly facilitated by the similarity of the three filters.

The implementation of the CAR algorithm is very flexible. It is convenient to implement different models in the three filters (stages). The basic CAR algorithm, with each filter making use of a basic geometry-based model, will be realized and tested in Chapter 7 over short baselines. As an extension of the basic CAR algorithm, efforts in ionospheric modeling are also incorporated into the third filter (stage) to improve L1/E1 ambiguity

resolution over medium baselines in Chapter 8. In addition, the number of filters is not restricted to three. In Chapter 7, a similar cascading ambiguity resolution process will be tested with two frequency data. In the dual-frequency cases, only two filters have been formed, with the first one utilizing a kind of code measurement (the most precise code measurements available) and WL phase measurements, the second making use of the fixed WL ranges and L1/E1 phase measurements. The two-filter approach is also nominally called a cascading ambiguity resolution technique.

Since all the ambiguities are divided into three groups and resolved in three independent filters, the number of ambiguities in each filter is decreased, which results in much smaller amount of ambiguity candidate sets, and much faster ambiguity fixing through LAMBDA searching.

Additionally, this three-filter approach makes the most of the stepwise improvement in the range's precision. The identified ambiguities in each step (filter) directly assist with improved precision of the range in the subsequent stage (filter), which speeds up the convergence of the user position and therefore directly benefits the estimation of the ambiguities in the next step.

However, this approach complicates the procedure of switching the base satellite(s), especially in the combined GPS/GALILEO case, in which each system adopts its own base satellite. With one base satellite changed, the ambiguities in each stage (filter) must be switched with respect to the new base satellite. Such a change may take place in any of

the three steps (filters). Once it happens, corresponding ambiguity switches must be made in all previous step(s).

This approach is unable to deal well with new satellites appearing during the second or third stage (filter) because the ambiguities in the preceding stages have not been estimated or even fixed yet for the new satellite. Two choices for this case are:

(1) Resetting the filters so that the new satellite can be validated;

(2) Discarding the new satellite.

However, neither is perfect. The first choice risks losing many epochs of information for the previously fixed ambiguities, whereas the second does not make full use of all the available satellites and will lead to a decrease in the number of satellites over time.

6.2.2 One Filter

The shortcomings of the three-filter cascading ambiguity resolution approach can be overcome by using one filter for all ambiguities. In this case, the ambiguities of all the frequency combinations are resolved at the same time, in which new satellites appearing no longer need to be discarded. Base satellite changes are also simplified and can be performed in one step.

However, since all ambiguities are included in one filter, the high number of ambiguities to fix amounts to a burden for the searching and fixing part of the algorithm (Alves,

2001; Julien et al., 2003). Meanwhile, no step-wise improved precision is available, and the initial values of all ambiguities can only be estimated through code measurements. This single filter approach using cascading wide lanes is not expected to have better performance than the three filter approach, and therefore will not be adopted in the tests.

6.3 SWITCH OF BASE SATELLITES

Forming DD measurements for GPS and GALILEO systems requires two different base satellites. In the research of this thesis, the satellite at the highest elevation angle is selected as the base satellite for each system.

The elevation of each satellite alters along with the movement of each satellite in orbit. Therefore, according to the above selection strategy, new satellites appearing at the highest elevation for each system are selected to replace the old base satellites, and the DD ambiguities in state vector and the state VC matrix of each step need to be switched with respect to the new base satellite. Equations (6.7) and (6.8) demonstrate the principle of the switches:

$$\mathbf{X}_j = \mathbf{G}_{j,k} \cdot \mathbf{X}_k \tag{6.7}$$

$$\mathbf{Q}_j = \mathbf{G}_{j,k} \cdot \mathbf{Q}_k \cdot \mathbf{G}_{j,k}^T \tag{6.8}$$

where $\mathbf{X}_k$ is the DD ambiguity vector when satellite k is selected as the base satellite, and $\mathbf{Q}_k$ is the corresponding VC matrix; $\mathbf{X}_j$ is the new DD ambiguity vector when the

old base satellite k is replaced by satellite j, and $\mathbf{Q}_j$ is the corresponding VC matrix; $\mathbf{G}_{k,j}$ is the ambiguity transition matrix from old base satellite k to new base satellite j.

Two cases need to be taken into account when constructing the transition matrix $\mathbf{G}_{k,j}$:

(1) For any satellite i other than the new base satellite, the DD ambiguity with respect to the new base satellite j can be obtained in the following equation:

$$\nabla\Delta N_{AB}^{ij} = \nabla\Delta N_{AB}^{ik} - \nabla\Delta N_{AB}^{jk} \tag{6.9}$$

where the old base satellite number is k, and the superscript letters indicate satellite numbers, with the second being the base satellite number; the subscript letters indicate station id, with the second being the reference station id.

(2) For the old base satellite k, the DD ambiguity with respect to the new base satellite can be obtained through:

$$\nabla\Delta N_{AB}^{kj} = (-1)\cdot\nabla\Delta N_{AB}^{jk} \tag{6.10}$$

The following gives an example of ambiguity switching from base satellite '6' to '4'. The ambiguity vector with respect to old base satellite '6' is:

$$\mathbf{X}_6 = \begin{bmatrix}\nabla\Delta N_{AB}^{16} & \nabla\Delta N_{AB}^{26} & \nabla\Delta N_{AB}^{36} & \nabla\Delta N_{AB}^{46} & \nabla\Delta N_{AB}^{56}\end{bmatrix}^T \tag{6.11}$$

After switching to new base satellite '4', the ambiguity vector becomes:

$$\mathbf{X}_4 = \begin{bmatrix}\nabla\Delta N_{AB}^{14} & \nabla\Delta N_{AB}^{24} & \nabla\Delta N_{AB}^{34} & \nabla\Delta N_{AB}^{64} & \nabla\Delta N_{AB}^{54}\end{bmatrix}^T \tag{6.12}$$

Therefore, the transition matrix is of the following form:

$$\Gamma_{4,6} = \begin{bmatrix} 1 & 0 & 0 & -1 & 0 \\ 0 & 1 & 0 & -1 & 0 \\ 0 & 0 & 1 & -1 & 0 \\ 0 & 0 & 0 & -1 & 0 \\ 0 & 0 & 0 & -1 & 1 \end{bmatrix} \tag{6.13}$$

In Equation (6.13), all the elements of the 4th column are '-1' since the 4th satellite is selected as the new base satellite, as explained in Equation (4.9). In addition, all the elements of the 4th row are '0' except the 4-th element being '-1', as explained in Equation (4.10). For other cases, the transition matrices can be derived in the same way.

7 SIMULATION AND TEST RESULTS

7.1 DEFINITION OF FIGURES OF MERIT

For tests of ambiguity resolution over different baselines, different time limits are specified as shown in Table 7.2. Once the fixing of an ambiguity set is achieved or it fails, the filters are reset immediately. This process is carried out throughout the whole dataset to generate a statistical sample. The performance of the proposed algorithms were evaluated in terms of the following figures of merit.

- **Mean Time To Correctly Fix Ambiguities (MTTCF)**

In cascading ambiguity resolution, the time to fix any ambiguity is counted from the start of the EWL filter. To assess the suitability of a system for carrier phase ambiguity resolution, a large number of trials are adopted and this figure of merit can be calculated by averaging the time required to fix ambiguities in each attempt throughout a dataset under the specified conditions, such as specific baseline lengths and ionospheric levels. In the calculation of the mean time to fix, only the correctly fixed ambiguity sets are taken into account in the sample.

- **Percentage of Single-Epoch Ambiguity Resolution (PSE)**

This figure of merit has been used in Zhang et al. (2003) to assess the ability of instantaneous ambiguity resolution for a system or systems, which is defined as the result

of the number of ambiguity sets fixed within one epoch divided by the total number of epochs of the datasets.

- **Ambiguity Resolution Percent Correct (PC)**

This figure of merit has been used by the University of Calgary in the GALA project report (Lachapelle et al., 2001). As an empirical quantity, it is the result of the number of fully correctly fixed ambiguity sets over the total number of fixed ambiguity sets, which is different from the ambiguity success rate used by Delft University (Teunissen, 1998) that is a probabilistic value derived from the covariance matrix of the float solution of the ambiguities.

- **Number of Failures in Ambiguity Resolution**

This quantity is able to indicate how much of the dataset contributes to the statistics of the above figures of merit. A failure in ambiguity resolution is defined as an ambiguity set that fails to fix within a given time limit due to solution divergence or timeout. Once the ambiguity resolution is carried out through the entire dataset, the total number of failed ambiguity sets is referred to as the number of failures in ambiguity resolution.

- **Number of Fixes in Ambiguity Resolution**

This figure of merit is defined as the total number of fixed ambiguity sets throughout the test dataset, acting as a complement figure of merit to the PSE. In a comparison of the two systems in terms of ambiguity resolution performance, the Ambiguity Resolution

Percent Correct makes sense only when there are equivalent Numbers of Fixes for both systems.

- **Accuracy with Correct Ambiguity Fixing**

This figure of merit shows the accuracy in the position domain when the ambiguities have been correctly fixed. It allows for an evaluation of the remaining errors after correct ambiguity resolution. So only when the ambiguities are correctly fixed, can the positioning accuracy be used in the statistics.

- **Accuracy with Partially Correct Ambiguities**

This figure of merit aims to evaluate the impact of partially correct ambiguities in the position domain. So once the ambiguities are failed, the resulting positioning accuracy is used in statistics.

7.2 DATA SIMULATION

7.2.1 GPS/GALILEO Simulator

A software-based GPS/GALILEO simulator SimGNSS2™ has been developed at the University of Calgary (Luo, 2000). This simulator has been used in many other GPS and GALILEO system evaluations (Alves, 2001; Lachapelle et al., 2002; Julien et al., 2003; Zhang et al., 2003). The GALILEO constellation in simulation consists of 27 satellites

(the 3 spares are not considered) according to parameters described in Chapter 2 and the GPS constellation consists of 24 satellites in circular orbits, with the assumption that the time and coordinate reference frames of GPS and GALILEO have been reconciled to GPS system. With user input error scaling factors, the sampling rate, the masking angle, the coordinates of reference and user stations, this software is able to simulate pseudorange and carrier-phase measurements on three carrier frequencies for both GPS and GALILEO. Ionospheric errors, tropospheric errors, orbital errors, receiver noise and multipath are included. For each carrier-phase measurement, an ambiguity of zero cycles is simulated. So the true value of each ambiguity is zero, which facilitates the check of the correctness of each ambiguity resolution trial.

7.2.2 Simulated Baselines

In an effort to evaluate the efficiency of the proposed ambiguity resolution algorithms, both GPS and GALILEO observations were simulated with the above software simulator at a one second sampling rate over 1, 10, 20, 30, 50 and 70 km baselines for 24 hours. The coordinates of the simulated stations A, B, C, D, E, F and G are listed in Table 7.1.

Table 7.1 Coordinates of the Simulated Stations

Station #	Latitude	Longitude	Altitude	Baseline Length from A
A	51° 00' 00.000?	-114° 00' 00.000?	1000 m	0 km
B	51° 00' 32.340?	-114° 00' 00.000?	1000 m	1 km
C	51° 05' 23.400?	-114° 00' 00.000?	1000 m	10 km
D	51° 10' 46.799?	-114° 00' 00.000?	1000 m	20 km
E	51° 16' 10.200?	-114° 00' 00.000?	1000 m	30 km
F	51° 26' 56.969?	-114° 00' 00.000?	1000 m	50 km
G	51° 37'44.418?	-113° 59' 27.660?	1000 m	70 km

7.2.3 Simulated Error Levels

Both the pseudorange and carrier-phase measurements for GPS and GALILEO observations were simulated at typical and realistic error levels as follows:

- Atmospheric errors (within the levels 90% of the time)

  DD tropospheric error: 0.2 ppm

  DD ionospheric error: 3.0 ppm and 6.0 ppm (2 cases)

  DD orbital error (1 σ): 0.1 ppm

- Multipath (Single measurement 1 σ):

  Phase: 0.025 cycles

  L5/E5a Code: 0.14 m

- Receiver noise (1 σ):

  Code:

	L1:	0.36 m
	L5:	0.04 m
	E1:	0.10 m
	E5a:	0.045 m
Phase:		0.003 cycles

The DD atmospheric errors are defined in ppm over specified baselines. The level '*x*' ppm is defined that 90% of the time, the DD error is less than '*x*' ppm. The tropospheric error level as shown above is the residual errors after applying a tropospheric correction. For both GPS and GALILEO, the ionospheric errors were simulated over 24 hours and presented in Figure 7.1 and Figure 7.2, in which the 3 ppm error is regarded as a medium level, whereas 6 ppm is considered as a high level. The multipath and noise variances adopted are single measurement errors. It is important to notice that the code noise errors were chosen optimistically for L5, E1 and E5a compared to current signal structures, but a little pessimistic for L1, as the front-end bandwidth and tracking techniques by 2008 will be wider and better respectively.

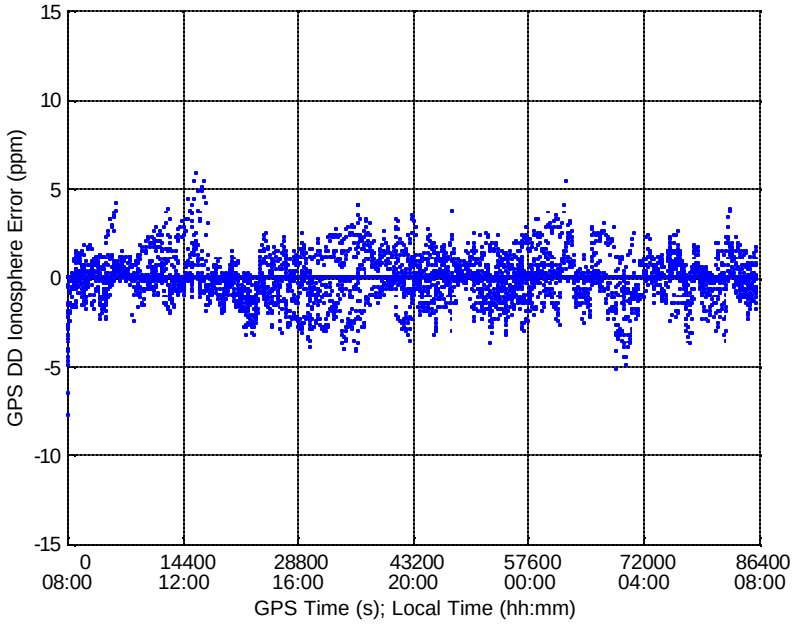

(GPS)

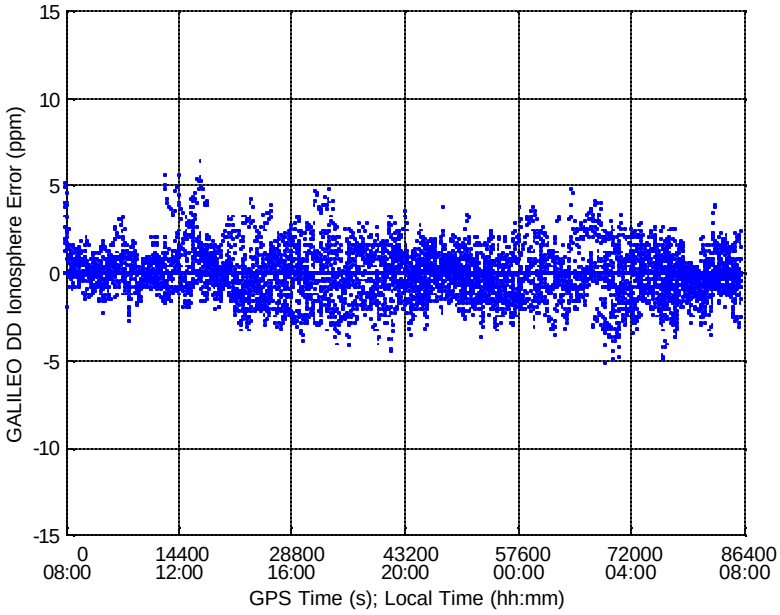

(GALILEO)

Figure 7.1 Simulated DD Ionospheric Errors at the level of 3 ppm

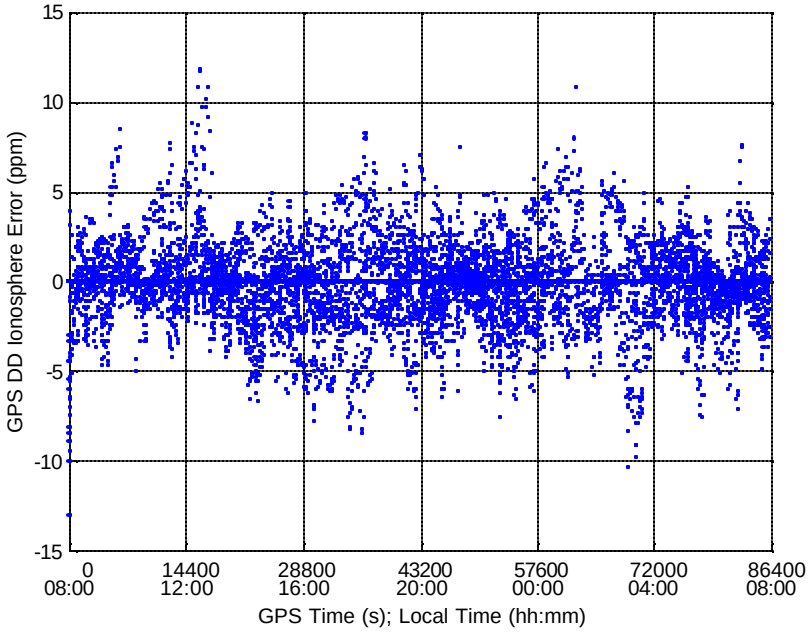

(GPS)

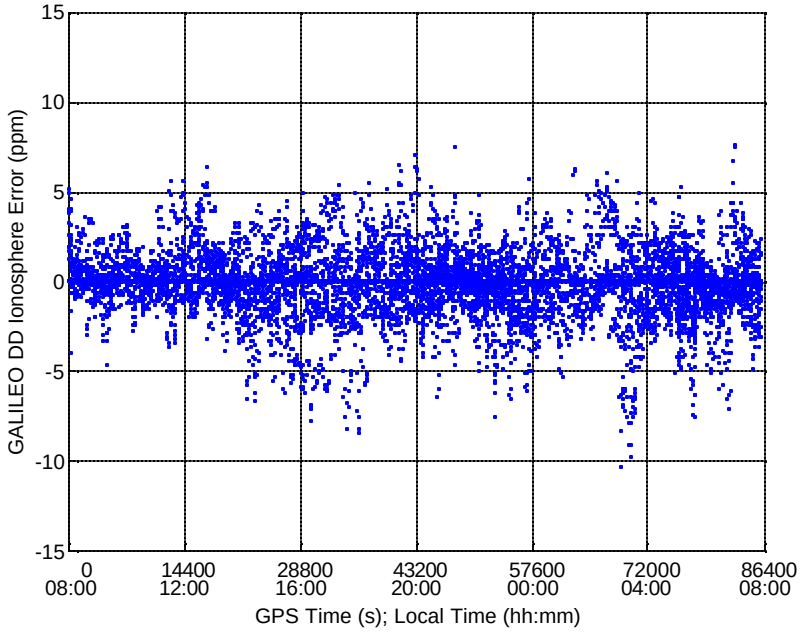

(GALILEO)

Figure 7.2 Simulated DD Ionospheric Errors at the level of 6 ppm

7.2.4 Limits of Time To Fix

Static tests were performed using the simulated measurements over the above baselines. For the ambiguity resolution tests over each baseline, a limit of time to fix was specified as shown in Table 7.2. The selection of the limits was based on experience. The purpose of the time limit was to avoid accounting for too many epochs when divergence occurs in the ambiguity resolution process. Ambiguity sets that did not fix within the time limit were regarded as failures.

Table 7.2 Specified Limits of Time To Fix over Simulated Baselines

Baselines (km)	Limit of Time to Fix (s)
1	300
10	600
20	1500
30	1800
50	2400
70	3000

For each scenario, ambiguity resolution tests in the cases of GPS only, GALILEO only and combined GPS/GALILEO were repeated throughout the entire dataset.

7.2.5 Number of Visible Satellites

As shown in Figure 2.4, the simulated GALILEO constellation consists of 27 satellites and the GPS constellation consists of 24 satellites. The following figure shows the number of visible satellites for both systems above an elevation mask of 15° during the

24-hour simulation. The number of visible GPS satellites was always between 5 and 7, while 6 to 8 satellites were usually visible for the GALILEO constellation.

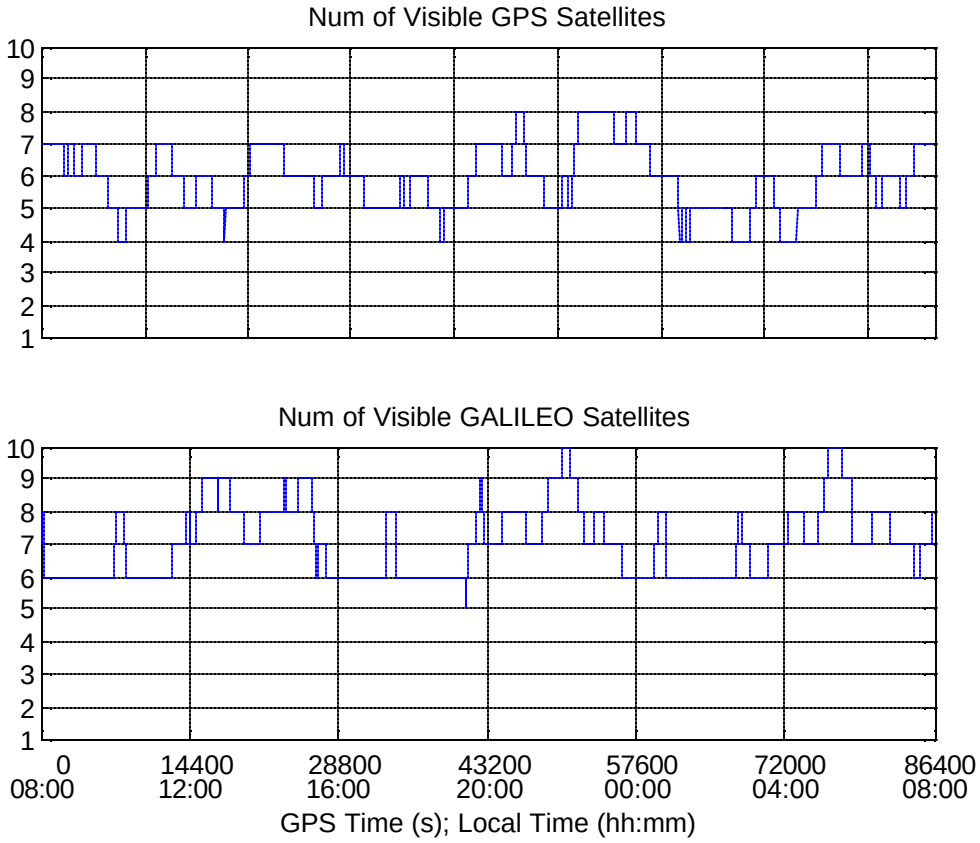

Figure 7.3 Number of visible satellites for GPS and GALILEO

7.3 TEST OF INTEGER ROUNDING

As a supplement to the theoretical analysis in Section 5.1, this section presents test results of integer rounding for GPS only with simulated data at a 3-ppm ionosphere level over 1, 10 and 20 km baselines.

7.3.1 Test Methods

Summarizing Equations (5.1), (5.5) and (5.6) gives:

$$x = \nabla\Delta\tilde{N}_{(\cdot)} - \nabla\Delta N_{(\cdot)} \tag{7.1}$$

where $(\cdot)$ represents 'EWL', 'WL' or 'L1/E1'. Since the true values of the simulated ambiguities are always zero (Section 7.2.1), Equation (7.1) can be simplified to:

$$x = \nabla\Delta\tilde{N}_{(\cdot)} \tag{7.2}$$

Therefore, by directly analyzing the distribution of the float ambiguities, $\nabla\Delta\tilde{N}_{(\cdot)}$, in each step of CAR, the probability of successful rounding can be obtained and the following steps are adopted in the investigation:

(1) Repeatedly run the EWL ambiguity resolution over 24 hours, and each time reset the EWL filter no matter whether the EWL can be fixed or not. The probability of successful EWL ambiguity rounding is the percentage of the float EWL ambiguities distributed in the range of [–0.5, 0.5] cycles among all EWL ambiguities, namely:

$$f(x_{EWL}) = \left\{ \left| x_{EWL} \right| < 0.5 \right\}$$

(2) Set the EWL ambiguities to zero (true value) and repeatedly run WL ambiguity resolution over 24 hours, and each time reset the WL filter no matter whether the WL can be fixed or not. Under the condition of correct EWL fixing, the probability of successful WL ambiguity rounding should be the percentage of the float WL ambiguities distributed in the range of [–0.5, 0.5] cycles, namely:

$$f(x_{WL} \mid x_{EWL} = 0) = \left\{ \left| x_{WL} \right| < 0.5 \right\}$$

(3) Set both the EWL and WL ambiguities to zero and repeatedly run the L1/E1 ambiguity resolution over 24 hours, and each time reset the L1/E1 filter no matter whether the L1/E1 can be fixed or not. Under the condition of correct EWL and WL fixing, the probability of successful L1/E1 ambiguity rounding should be the percentage of the float L1/E1 ambiguities distributed in the range of [-0.5, 0.5] cycles, namely:

$$f(x_{L1} \mid x_{EWL} = 0, x_{WL} = 0) = \{|x_{L1}| < 0.5\}$$

(4) The probability of successful L1/E1 ambiguity rounding therefore can be obtained as:

$$f(x_{L1}) = f(x_{EWL}) \cdot f(x_{WL} \mid x_{EWL} = 0) \cdot f(x_{L1} \mid x_{EWL} = 0, x_{WL} = 0)$$

In case of dual frequency data, similar two-step cascading integer rounding is adopted. Since the EWL is not available, WL ambiguities are directly estimated through the most precise code measurement that is available, so the probability of successful L1/E1 ambiguity rounding becomes:

$$f(x_{L1}) = f(x_{WL}) \cdot f(x_{L1} \mid x_{WL} = 0)$$

The probability of successful rounding is approximated by the percentage of correct rounding in statistics.

7.3.2 Results Description

The distribution of the EWL/WL/L1 float ambiguities obtained over 1, 10 and 20 km baselines through the aforementioned steps is presented in Figure 7.5, Figure 7.6 and

Figure 7.7. Figure 7.4 also depicts the distribution of the WL/L1 float ambiguities obtained over the 1 km baseline through two-step cascading integer rounding. In each figure, the x axis represents the ambiguity bins in the range of [-1, 1] cycles, and the y axis represents the percentile of the ambiguities distributed in each bin. The red dashed lines in each figure mark ± 0.5 cycles, and the percentage of the ambiguities distributed in the range of [-0.5, 0.5] is displayed, which actually represents the percentage of correct rounding of the ambiguities. The results are also presented in Figure 7.5 in a summary form.

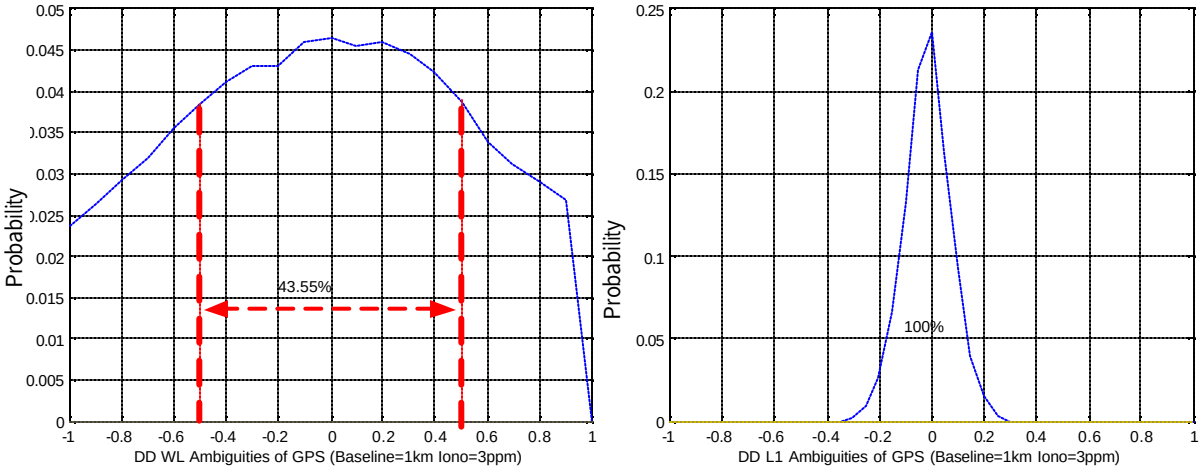

(1) WL (2) L1

Figure 7.4 Distribution of GPS WL/L1 Float Ambiguities using the Two-step Cascading Approach over the 1 km Baseline at the 3 ppm Ionospheric Level

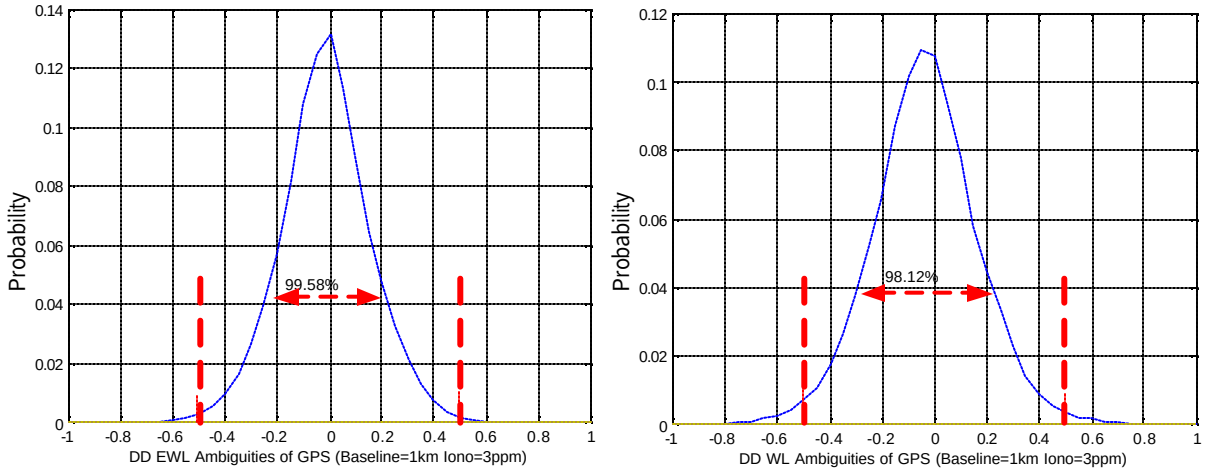

(1) EWL

(2) WL

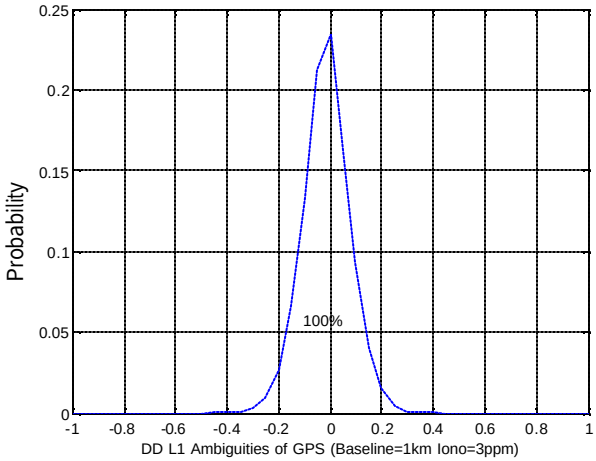

(3) L1

Figure 7.5 Distribution of GPS EWL/WL/L1 Float Ambiguities using the Three-step Cascading Approach over the 1 km Baseline at the 3 ppm Ionospheric Level

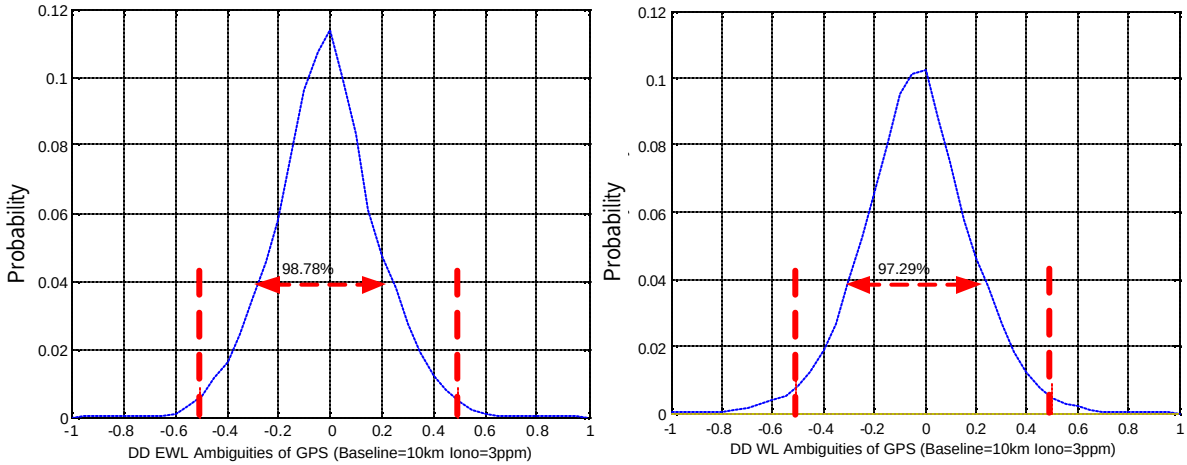

(1) EWL (2) WL

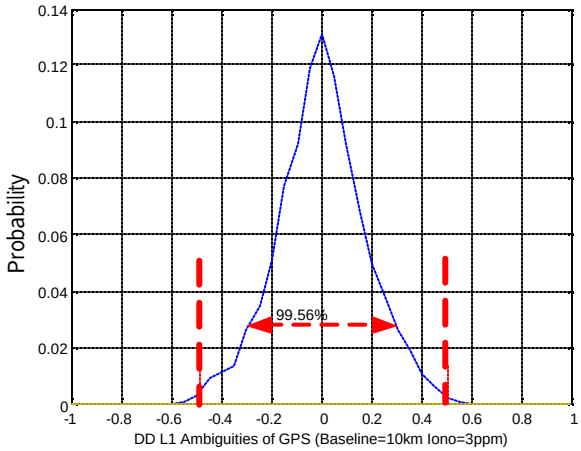

(3) L1

Figure 7.6 Distribution of GPS EWL/WL/L1 Float Ambiguities using the Three-step Cascading Approach over the 10 km at the 3 ppm Ionospheric Level

Table 7.3 Percentage of Correct Cascading Integer Rounding over the 1, 10 and 20 km baselines at the 3 ppm Ionospheric level for GPS only

Baselines	PC for each Cascading Step			PC of L1
	EWL	WL	L1	
1 km	99.58%	98.12%	100.0%	97.71%
	[redacted]	43.55%	100.0%	43.55%
10 km	98.78%	97.29%	99.56%	95.68%
20 km	97.84%	98.59%	90.39%	87.19%

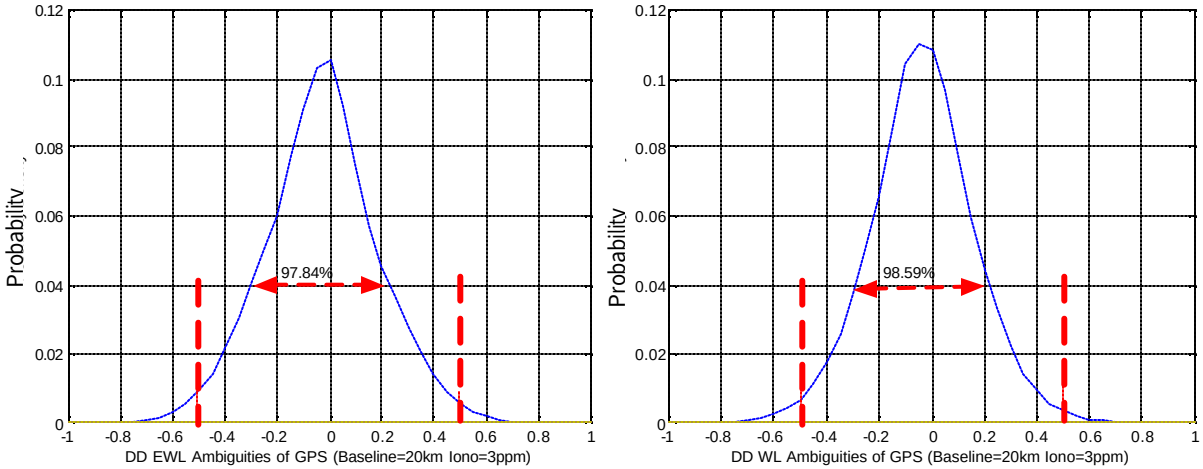

(1) EWL (2) WL

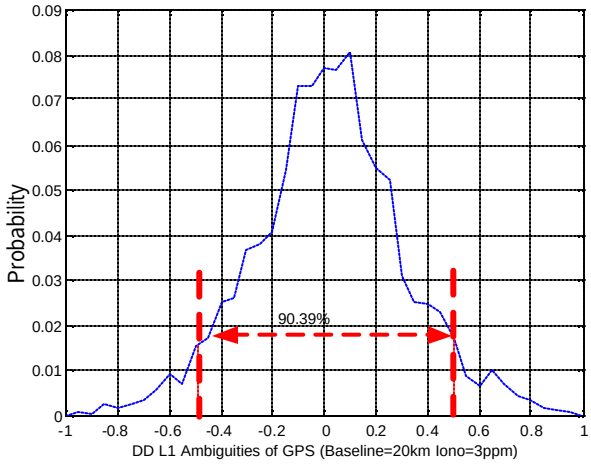

(3) L1

Figure 7.7 Distribution of GPS EWL/WL/L1 Float Ambiguities using the Three-step Cascading Approach over the 20 km Baseline at the 3 ppm Ionospheric Level

According to the results in the above figures and the summary in Figure 7.5, the following observations can be made:

(1) Over the 1 ~10 km baselines, it is easier to bridge WL to L1 than to bridge EWL to WL because the influence of WL measurement noise on L1 ambiguity estimation is smaller than that of EWL on WL as indicated in Table 4.2;

(2) Over the 20 km baselines, it becomes more challenging to bridge WL to L1 than to bridge EWL to WL, because the residual ionospheric errors become predominant, and

the influence of residual ionospheric error on L1 ambiguity estimation exceeds WL as indicated in Table 4.1;

(3) Over the 1 km baseline, Figure 7.4 shows significantly worse integer rounding results of the WL from code measurements compared to from the fixed EWL range as shown in Figure 7.5, which indicates that EWL ambiguity fixing is so crucial that it leads to a great improvement in the range precision from code measurement level to the EWL phase measurement level;

(4) Over the 1 ~ 10 km baselines, the L1 ambiguities can be instantaneously fixed through integer rounding with over a 95% confidence at the 3 ppm ionospheric level.

7.4 TEST OF CAR OVER SHORT BASELINES (1 ~ 20 km)

In this section, CAR was tested over short baselines ranging from 1 to 20 km with triple and dual frequencies. With dual frequency data, the ambiguity resolution only consists of two steps (WL and L1/E1), and the first step is to resolve WL ambiguities directly from the most precise code measurement that is available. For convenience, both the triple and dual frequency cascading ambiguity resolution methods here are both referred to as CAR.

7.4.1 Triple Frequency Ambiguity Resolution

7.4.1.1 Medium Ionosphere

The first tests were conducted using data at the medium ionospheric level (3 ppm). Table 7.8 shows that the combination of GPS/GALILEO performs better than either system alone in terms of MTTCF for all baselines from 1 to 20 km. As the length of the baseline increases, the advantage of combined GPS/GALILEO over either system alone becomes significant, which clearly indicates the improvements brought by the interoperability of the two systems.

In Figure 7.8, GPS performs slightly better than GALILEO within 10 km, but worse on the 20 km baseline. It can be understood through the two error sources: measurement noise and residual ionospheric errors. Under medium ionospheric level conditions, whereby ionospheric errors can be efficiently eliminated through double differencing over the 1 and 10 km baselines, measurement noise becomes the dominant error source, which explains the better performance of GPS as indicated in Table 4.2. However, over the 20 km baseline, the ionospheric residual turns to be the main error source, and GALILEO outperforms GPS. Over all the baselines, combined GPS/GALILEO always performs the best in terms of MTTCF, which exhibits the exclusive advantage of the combination of the two systems.

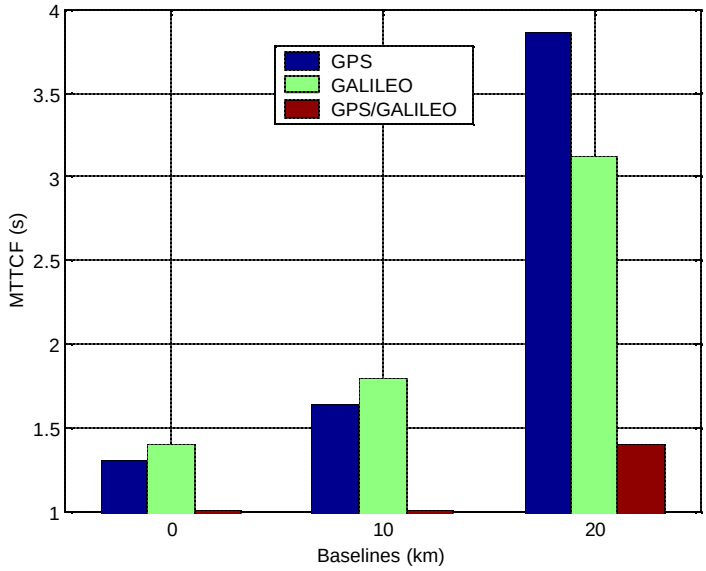

Figure 7.8 MTTCF of GPS Only, GALILEO Only and GPS/GALILEO at Medium Ionospheric Level (3 ppm) Using CAR in the Three-frequency Case

Another figure of merit, the PC, is shown in Figure 7.9. It can be noted that except for the GPS only case over the 20 km baseline, the PC in all cases, for all baselines, remains 100%. However, for the 20 km baseline, GPS shows worse performance than GALILEO and GPS/GALILEO due to the same aforementioned reason. Compared to the results in Table 7.3, the improvement of PC over the 1 ~ 20 km baselines in Figure 7.9 is obvious, which is due to the implementation of the LAMBDA searching algorithm implemented in Figure 6.1.

Both Figure 7.8 and Figure 7.9 also exhibit that instantaneous ambiguity resolution for combined GPS/ GALILEO within 10 km from a reference station is possible according to the results under the medium ionospheric conditions. In this case, only GPS only on the 20 km baseline has a few incorrectly fixed ambiguities.

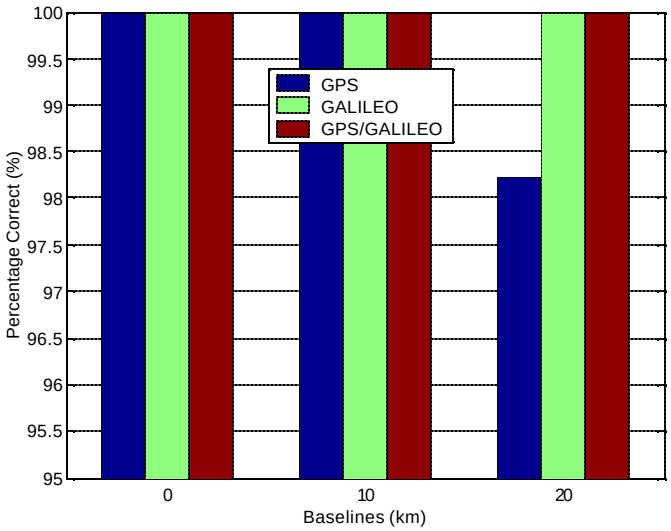

Figure 7.9 PC of GPS Only, GALILEO Only and GPS/GALILEO at Medium Ionospheric Level (3 ppm) Using CAR in the Three-frequency Case

Table 7.4 shows the PC in the incorrectly fixed sets, which indicates that even among the few incorrectly fixed ambiguity sets, the percentage of correct ambiguities is still quite high for GPS only.

Table 7.4 PC in a Set of Incorrectly Fixed Ambiguities for GPS Only, GALILEO Only, GPS/GALILEO at the Medium Ionospheric Level (3 ppm) using CAR in Case of Three Frequencies

Baselines	GPS Only	GALILEO Only	GPS/GALILEO
1 km	N/A	N/A	N/A
10 km	N/A	N/A	N/A
20 km	74.9	N/A	N/A

7.4.1.2 High Ionosphere

The second tests were conducted under a high ionospheric level (6 ppm). Figure 7.10 shows the MTTCF for baselines ranging from 1 to 20 km. As expected, shorter baselines

(1 and 10 km) are accompanied by better results due to the short time it takes to correctly fix the ambiguities. However, the performance in all three cases on the 20 km baseline is much worse, among which GPS only degrades more than ten times with respect to the 10 km case, and GALILEO performs considerably better than GPS only, and even better than GPS/GALILEO. The good performance over short baselines (1 ~ 10 km) is due to correlated errors (ionosphere and troposphere) cancelled through differencing. The worse performance on the 20 km baseline is directly related to increased residual errors. In Figure 7.10, although combined GPS/GALILEO has longer MTTCF than GALILEO only on 20 km, it has a much higher PC in Figure 7.11. The longer MTTCF for the combined GPS/GALILEO case might be due to the much larger number of ambiguities to resolve than GALILEO only.

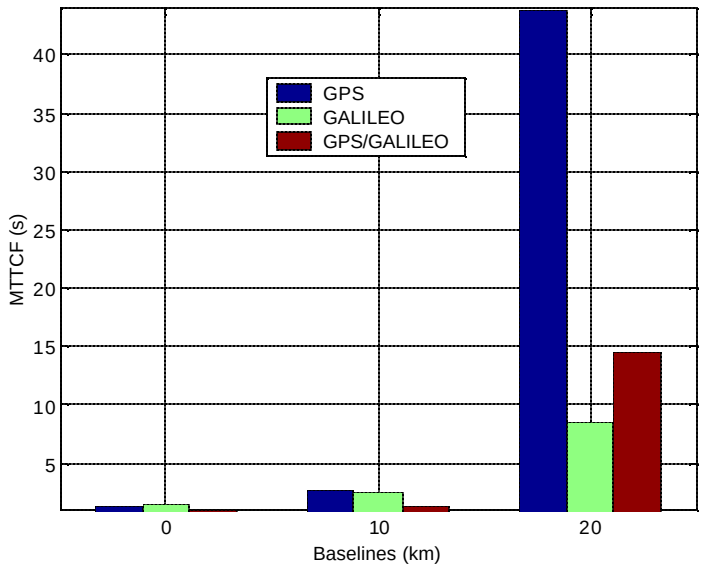

Figure 7.10 MTTCF of GPS Only, GALILEO Only and GPS/GALILEO at High Ionospheric Level (6 ppm) Using CAR in the Three-frequency Case

The PC under high ionospheric conditions is shown in Figure 7.11, where two consistent trends with previous results can be identified. One is both the individual and combined

systems perform very well over short baselines (1 ~ 10 km), but worse on the 20 km baseline in terms of the percentage of correctly fixed ambiguities. The other is that GALILEO only performs much better than GPS only on the 20 km baseline. The combined GPS/GALILEO case has the highest percentage of correct ambiguities (98.6%), which means that combined GPS/GALILEO has the highest reliability in ambiguity resolution due to the interoperability between GPS and GALILEO. Compared with the performance on the 10 km baseline, the PC of GPS only drops drastically from 99.9% to 33.1%, and GALILEO degrades much less from 99.9% to 88.9%, whereas combined GPS/ GALILEO only decreases slightly from 100.00% to 98.6%.

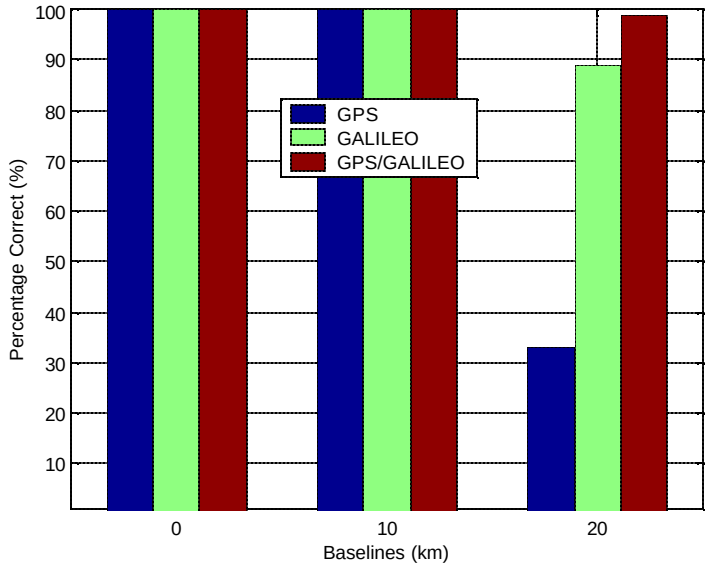

Figure 7.11 PC of GPS Only, GALILEO Only and GPS/GALILEO at High Ionospheric Level (6 ppm) Using CAR in the Three-frequency Case

At the high ionospheric level, the PCs remain 100% only on the 1 km baseline. The PC in the incorrectly fixed sets listed in Table 7.5 shows that the shorter the baseline, the higher the percentage of correct as expected.

Table 7.5 PC in a Set of Incorrectly Fixed Ambiguities for GALILEO Only, GPS Only, GPS/GALILEO for the Medium Ionospheric Level (6 ppm) Using CAR In Case of Three Frequencies

Baselines	GPS Only	GALILEO Only	GPS/GALILEO
1 km	N/A	N/A	N/A
10 km	73.3	60.0	N/A
20 km	39.8	40.4	56.3

It should be mentioned that under high ionospheric conditions, the influence of one limitation of the CAR becomes obvious. The problem is that if any new satellite appears in the second or third step of CAR (i.e. the step of EWL to WL or WL to L1/E1), CAR must either be reset or the new satellite discarded because each cascading step is based on the previous step. Under high ionospheric conditions it takes a longer time to fix the ambiguities, so the problem occurs at higher frequencies than under medium ionospheric conditions. In the results presented, the new satellites appearing in the second or third step are discarded.

7.4.1.3 Comparison of the Ionospheric Effects

As the main error source, the ionosphere always has a large influence on ambiguity resolution. To assess the impact of the ionosphere on the performance of individual and combined systems, the research conducts comparative analysis on MTTCF versus ionospheric level with respect to different baselines.

The results in Figure 7.12 shows that on the 1 km baseline, the MTTCF remains almost unchanged under both medium and high ionospheric conditions for GPS only, GALILEO only and combined GPS/GALILEO. This results from a very short baseline, whereby the ionospheric errors at the reference station and remote station are highly correlated and hence are efficiently cancelled by double differencing. Figure 7.12 shows that for combined GPS/GALILEO on a 1 km baseline, instantaneous ambiguity resolution is always feasible for both medium and high ionospheric activities.

Figure 7.13 shows a longer MTTCF with respect to Figure 7.12 due to the longer baseline length. Along with the increase of the baseline length, the correlation between the ionospheric errors at the reference station and those at remote station diminishes, which therefore leads to decreasing efficiency of canceling inonspheric errors. In addition, the increased ionospheric level also results in increased residual ionospheric errors. As a result, the MTTCFs at medium and high ionospheric levels are no longer the same.

Figure 7.14 shows an even longer MTTCF with respect to Figure 7.12 and Figure 7.13, which is again due to the increased baseline length, where the residual ionospheric errors increase accordingly. The results in the figures show that the longer the baseline, the longer the MTTCF. In addition, the results also indicate that the ionospheric errors can only be cancelled efficiently on very short baselines such as 1 km and 10 km, and on longer baselines such as 20 km they will become the main factor impairing the performance of ambiguity resolution. As shown in Figure 7.14, although combined GPS/GALILEO has longer MTTCF than GALILEO only due to the larger number of

ambiguities to resolve, the PC for combined GPS/GALILEO is obviously higher than GALILEO only.

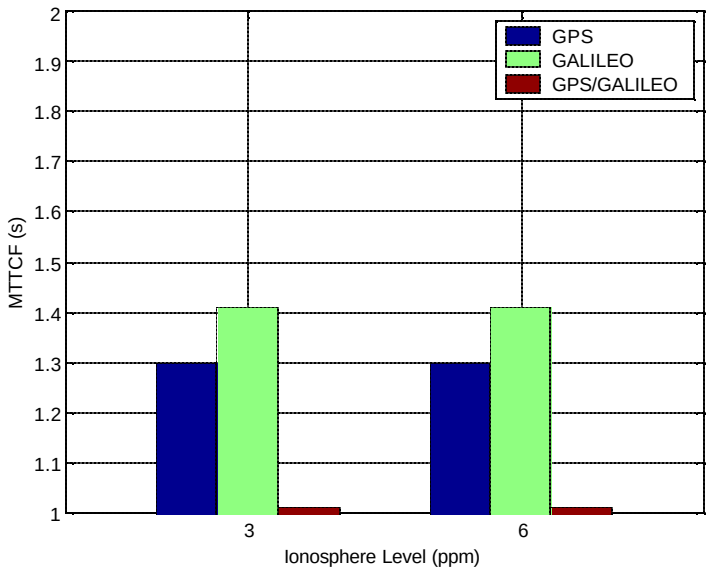

Figure 7.12 Ionospheric Effect on the MTTCF for GALILEO Only, GPS Only and GPS/GALILEO on the 1 km Baseline Using CAR in the Three-frequency Case

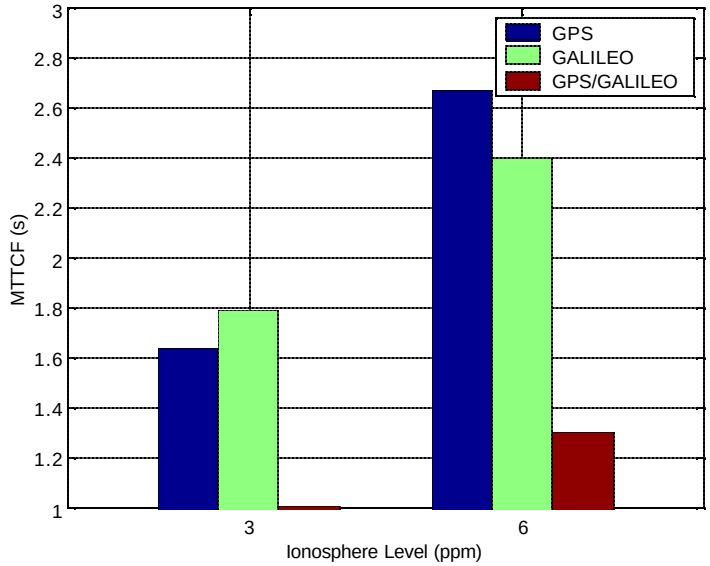

Figure 7.13 Ionospheric Effect on the MTTCF for GALILEO Only, GPS Only and GPS/GALILEO on the 10 km Baseline Using CAR in the Three-frequency Case

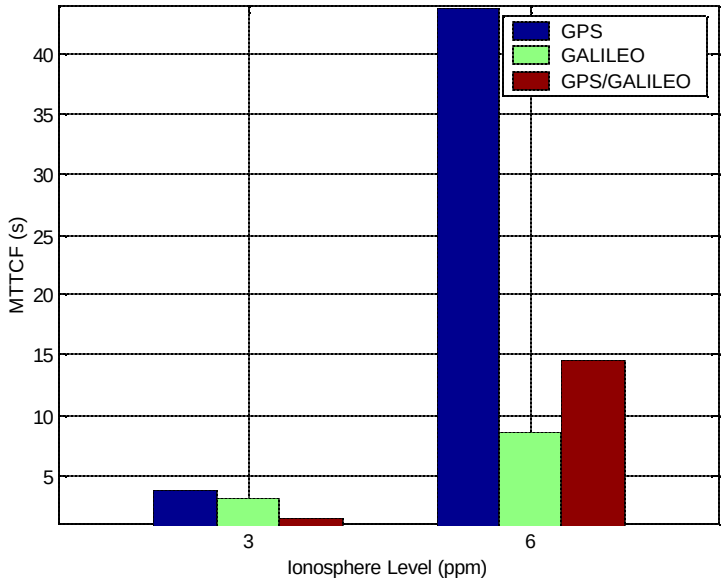

Figure 7.14 Ionospheric Effect on the MTTCF of GPS Only, GALILEO Only, and GPS/GALILEO on the 20 km Baseline using CAR in the Three-frequency Case

The ionospheric impact on the PC remains unremarkable until the baseline length extends to 20 km. Under medium ionospheric conditions, the ambiguity sets on the 1 ~ 20 km baselines can almost be 100% correctly fixed (There is only one exception for GPS only on 20 km, see Figure 7.9), however only on the 1 km baseline can the ambiguities be 100% correctly fixed at a high ionospheric level.

7.4.2 Dual Frequency Ambiguity Resolution

For the purpose of comparison, two frequencies (L1 and L2 for GPS, E1 and E5b for GALILEO) were also tested using a two-step cascading approach (WL and L1/E1).

7.4.2.1 Medium Ionosphere

First, the dual frequency cascading ambiguity resolution approach was tested at the medium ionospheric level. Figure 7.15 exhibits the performance of GALILEO only, GPS only and combined GPS/GALILEO on different baselines in terms of MTTCF, where a consistent phenomenon is obvious that combined GPS/GALILEO always performs the best on all baselines, GALILEO only the second, and GPS only the worst. Increases in the baseline length do not result in significant increases in MTTCF, (for example, the MTTCF for the combined GPS/GALILEO case only increases very slightly from 1.0 s on the 1 and 10 km baselines, to 1.5 s on the 20 km baseline). In another words, very fast ambiguity resolution is possible with two frequencies under medium ionospheric conditions on a 1 km baseline. The increase in the MTTCF for GALILEO only is also small (from 2.6 s on the 1 km, to 3.3 s on the 10 km, and to 7.3 s on the 20 km baseline) with the increase of baseline length. However, the MTTCF for GPS only increases drastically as the baseline length increases, especially on the 20 km baseline, the MTTCF has increased almost nine times compared to that on the 1 km, and five times compared to that on the 10 km baseline. Meanwhile, the increase of the MTTCF from 10 to 20 km exceeds significantly that from 1 to 10 km, which means that the residual errors rise greatly on a 20 km baseline. Since on this baseline, the MTTCF for GPS only increases most significantly compared to the slight increase for combined GPS/GALILEO, GPS only is the most susceptible to residual errors and combined GPS/GALILEO is the most immune.

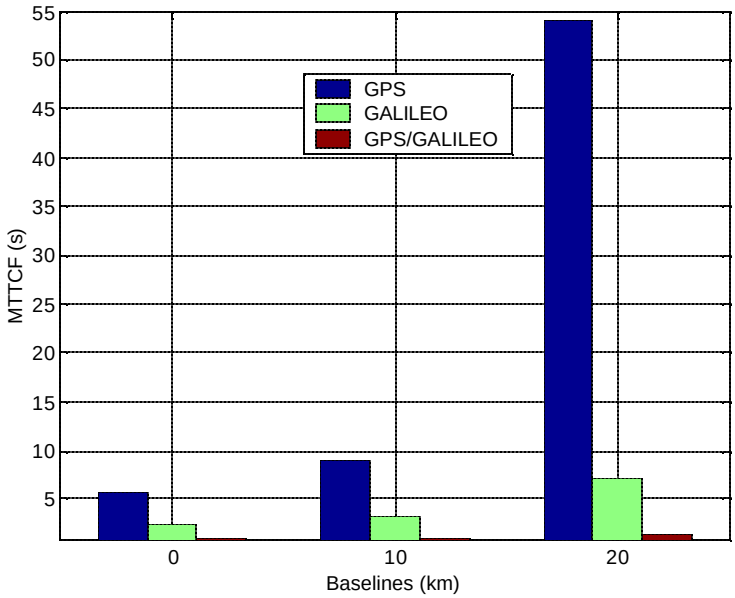

Figure 7.15 MTTCF of GPS Only, GALILEO Only, and GPS/GALILEO at Medium Ionospheric Level (3 ppm) Using CAR in the Two-frequency Case

At medium ionospheric levels, the ambiguities are almost 100% correctly fixed on both the 1 and 10 km baselines for GALILEO only, GPS only and the combined GPS/GALILEO cases as shown in Figure 7.16. Since GPS only is the most susceptible to residual errors, its PC drops slightly to 97.7% on the 20 km baseline, whereas GALILEO only and combined GPS/GALILEO remain almost 100%.

In a comparison to the results in Figure 7.4, Figure 7.16 shows a significant difference in PC with two frequencies. Due to the implementation of LAMBDA in Figure 6.1, the PC has been greatly improved.

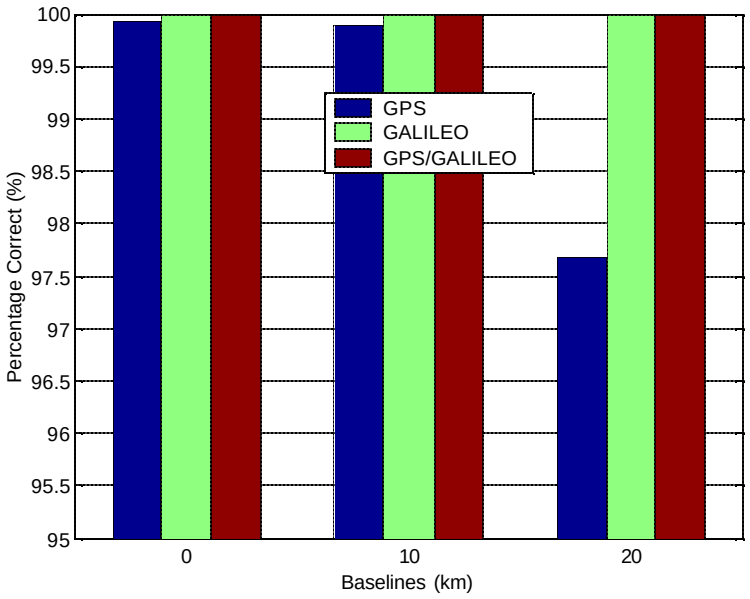

Figure 7.16 PC of GPS Only, GALILEO Only, GPS/GALILEO at Medium Ionospheric Level (3 ppm) Using CAR in the Two-frequency Case

7.4.2.2 High Ionosphere

At high ionospheric levels, the MTTCF shown in Figure 7.17 increases tremendously, not only for GPS only as the baseline length increases, but also for GALILEO only and combined GPS/GALILEO. Even for combined GPS/GALILEO, the MTTCF on the 20 km baseline increases to 34.87 s from 1.0 s on the 1 km baseline (Table 7.8). For GALILEO only and GPS only, the increased magnitude of the MTTCF is even larger, both increasing almost 100 times compared to that on the 1 km baseline. As the number of fixes for both GPS only and GALILEO only is very small on the 20 km baseline, the MTTCF for both may not be representative, however they indicate a trend that under high ionospheric conditions, the performance of both GPS only and GALILEO only in terms of MTTCF degrades significantly. Although the performance of combined

GPS/GALILEO also degrades, the degradation is obviously less significant than GPS only and GALILEO only.

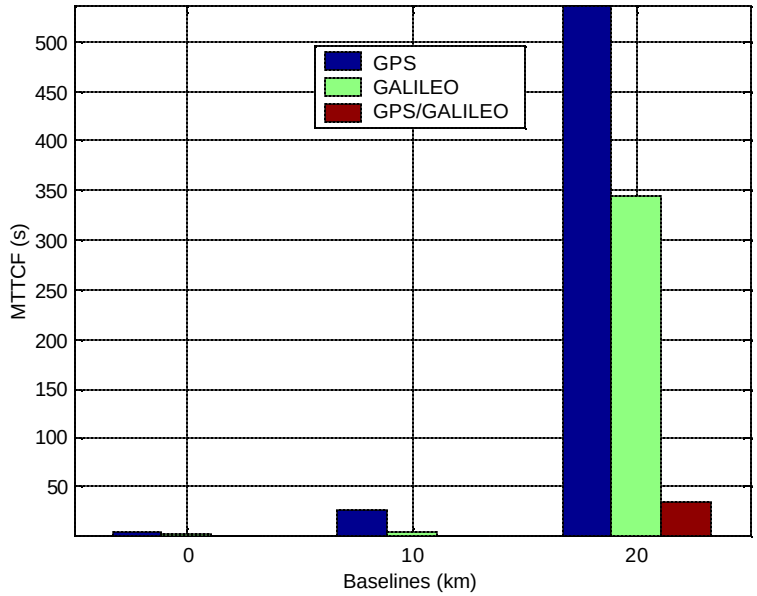

Figure 7.17 MTTCF of GPS Only, GALILEO Only, GPS/GALILEO at High Ionospheric Level (6 ppm) Using CAR in the Two-frequency Case

Under the high ionospheric conditions, 100%-fix case, which appears under medium inonspheric conditions, vanishes for both the individual and combined systems on the 20 km baseline according to the results shown in Figure 7.18. Again, the results show identical performance for all systems (individual and combined) except for the case of 20 km baseline where large differences appear. Combined GPS/GALILEO has the highest PC, GALILEO only the second, and GPS only the lowest, which exhibits a consistent trend with that at medium inonspheric level.

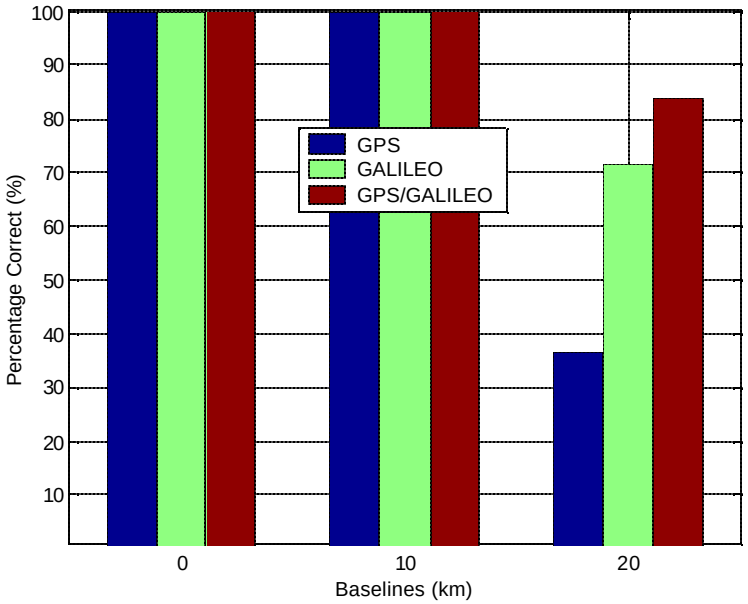

Figure 7.18 PC of GPS Only, GALILEO Only, GPS/GALILEO at High Ionospheric Level (6 ppm) Using CAR in the Two-frequency Case

7.4.2.3 Comparison of the Ionospheric Effect

In an effort to evaluate the influence of the ionosphere on two-frequency ambiguity resolution, the performances of GPS only, GALILEO only and combined GPS/GALILEO under the two ionospheric conditions on different baselines were compared. Figure 7.19 gives the comparisons based on the MTTCF, and Figure 7.22 to Figure 7.24 provide the comparisons according to PC.

From Figure 7.19, a small difference between medium (3 ppm) and high (6 ppm) ionospheric levels can be found in MTTCF for GPS only, GALILEO only and combined GPS/GALILEO, which means that the influence of the ionosphere on ambiguity resolution on a 1 km baseline is too trivial to take into account.

Figure 7.20 shows a comparison on the 10 km baseline. As the ionospheric level increases from 3 to 6 ppm, the MTTCF increases accordingly for all the cases of GPS only, GALILEO only and combined GPS/GALILEO, among which, the increase of GPS only is the largest, from 9.0 s at 3 ppm level to 26.6 s at 6 ppm. The MTTCF for GALILEO only and combined GPS/GALILEO under the two ionospheric conditions is at the same level. This reconfirms that GPS only is more susceptible to ionospheric levels than GALILEO only and GPS/GALILEO.

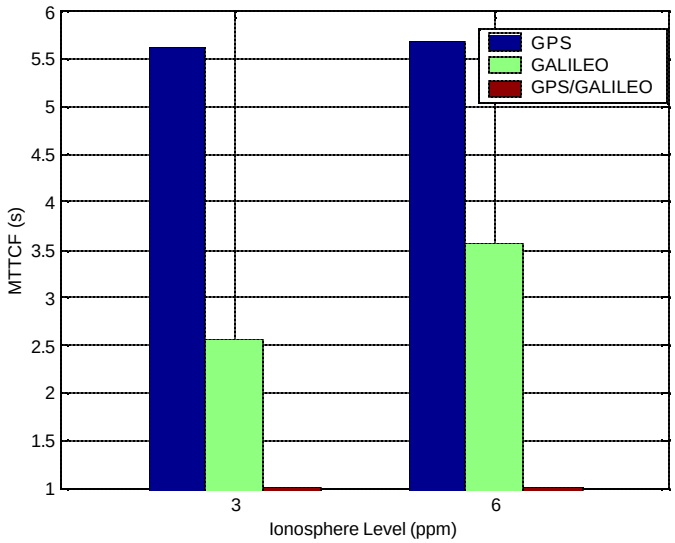

Figure 7.19 Ionospheric Effect on the MTTCF of GPS Only, GALILEO Only, and GPS/GALILEO on the 1 km Baseline Using CAR in the Two-frequency Case

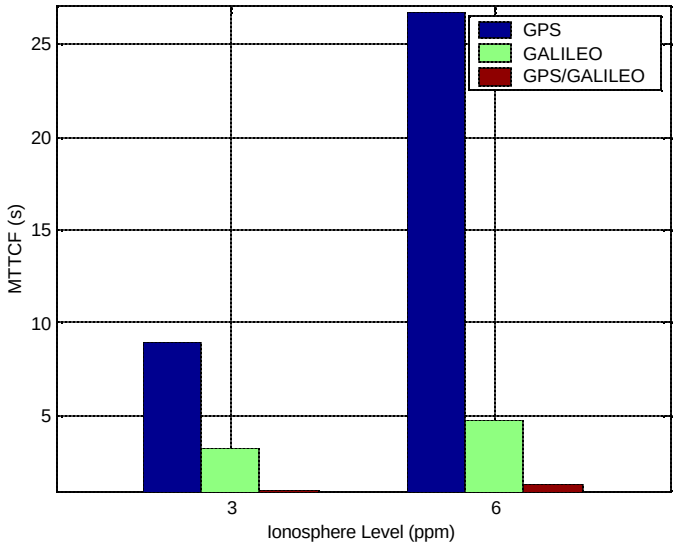

Figure 7.20 Effect of the Ionospheric Level on the MTTCF of GPS Only, GALILEO Only, and GPS/GALILEO on the 10 km Baseline Using CAR in the Two-frequency Case

On the 20 km baseline, the ionospheric level shows much greater influence on ambiguity resolution as shown in Figure 7.21. As the ionospheric level increases from 3 to 6 ppm, even for combined GPS/GALILEO, the MTTCF increases 10 times from 1.4 s to 14.9 s. The MTTCF for GPS only and GALILEO only increases almost 100 times and 40 times at the 6 ppm level with respect to that at the 3 ppm level. Although the results of GPS only and GALILEO only on the 20 km baseline at the 6 ppm ionospheric level might not be representative because there are very few fixes for both. The trend indicates that only combined GPS/GALILEO has the least susceptibility to the ionosphere even on a 20 km baseline.

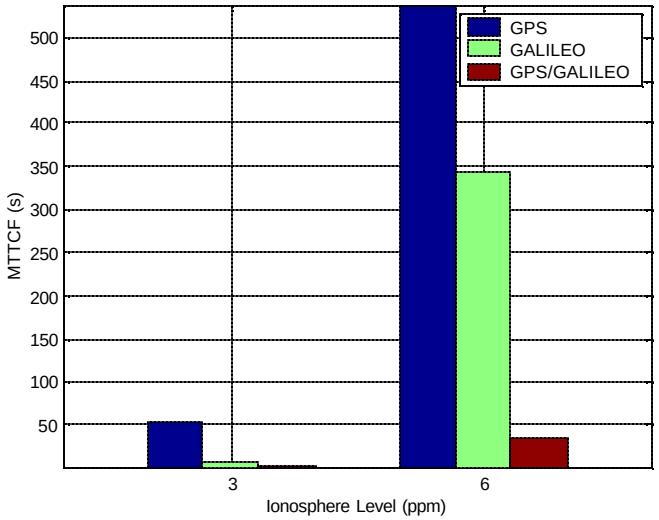

Figure 7.21 Ionospheric Effect on the MTTCF of GPS Only, GALILEO Only, and GPS/GALILEO on the 20 km Baseline Using CAR in the Two-frequency Case

The influence of the ionospheric level on ambiguity resolution on the 1 km baseline is insignificant according to the PC shown in Figure 7.22, which exhibits little difference between the PCs at the two ionospheric levels.

However, on the 10 km baseline, ionospheric influence turns larger on the PC as shown in Figure 7.23. It seems that only the PC of GPS only at the 6 ppm ionospheric level is influenced. The ionospheric influence on the ambiguity for the 10 km baseline is still small.

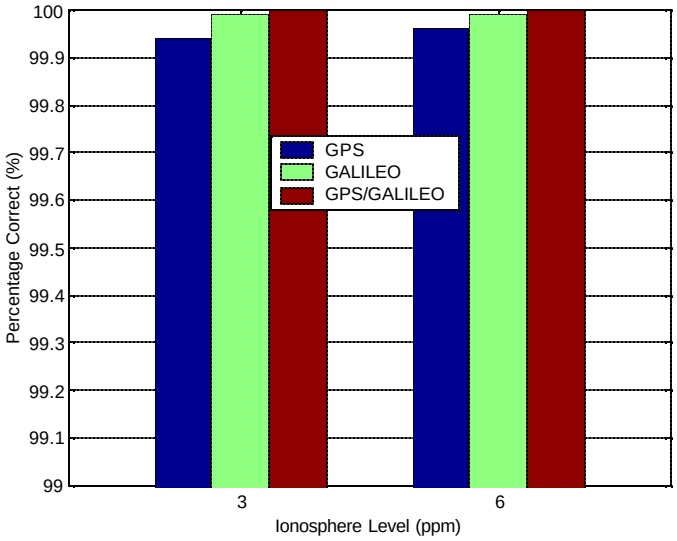

Figure 7.22 Ionospheric Effect on PC of GPS Only, GALILEO Only, and GPS/GALILEO on the 1 km Baseline Using CAR in the Two-frequency Case

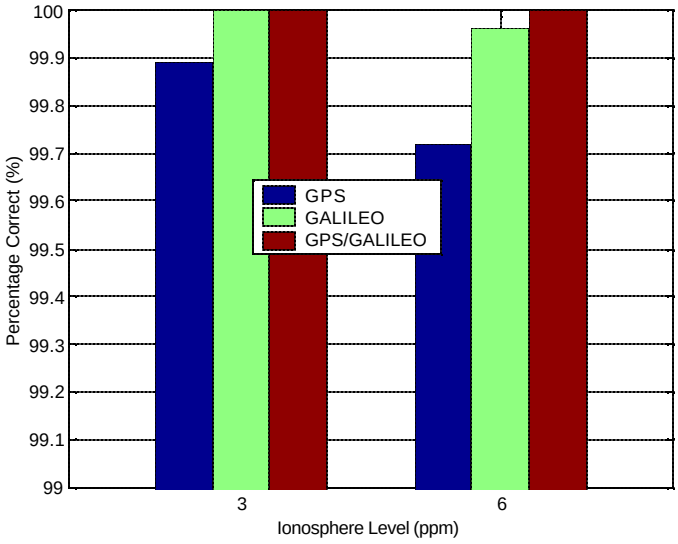

Figure 7.23 Ionospheric Effect on PC of GPS Only, GALILEO Only, and GPS/GALILEO on the 10 km Baseline Using CAR in the Two-frequency Case

Figure 7.24 shows a much greater ionospheric impact at the 3 ppm ionospheric level, the PC for all the cases of GPS only, GALILEO only and GPS/GALILEO combined is over 97%. However, the PC degrades significantly as the ionospheric level increases to 6 ppm.

The PC of GPS only degrades the most severely from 97.7% to 36.4%. The PC of GPS/GALILEO at the 6 ppm level remains the highest, but still decreases to 83.9% from 100% at the 3 ppm level.

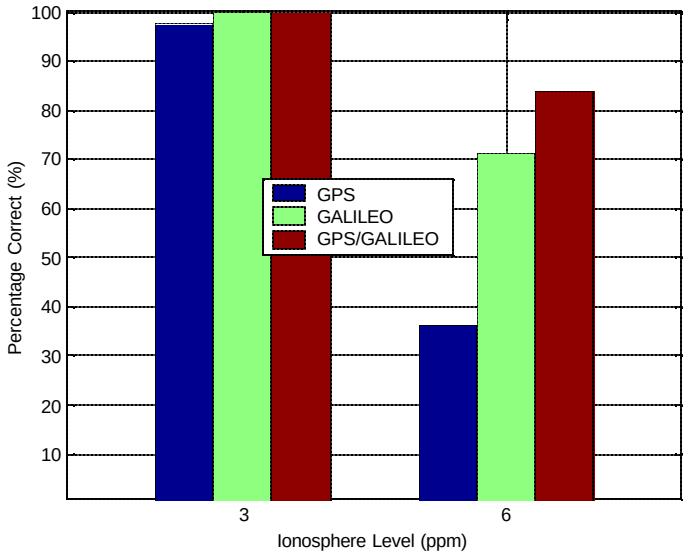

Figure 7.24 Ionospheric Effect on PC of GPS Only, GALILEO Only, and GPS/GALILEO on the 20 km Baseline Using CAR in the Two-frequency Case

It can be concluded that ionosphere has significant influences on two-frequency ambiguity resolution for baselines around 20 km. GPS only with two frequencies is the most susceptible to ionospheric influence, and combined GPS/GALILEO is of the highest insusceptibility.

7.4.3 Comparison between Dual and Triple Frequency Results

Table 7.6 and Table 7.7 list the comparisons of the results of dual and triple frequency ambiguity resolution using CAR under medium and high ionosphere conditions.

Under medium ionospheric condition, with three frequencies, all the cases of GPS only, GALILEO only and GPS/GALILEO combined always come out better results than those with only two frequencies in terms of MTTCF, PC and Number of Failures shown in Table 7.6.

Table 7.6 Comparison of Dual and Triple Frequency Ambiguity Resolution Performance at the Medium Ionospheric (3 ppm) Level Using CAR

	Number of Freq	GPS (km)			GALILEO (km)			GPS/GALILEO (km)		
		1	10	20	1	10	20	1	10	20
MTTCF (s)	3	1.3	1.6	3.9	1.4	1.8	3.1	1.0	1.0	1.4
	2	5.6	9.0	54.1	2.6	3.3	7.3	1.0	1.0	1.5
PC (%)	3	100	100	98.2	100	100	100	100	100	100
	2	99.9	99.9	97.7	99.9	100	100	100	100	100
Number of Failures	3	0	17	24	0	15	20	0	0	7
	2	28	30	27	1	15	22	0	0	7

Table 7.6 shows that improvements in GPS only due to the additional frequency L5 introduced by GPS modernization are most significant, while such improvements in GALILEO appears much smaller. Combined GPS/GALILEO is accompanied by the slightest changes in results due to the improvements from two-frequency to three-frequency results, which indicates that the interoperability between GPS and GALILEO benefits ambiguity resolution regardless of using two or three frequencies, and the number of correct fixes in Table 7.7 also shows the same fact. For the Number of Failures, the three-frequency results are slightly better than the two-frequency results. However, compared to GPS only and GALILEO only, combined GPS/GALILEO has much less Number of Failures due to the interoperability of GPS and GALILEO.

Table 7.7 Comparison of the Number of Correctly Fixed Ambiguities for Dual and Triple Frequency Ambiguity Resolution at the Medium Ionosphere (3 ppm) Using CAR, over 24 Hours

Number of Correct Fixes		1 km	10 km	20 km
GPS	3 Freq	65375	43498	7234
	2 Freq	12055	6214	337
GALILEO	3 Freq	61040	41879	9640
	2 Freq	31104	20847	3592
GPS/GALILEO	3 Freq	86394	85404	29064
	2 Freq	86093	84437	27390

Table 7.7 shows that switching from two to three frequencies enables an increase in the fixed ambiguities. Meanwhile, in terms of the number of fixed ambiguities, combined GPS/GALILEO is shown to possess a stronger capability of fixing ambiguities than GPS only and GALILEO only on all baselines using both three and two frequencies.

The results listed in Table 7.8 also show the advantages of three frequencies over two frequencies under high ionospheric conditions. As shown in the table, three frequencies produce better results than two frequencies in terms of the MTTCF, PC and Percent Correct in an Incorrect Set. However, several exceptions exist on the 20 km baseline. Since under high ionosphere conditions, the Number of Correctly Fixed Ambiguities falls significantly, especially on the 20 km baseline (only about 200 over a day), the statistics of the MTTCF and PC becomes less representative. As to the Number of Failures, the combined GPS/GALILEO case always has fewer failures on all the baselines than for the GPS only and GALILEO only cases.

Table 7.8 Comparison of Dual and Triple Frequency Ambiguity Resolution Performance for the High Ionospheric (6 ppm) Level Using CAR

	Number of Freq	GPS (km)			GALILEO (km)			GPS/GALILEO (km)		
		1	10	20	1	10	20	1	10	20
MTTCF (s)	3	1.30	2.67	43.76	1.41	2.40	8.56	1.0	1.30	14.87
	2	5.69	26.63	537.7	3.56	4.78	345.0	1.0	1.32	34.87
PC (%)	3	100	99.95	33.07	100	99.97	88.96	100	100	98.59
	2	99.9	99.72	36.36	99.99	99.96	71.43	100	100	83.88
Number of Failures	3	0	87	32	0	82	33	0	40	21
	2	23	79	32	1	64	21	0	40	21

As the ionospheric level increases from 3 to 6 ppm, the number of correct fixes drops significantly even for combined GPS/GALILEO. On the 20 km baseline, even combined GPS/GALILEO only has 140 and 228 correct fixes using three and two frequencies respectively, which means that the statistics of the MTTCF in this case is no longer representative.

7.5 TEST OF CAR OVER MEDIUM BASELINES (30 ~ 70 km)

As a continuous effort, the cascading ambiguity resolution approach was further tested over medium baselines ranging from 30 to 70 km augmented with ionospheric modeling techniques.

7.5.1 WL Ambiguity Resolution

Over the 20 km baseline, it has become somehow difficult to fix L1/E1 ambiguities using the basic CAR, especially at the 6 ppm ionospheric level for GPS only and GALILEO only as shown in Figure 7.8. It is estimated that it would become even more difficult for L1/E1 ambiguity resolution over medium baselines. The purpose of this section is to find the weak point of the basic CAR method when applied over medium baselines, by investigating the ambiguity resolution performance step by step using CAR.

The investigation was started with the step of bridging EWL to WL by carrying out the first two cascading steps as represented in Figure 6.1. The WL ambiguity resolution was set as the destination instead of the L1/E1 ambiguity resolution in the tests, and the limits for TTF shown in Table 7.2 were selected.

Table 7.9 lists the number of failures, PC and MTTCF for WL ambiguity resolution over the 30 to 70 km baselines, and the MTTCF is also plotted in Figure 7.25. It is evident that there are very few failures for GPS only, GALILEO only and the combined GPS/GALILEO cases. Although the number of failures in WL ambiguity resolution increases with an increase in ionospheric level from 3 to 6 ppm, the PC for all cases remains at 100%. In addition, according to the MTTCF, the WL ambiguities can be fixed at an instantaneous level under medium ionospheric conditions for GALILEO only and combined GPS/GALILEO. The increase of ionsopheric level leads to the MTTCF increases accordingly which however is less significant than depicted in Table 7.13 in

terms of magnitude. In a comparison, at both 3 and 6 ppm ionospheric levels, GALILEO only outperforms GPS in terms of MTTCF, which is consistent with the results obtained in Section 7.4.1 when ionospheric residuals become the main error source. The combination of GPS and GALILEO definitely benefits, as the combined case always performs the best at both ionospheric levels over all the medium baseline lengths.

Table 7.9 MTTCF, PC and Number of Failures of WL Ambiguity Resolution through CAR over Medium Baselines during 24 Hours

		GPS (km)			GALILEO (km)			GPS/GALILEO (km)		
		30	50	70	30	50	70	30	50	70
MTTCF (s)	3 ppm	1.7	2.3	2.9	1.1	1.1	1.3	1.0	1.1	1.2
	6 ppm	2.6	4.6	9.3	1.8	2.8	4.2	1.2	2.6	3.1
PC (%)	3 ppm	100	100	100	100	100	100	100	100	100
	6 ppm	100	100	100	100	100	100	100	100	100
Number of Failures	3 ppm	0	0	0	0	1	1	0	0	1
	6 ppm	0	4	5	8	8	9	1	4	5

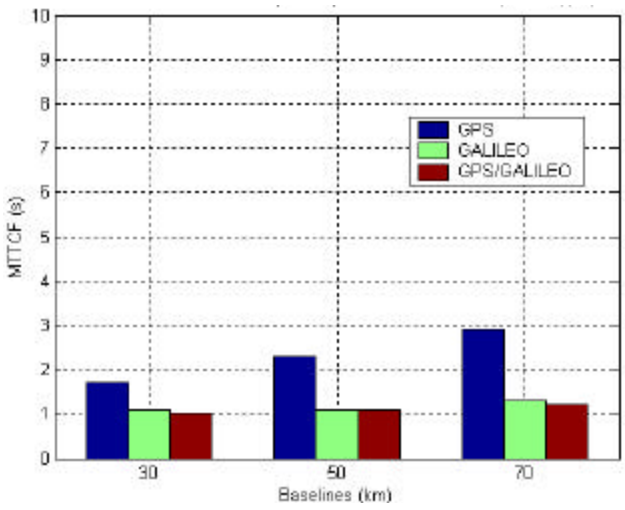

(3 ppm)

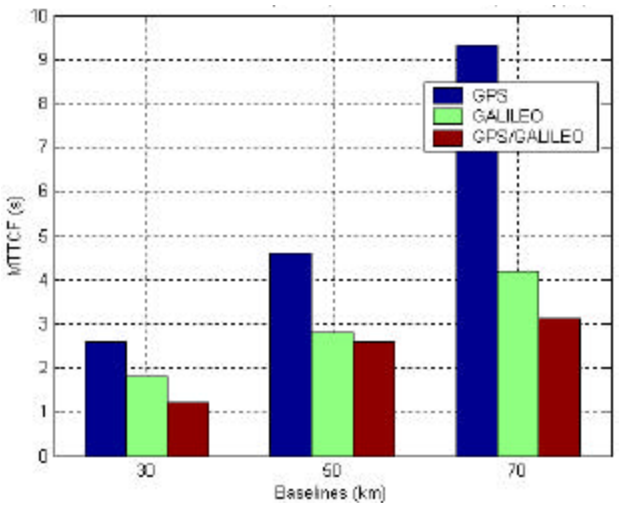

(6 ppm)

Figure 7.25 MTTCF of WL Ambiguity Resolution through CAR over Medium Baselines during 24 Hours

It has been shown in Section 7.4.1 that the lack of ionospheric modeling results in an increasing impracticability of the L1/E1 ambiguity resolution through the three-step CAR at the 20 km baseline, especially at the 6 ppm ionospheric level for GPS only and GALILEO only. However, the results here show that ionospheric modeling causes little influence on the first two steps of CAR, where the ambiguities, namely the WL ambiguity resolution, still can be 100% correctly fixed within only a few epochs even over the 70 km baseline at the high ionospheric level until the third step. Therefore, the final step of CAR (L1/E1) plays crucial role in the degradation of the overall performance in ambiguity resolution and the weak point of the three-step CAR must lie in the step bridging WL to L1/E1. This necessitates the implementation of ionospheric modeling techniques in the last step of CAR to extend acceptable performance of L1/E1 ambiguity resolution to medium baselines.

7.5.2 Stochastic Ionospheric Modeling

To overcome the weak point in the basic CAR, the stochastic ionospheric model described in Section 5.3 was implemented in the final step of CAR. In this section, the test results of this approach over medium baselines at the 3 and 6 ppm ionospheric levels are presented.

7.5.2.1 Number of Failures

The number of failures in Table 7.10 indicates that the failed trials account for a large part of the test duration (86400 s) over each baseline at both ionospheric levels. Generally speaking, combined GPS/GALILEO possess fewer failures than GPS only and GALILEO only (with one exception in green). Comparison of the number of failures among varying baselines is meaningless. But when taking into account the different limits of TTF, longer baselines are provided with more epochs of failed trials than shorter baselines.

Table 7.10 Number of Failures over medium Baselines using Stochastic Ionospheric Modeling in CAR during 24 hours

Ionospheric Level	Baseline Length	Number of Failures		
		GPS	GALILEO	GPS/GALILEO
3 ppm	30 km	23	22	19
	50 km	21	21	17
	70 km	15	17	9
6 ppm	30 km	13	24	21
	50 km	23	17	20
	70 km	19	15	13

7.5.2.2 Number of Fixes

The total number of fixes (including both correct and incorrect ones) shown in Table 7.11 reflects the efficacy of each system or combined systems from another perspective. As shown, in most cases, neither GPS nor GALILEO works well alone, but combined GPS/GALILEO performs far better.

Table 7.11 Number of Fixes over medium Baselines using Stochastic Ionospheric Modeling in CAR during 24 hours

Ionospheric Level	Baseline Length	Number of Fixes		
		GPS	GALILEO	GPS/GALILEO
3 ppm	30 km	1842	2817	23123
	50 km	375	403	8828
	70 km	397	44	2962
6 ppm	30 km	243	314	18016
	50 km	278	135	2162
	70 km	79	41	216

7.5.2.3 Percentage of Correct (PC)

As shown in Table 7.12, for combined GPS/GALILEO, the PC is always impressive over different baselines at both 3 and 6 ppm, which shows that once the ambiguities are fixed, they are almost always correct. For GPS only and GALILEO only, the statistics of PC in red is not representative since the total number of fixed ambiguity sets is very small. In most cases, neither GPS nor GALILEO performs well by their own. The advantage of combining GPS and GALILEO is more significant over the 30 to 70 km baselines than over the 1 to 20 km baselines when implementing the stochastic ionospheric model.

Table 7.12 PC over medium Baselines using Stochastic Ionospheric Modeling in CAR during 24 hours

Ionospheric Level	Baseline Length	PC		
		GPS	GALILEO	GPS/GALILEO
3 ppm	30 km	67.30 %	87.00 %	99.98 %
	50 km	9.06 %	71.96 %	99.90 %
	70 km	2.27 %	43.18 %	99.67 %
6 ppm	30 km	4.53 %	70.06 %	99.95 %
	50 km	3.24 %	8.89 %	99.21 %
	70 km	0.50 %	1.46 %	93.06 %

7.5.2.4 Mean Time To Correctly Fix (MTTCF)

Since only the correct fixes are adopted in the calculation of MTTCF statistics, the fewer correct fixes, the less the MTTCF is representative. In Table 7.13, the statistics of MTTCF in red is not representative because the total number of correctly fixed ambiguity sets does not exceed 100. But fast L1/E1 ambiguity resolution can still be obtained through combined GPS/GALILEO over 30 to 70 km baselines at both medium and high ionospheric levels.

Table 7.13 MTTCF over medium Baselines using Stochastic Ionospheric Modeling in CAR during 24 hours

Ionospheric Level	Baseline Length	MTTCF		
		GPS	GALILEO	GPS/GALILEO
3 ppm	30 km	21.5 s	17.8 s	1.8 s
	50 km	39.3 s	25.0 s	1.9 s
	70 km	77.0 s	40.4 s	3.0 s
6 ppm	30 km	36.1 s	50.3 s	1.6 s
	50 km	35.7 s	139.9 s	8.2 s
	70 km	165.2 s	47.0 s	49.1 s

7.5.2.5 Ionospheric Estimations

In Figure 7.26 and Figure 7.27, there are some representative segments extracted from 24-hour results illustrating the convergence process of GPS and GALILEO ionospheric estimations over the 50 km baseline at the 3 ppm ionospheric level. Since the ionospheric modeling is only implemented in the last step of CAR, the following figures only illustrate how the ionospheric estimation converges in the last step of CAR. The discontinuities existing in the following figures correspond to the first two steps of CAR

(EWL/WL) in those trials, during which ionosphere is not estimated. However, due to the density of points, the discontinuity is visible only when the first two steps take a long time.

The filters are reset, following where either all ambiguities are fixed, or the ambiguity resolution times out (as shown in Table 7.3, different time limits for different baselines). Some of the resets are marked with vertical solid lines. During 24-hour tests, the duration of convergence of the ionospheric estimation in each trial varies, ranging from several epochs to several thousand epochs. For some trials, the ionospheric estimation even fails to converge, due to the variation of the ionospheric level during the 24-hour period or the mismatching of the tuned variances and actual ionospheric error levels. The tuning strategy of the ionospheric variances adopted in the test was simply based on baseline lengths and the predefined ionospheric levels. Therefore, variance tuning is unable to reflect the complicated variations of the ionospheric errors and very slow convergence or even divergence is likely. Analysis shows that:

(1) Successful L1/E1 ambiguity resolution always corresponds to successful convergence of the ionospheric estimate;

(2) Failures of L1/E1 ambiguity resolution usually correspond to divergence of the ionospheric estimates.

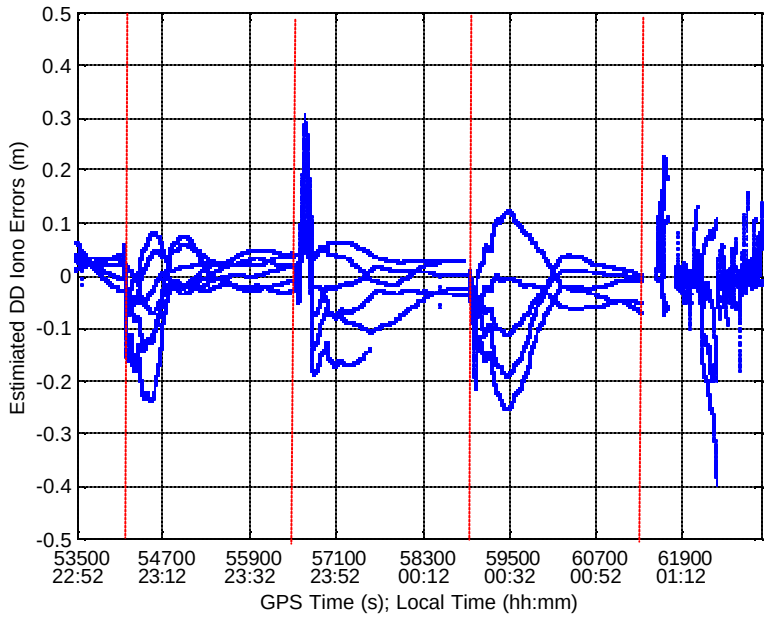

(1) GPS

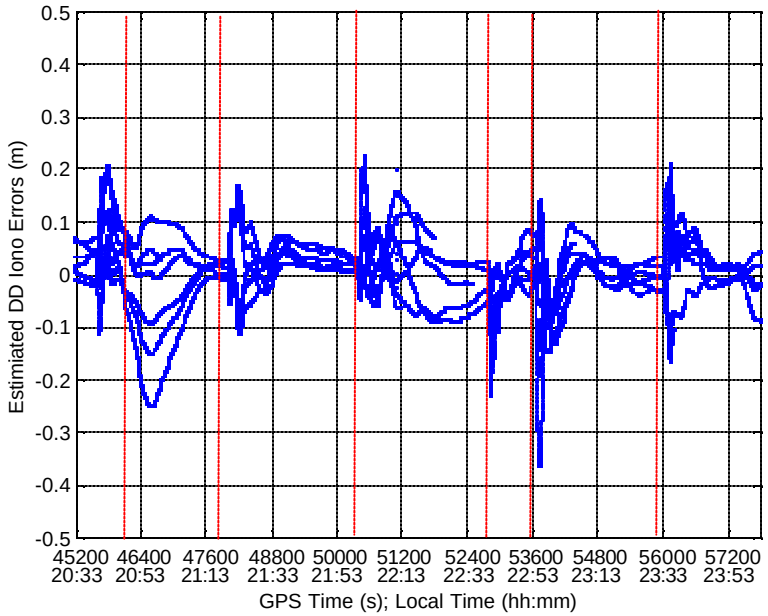

(2) GALILEO

Figure 7.26 Ionospheric Estimations of GPS and GALILEO over the 50 km Baseline at the 3 ppm Ionospheric Level

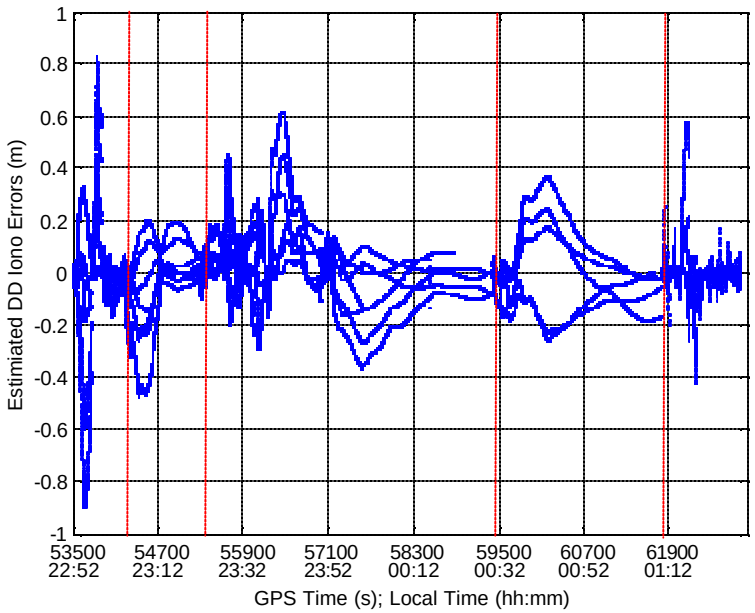

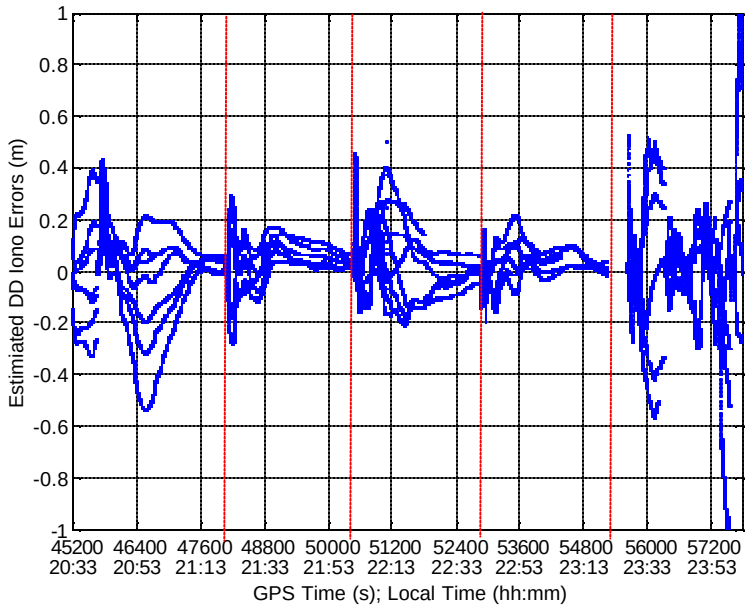

(2) GALILEO

Figure 7.27 Ionospheric Estimations of GPS and GALILEO over the 50 km Baseline at the 6 ppm Ionospheric Level

7.5.2.6 Positioning Errors

The positioning errors that correspond to the convergence of ionospheric estimates at the 3 ppm ionospheric level over the 50 km baseline are shown in Figure 7.29. The resets of filters are marked with vertical solid lines. Some resets in the dashed box are too frequent to mark. Frequent filter resets represent fast ambiguity fixing and position convergence. An analysis shows that:

(1) The initial positioning accuracy in the last step of CAR affects the time to fix the L1/E1 ambiguities;

(2) Large initial positioning errors may result in slow ambiguity fixing and slow convergence of position, or even lead to a failure in ambiguity fixing;

(3) Small initial positioning errors enable fast fixing of L1/E1 ambiguity sets;

(4) Once the L1/E1 ambiguities are fixed, a positioning accuracy can be obtained at the centimetre level.

The initial positioning errors in L1/E1 ambiguity resolution are caused during the first two steps, which, without the implementation of an ionospheric model, are subject to ionospheric errors.

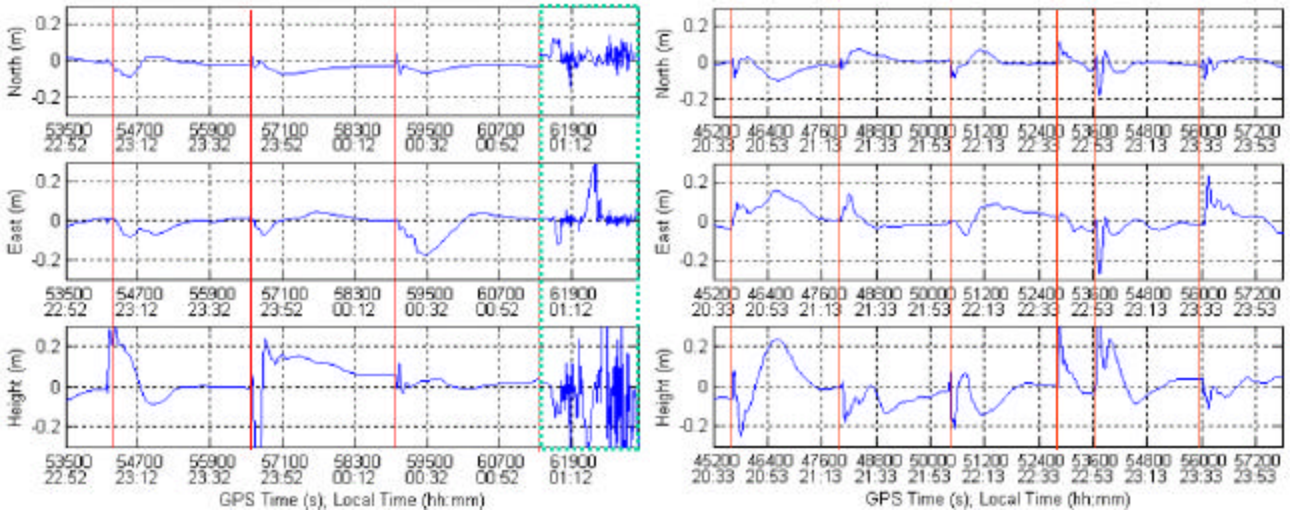

Figure 7.28 Positioning Errors of GPS and GALILEO over the 50 km Baseline at the 3 ppm Ionospheric Level

Figure 7.29 gives the positioning errors which correspond to the convergence of ionospheric estimates at the 6 ppm ionospheric level over the 50 km baseline shown in Figure 7.27. Although stochastic ionospheric modeling is implemented, the positioning results are still somehow subject to ionospheric changes according to the results at 3 and 6 ppm, which is due to the following reasons:

(1) Some ionospheric influence is introduced in the first two steps;

(2) The variance tuning for the pseudo-ionosphere observable does not exactly reflect the ionospheric variation.

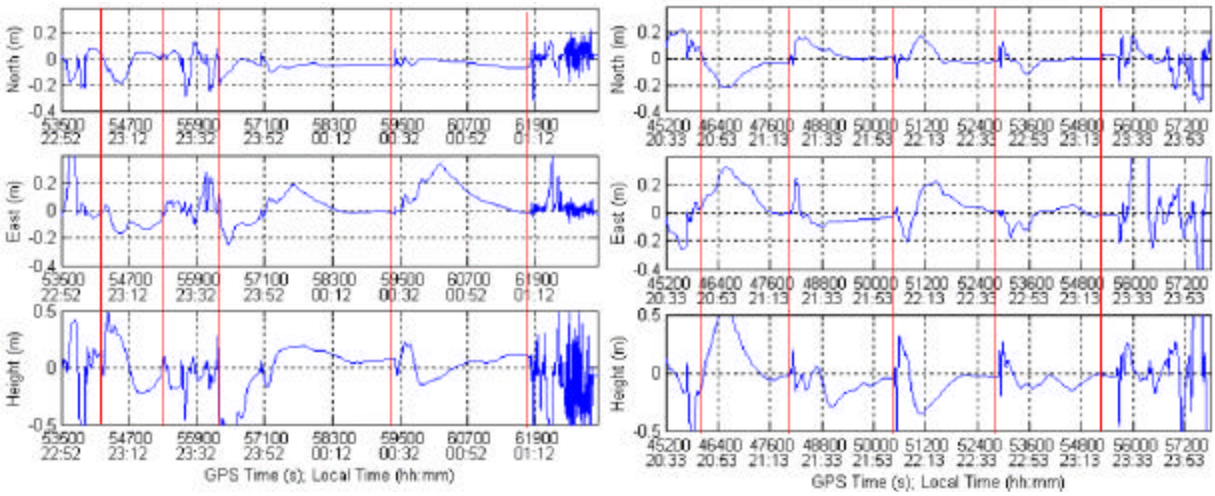

(GPS) (GALILEO)

Figure 7.29 Positioning Errors of GPS and GALILEO over the 50 km Baseline at the 6 ppm Ionospheric Level

7.5.2.7 Multipath influence on CAR when the Stochastic Ionospheric Model is implemented

The purpose of the tests in this section is to give some numerical ideas of the way in which multipath impacts PC and MTTCF for L1/E1 ambiguity resolution through CAR over medium baselines when the stochastic ionospheric model is implemented. After presenting some simulated tests, Joosten et al. (2002) concludes that the more satellites, the more robust ambiguity resolution is against multipath; and hence it is recommended to combine GPS and GALILEO to take advantage of all available satellites. The following are the multipath levels simulated in the tests conducted, with each referred through its scale factor (MpSf).

□ MpSf = 0 Multipath free

Phase: 0.00 cycles

L5/E5a/E5b Code: 0.00 m

- MpSf = 0.25

  Phase: 0.0125 cycles

  L5/E5a/E5b Code: 0.07 m

- MpSf = 0.50

  Phase: 0.025 cycles

  L5/E5a/E5b Code: 0.14 m

The above multipath errors are expressed by means of 1 sigma error on single measurements. The reason that the above scale factors are adopted is that they are used in the GPS/GALILEO simulator SimGNSS2™, where multipath at different levels are simulated by applying different scale factors to a pre-determined error level. For the scenario with a mulitpath scale factor of 0.50, it corresponds to multipath error at the pre-determined level multiplied by 0.50, which is usually regarded as a normal multipath level.

The statistics of the PC of the L1/E1 ambiguity resolution for combined GPS/GALILEO at the above three multipath levels over medium baselines is presented in Table 7.14, and is also plotted in Figure 7.30. It can be observed that on a specified baseline, with the increase of the multipath level, the PC of the combined GPS/GALILEO gets worse by 0.01% ~ 6.39%, and over different baselines, the influence of multipath on PC differs slightly except over the 70 km baseline at 6 ppm ionospheric level.

The multipath influence on the PC is more significant at higher ionospheric levels. At the 3 ppm ionospheric level, the difference is as trivial as 0 ~ 0.08%; at the 6 ppm ionospheric level, it ranges from 0 to about 6%.

Table 7.14 PC of Combined GPS/GALILEO over Medium Baselines at Different Multipath Levels

Ionospheric Level	Baseline Length	PC		
		MpSf = 0.0	MpSf =0.25	MpSf = 0.50
3 ppm	30 km	99.99 %	99.99 %	99.98 %
	50 km	99.98 %	99.97 %	99.90 %
	70 km	99.67 %	99.66 %	99.63 %
6 ppm	30 km	99.99 %	99.99 %	99.95 %
	50 km	99.93 %	99.78 %	99.21 %
	70 km	99.45 %	94.97 %	93.06 %

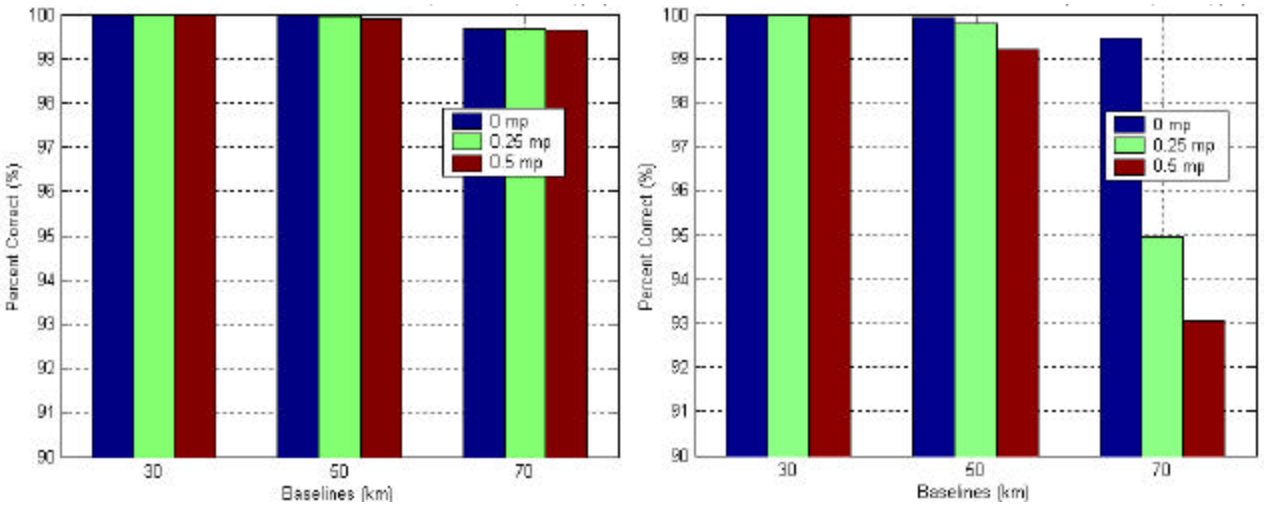

(3 ppm) (6 ppm)

Figure 7.30 Multipath Influence on PC of Combined GPS/GALILEO over Medium Baselines

The presence of multipath at high ionospheric level deteriorates the PC by a higher degree than at low ionospheric levels, as shown in Table 7.14 and Figure 7.30. For the errors in each phase measurement, there is a certain critical magnitude, exceeding which the ambiguity resolution turns impracticable. Under medium ionospheric condition where

the residual ionospheric errors are relatively small, the addition of multipath errors can only lead to limited paces closer to the critical magnitude for the errors in most measurements. However, under high ionospheric conditions the residual ionospheric errors are much larger and closer to the critical magnitude, so it is very likely that the addition of the multipath errors might cause the errors in much more measurements to exceed the critical magnitude. Therefore, at different ionospheric levels, changes in multipath errors even by the same magnitude might obviously cause different impacts on the performance of ambiguity resolution.

Table 7.15 represents the multipath influences on PC for GPS only and GALILEO only over the 30 km baseline, which is exhibited as well by Figure 7.31, together with the influence on combined GPS/GALILEO.

Table 7.15 Multipath Influence on PC of GPS Only and GALILEO Only over the 30 km Baseline at the 3 ppm Ionospheric Level

	System	**MpSf = 0.0**	**MpSf =0.25**	**MpSf = 0.50**
PC	GPS	90.28 %	83.47 %	67.30 %
	GALILEO	98.07 %	93.68 %	77.05 %

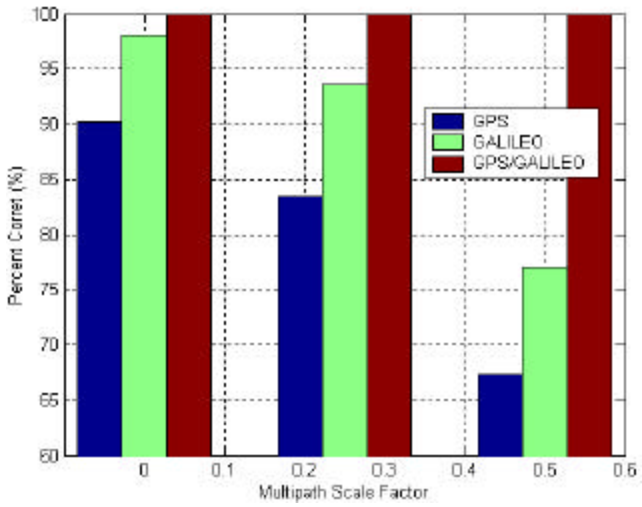

Figure 7.31 Multipath Influence on PC of GPS, GALILEO and combined GPS/GALILEO over the 30 km Baseline at the 3 ppm Ionospheric Level

According the above results, it can be noted that GPS is more subject to the increase of multipath errors than GALILEO, and combined GPS/GALILEO is the most immune to the multipath errors.

The statistics of MTTCF of L1/E1 ambiguity resolution for combined GPS/GALILEO at different multipath levels are presented in Table 7.16 and Figure 7.32. Similar to the phenomena existing in Table 7.14 and Figure 7.30, the multipath influence on MTTCF is more significant at the high ionospheric level than at the medium ionosheric level, and more significant over longer baselines than over the shorter baselines. It can be explained by the same interpretation as made for Table 7.14 and Figure 7.30.

Table 7.16 MTTCF of Combined GPS/GALILEO over Medium Baselines at Different Multipath Levels

Ionospheric Level	Baseline Length	MTTCF		
		MpSf = 0.0	MpSf =0.25	MpSf = 0.50
3 ppm	30 km	1.1 s	1.2 s	1.8 s
	50 km	1.2 s	1.6 s	1.9 s
	70 km	2.7 s	2.9 s	3.0 s
6 ppm	30 km	1.2 s	1.3 s	1.6 s
	50 km	3.2 s	3.8 s	8.2
	70 km	23.0 s	25.2 s	49.1 s

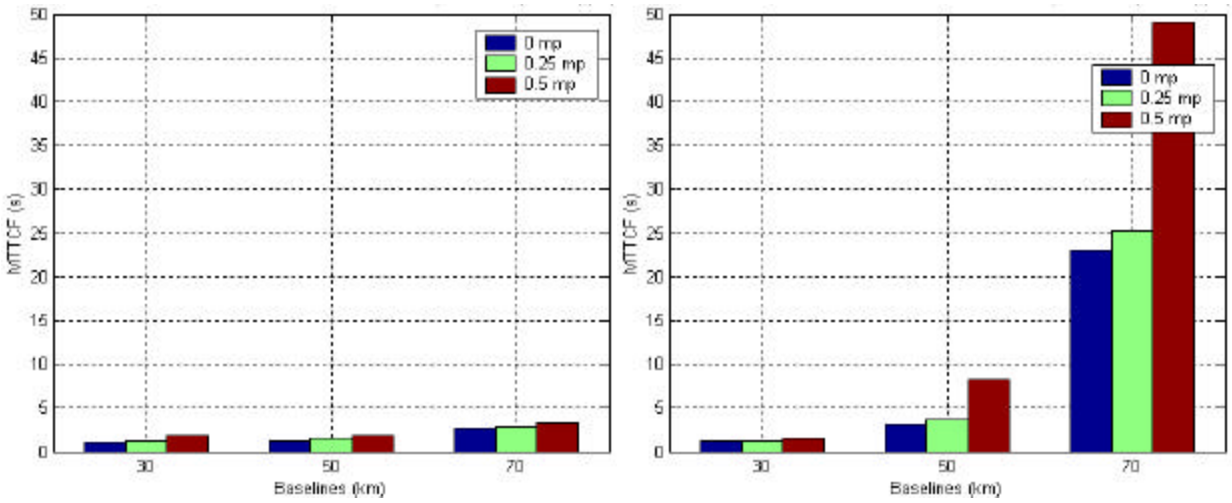

(3 ppm) (6 ppm)

Figure 7.32 Multipath Influence on MTTCF of Combined GPS/GALILEO over Medium Baselines

In Table 7.17, the multipath influence on MTTCF for GPS only and GALILEO only is compared over the 30 km baseline at the 3 ppm ionospheric level, and together with the influence on combined GPS/GALILEO, the results are plotted in Figure 7.33.

Table 7.17 Multipath Influence on MTTCF of GPS Only and GALILEO Only over the 30 km Baseline at the 3 ppm Ionospheric Level

	System	MpSf = 0.0	MpSf = 0.25	MpSf = 0.50
MTTCF	GPS	6.0 s	11.7 s	21.5 s
	GALILEO	2.3 s	9.5 s	17.8 s

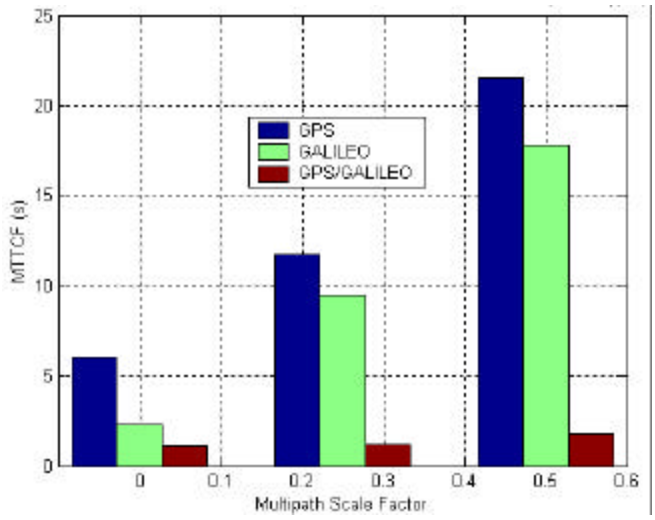

Figure 7.33 Multipath influence on MTTCF of GPS Only and GALILEO Only over the 30 km Baseline at the 3 ppm Ionospheric Level

In a summary, for a 3 ppm ionospheric level over the 30 km baseline, the increase of multipath from MpSf 0.25 to 0.5 deteriorates the GPS MTTCF by 5.7 ~ 15.5 s, and PC by 6.81% ~ 12.98%; the GALILEO MTTCF by 7.2 ~ 15.5 s, and PC by 5.35% ~ 11.02%; the combined GPS/GALILEO MTTCF by 0.1 ~ 0.7 s, and PC by 0.0% ~ 0.01%. The combination of GPS and GALILEO shows the lowest susceptibility to an increase in multipath errors. Under the same multipath condition, GALILEO always performs better than GPS, and also shows a slightly stronger ability to tolerate an increase in multipath errors. The results presented in this section are consistent with the conclusion drawn in Joosten et al. (2002).

7.5.3 IF Model

As another effort to overcome the weak point in the basic CAR, the ionosphere-free model described in Section 5.2 was implemented in the last step of CAR. Tests over medium baselines at the 3 and 6 ppm ionospheric levels were conducted and the results are presented below.

7.5.3.1 Number of Failures

According to the number of failures shown in Table 7.18, the implementation of the IF model in the third step of CAR is unable to exclusively eliminate the ionospheric influence due to the exposure to ionospheric influence in the first two steps. Generally speaking, an increase in the ionospheric level leads to the increase of failures for all scenarios, among which, the combined GPS/GALILEO case possesses less failures than GPS only and GALILEO only. Compared to Table 7.10, in most cases, the numbers of failures in Table 7.18 are usually smaller.

Table 7.18 Number of Failures over Medium Baselines when Implementing IF Model in the last Step of CAR during 24 Hours

Ionospheric Level	Baseline Length	Number of Failures		
		GPS	GALILEO	GPS/GALILEO
3 ppm	30 km	8	5	1
	50 km	12	11	3
	70 km	14	12	2
6 ppm	30 km	9	4	2
	50 km	7	12	7
	70 km	11	12	6

7.5.3.2 Number of Fixes

In Table 7.19, it can be noted that over 30 km, there are an equivalent number of fixes for 3 and 6 ppm; however, the difference between 3 and 6 ppm magnifies with an increase of the baseline length to 50 and 70 km. The advantage of combined GPS/GALILEO is significant with the number of fixes 1 ~ 2 magnitudes larger than GPS only and GALILEO only in all cases. In addition GALILEO always has more fixes than GPS (with one exception over 70 km at 6 ppm).

Table 7.19 Number of Fixes over Medium Baselines when Implementing IF Model in the last Step of CAR during 24 Hours

Ionospheric Level	Baseline Length	Number of Fixes		
		GPS	GALILEO	GPS/GALILEO
3 ppm	30 km	196	3820	23529
	50 km	179	1176	10694
	70 km	79	286	4795
6 ppm	30 km	205	2182	20755
	50 km	145	157	3911
	70 km	72	69	552

7.5.3.3 Percentage of Correct (PC)

As shown in Table 7.20 and Figure 7.34, for individual and combined systems over a specified baseline, the PCs under different ionospheric conditions are at an equivalent level. It can be further noted that, although the influence of the ionosphere on PC still exists, it is not too much. In terms of PC, the combined GPS/GALILEO case shows a consistent advantage over GPS only and GALILEO only on different baselines at different ionospheric levels. The GPS PC is always worse than GALILEO, the reason of

which is that the GPS IF L1/E1 integer ambiguities are always subject more to the enlarged measurement noise and geometrical errors according to Table 5.1.

Table 7.20 PC over Medium Baselines when Implementing IF Model in the last Step of CAR during 24 Hours

Ionospheric Level	Baseline Length	PC		
		GPS	GALILEO	GPS/GALILEO
3 ppm	30 km	45.92 %	98.95 %	100 %
	50 km	30.73 %	98.47 %	99.97 %
	70 km	31.65 %	97.90 %	100 %
6 ppm	30 km	39.02 %	99.13 %	100 %
	50 km	28.28 %	94.90 %	99.97 %
	70 km	25.0 %	88.41 %	99.77 %

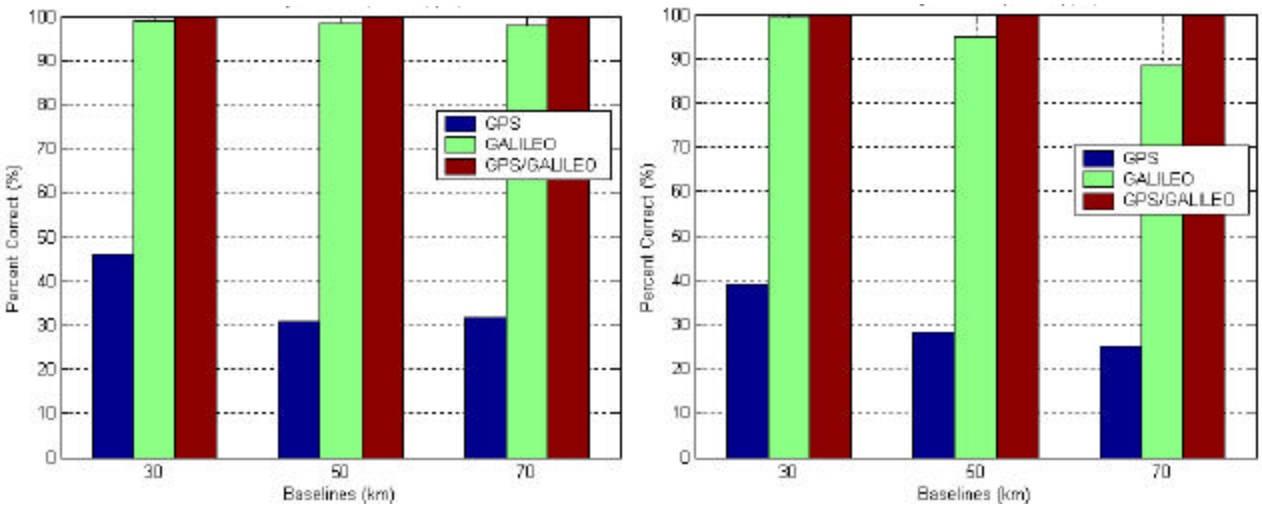

(3 ppm) (6 ppm)

Figure 7.34 PC over Medium Baselines when Implementing IF Model in the last Step of CAR during 24 Hours

7.5.3.4 Mean Time To Correctly Fix (MTTCF)

The advantage of combined GPS/GALILEO is very impressive as shown in Table 7.21 and Figure 7.35. Due to the same reason as explained in Section 7.5.3.3, GALILEO always performs better than GPS in terms of MTTCF. Compared to the results in Table

7.13, the MTTCF when implementing an ionospheric model in CAR is always longer than when implementing the stochastic model in CAR (except for GALILEO at over 30 km at 6 ppm). It is comprehensive since the influence of measurement noise and geometrical errors is enlarged when forming the ionosphere-free model (Table 5.1).

Table 7.21 MTTCF over Medium Baselines when Implementing IF Model in the last Step of CAR during 24 Hours

Ionospheric Level	Baseline Length	MTTCF		
		GPS	GALILEO	GPS/GALILEO
3 ppm	30 km	734.3 s	20.1 s	3.6 s
	50 km	560.38 s	47.9 s	7.4 s
	70 km	1323.3 s	152 s	16.8 s
6 ppm	30 km	688.0 s	31.1 s	4.0 s
	50 km	661.71 s	292.2 s	113.0 s
	70 km	1040.3 s	341.5 s	113.0 s

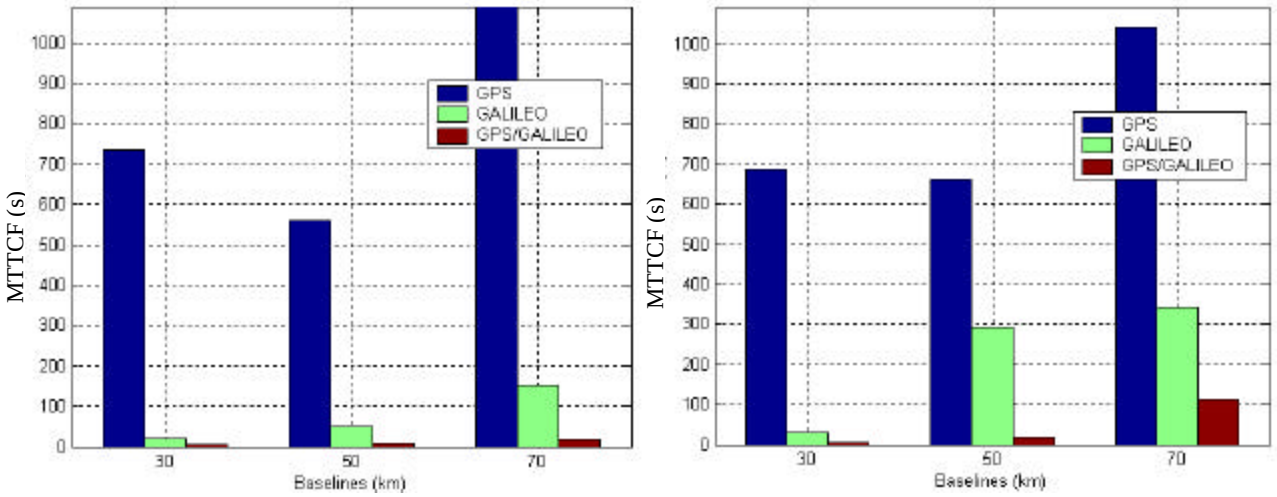

Figure 7.35 MTTCF over Medium Baselines when Implementing IF Model in the last Step of CAR during 24 Hours

7.5.3.5 Positioning Errors

The positioning errors for both GALILEO only and GPS only at both 3 and 6 ppm ionospheric levels are plotted in Figure 7.36 and Figure 7.37. The spikes in the figures

correspond to filter resets. For each filter run, the three-step procedure is demonstrated in Figure 7.38. In the first step, sub-metre positioning accuracy can be obtained with EWL, followed by the second step, where a positioning accuracy of the decimetre level can be obtained with WL. These two steps take place immediately after the filter starts, and then in the third step, the position is further converged to the centimetre level.

The process of positioning convergence shown in Figure 7.36 and Figure 7.37 corresponds to the convergence of the L1/E1 ambiguities. Before the L1/E1 ambiguities are fixed, a positioning accuracy of several tens of centimetres can be obtained, and once L1/E1 ambiguities are fixed, the positioning accuracy can immediately reach several centimetres. In Figure 7.36, only the positioning results of the third filter in CAR are presented. Those straight slopes in the figures correspond to the periods of the first two ambiguity resolution steps for the trials.

The positioning accuracies in Figure 7.36 and Figure 7.37 are calculated using both float and fixed L1/E1 ambiguities. So only taking into account the fixed solutions, the statistics of the positioning accuracy should be definitely better. In a comparison between Figure 7.36 and Figure 7.37, it can be seen that the GPS L1 positioning accuracy is lower than the GALILEO E1 positioning accuracy. In both figures, some positioning divergences can be observed, which always correspond to failures or incorrectness in ambiguity fixing. A degradation of constellation geometry might serve as one of the reasons for position divergence, since the new satellites appearing in the middle way of CAR are discarded. So, if the ambiguity fixing takes a long time, the number of

measurements will become smaller with time, so that the geometry will become worse with time. A comparison of Figure 7.36 and Figure 7.37 also shows that, although an IF model is implemented in the third filter in CAR, the positioning results are still somehow subject to ionospheric changes. The possible reasons are:

(1) Even if ionospheric influence has been completely removed in the last step with the IF model, some ionospheric influence has been introduced in the first two steps. Although the EWL/WL ambiguities can usually 100% correctly fixed (according to Table 7.9) during the first two steps, since the IF model is not used, the ionospheric influence is absorbed in the position estimates and passed to the last step.

(2) The variance tuning does not exactly reflect the measurement noise and residual errors at different ionospheric levels.

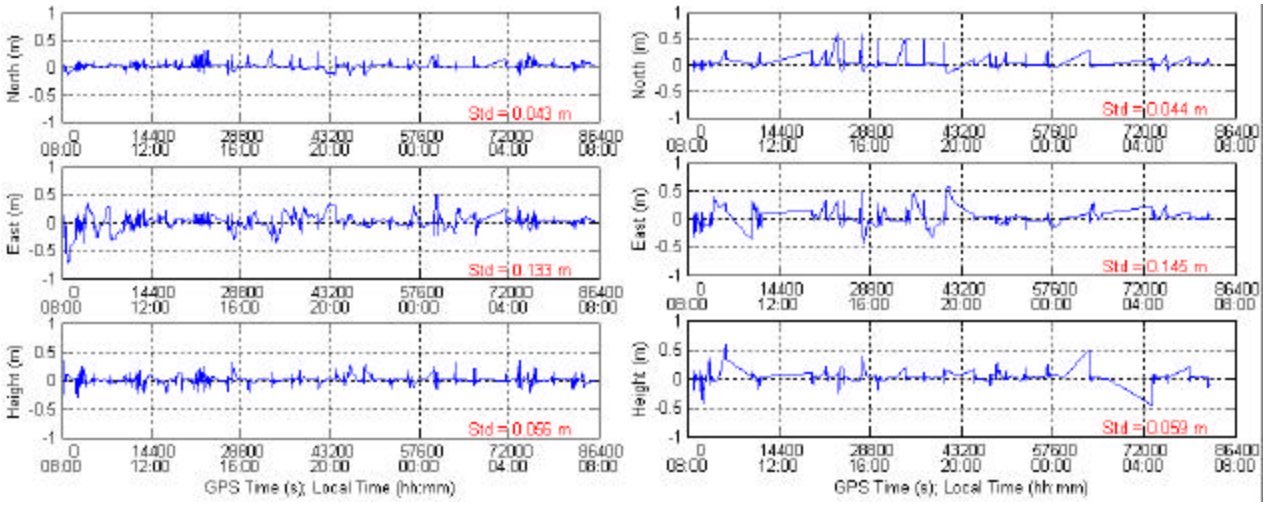

(3 ppm) (6 ppm)

Figure 7.36 Positioning Errors of GALILEO Only over the 70 km Baseline when Implementing IF Model in the Last step of CAR

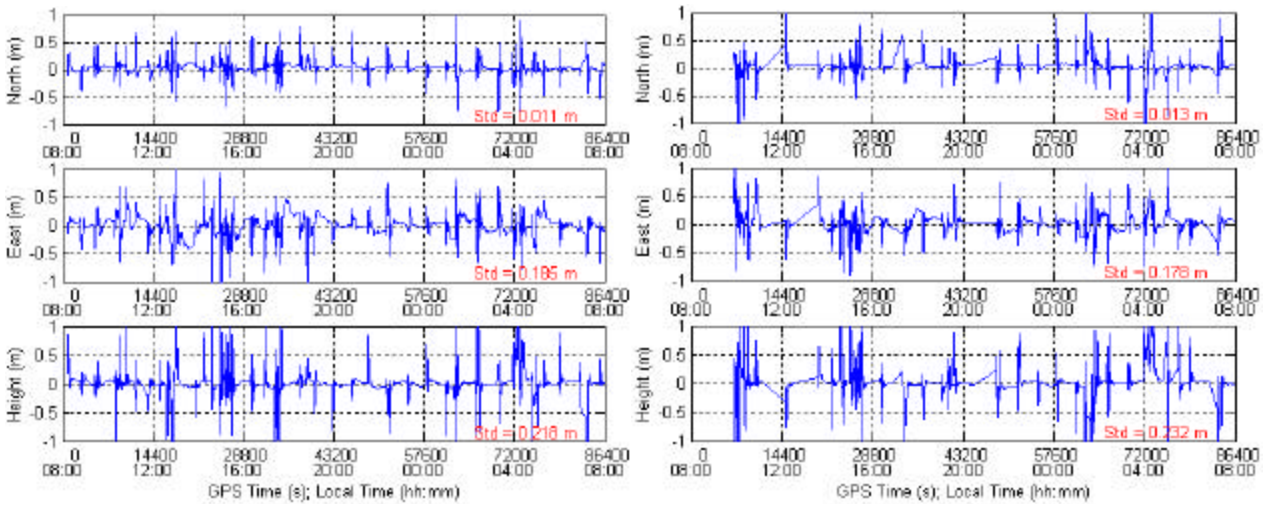

(3 ppm) (6 ppm)

Figure 7.37 Positioning Errors of GPS Only over the 70 km Baseline when Implementing IF Model in the Last step of CAR

Figure 7.38 is an illustration of the three-step position convergence procedure of CAR. A period of EWL, WL and E1 positioning results for GALILEO only over the 70 km baseline are plotted. As shown, it usually takes only a few epochs to fix EWL/WL ambiguities, however much more epochs to fix E1 ambiguities. Also, even if EWL ambiguities are fixed, the positioning errors might still remain as large as about 1 m. When WL ambiguities are fixed, the positioning accuracy is further improved. Only when E1 ambiguities are fixed, can a centimetre level positioning accuracy be obtained.

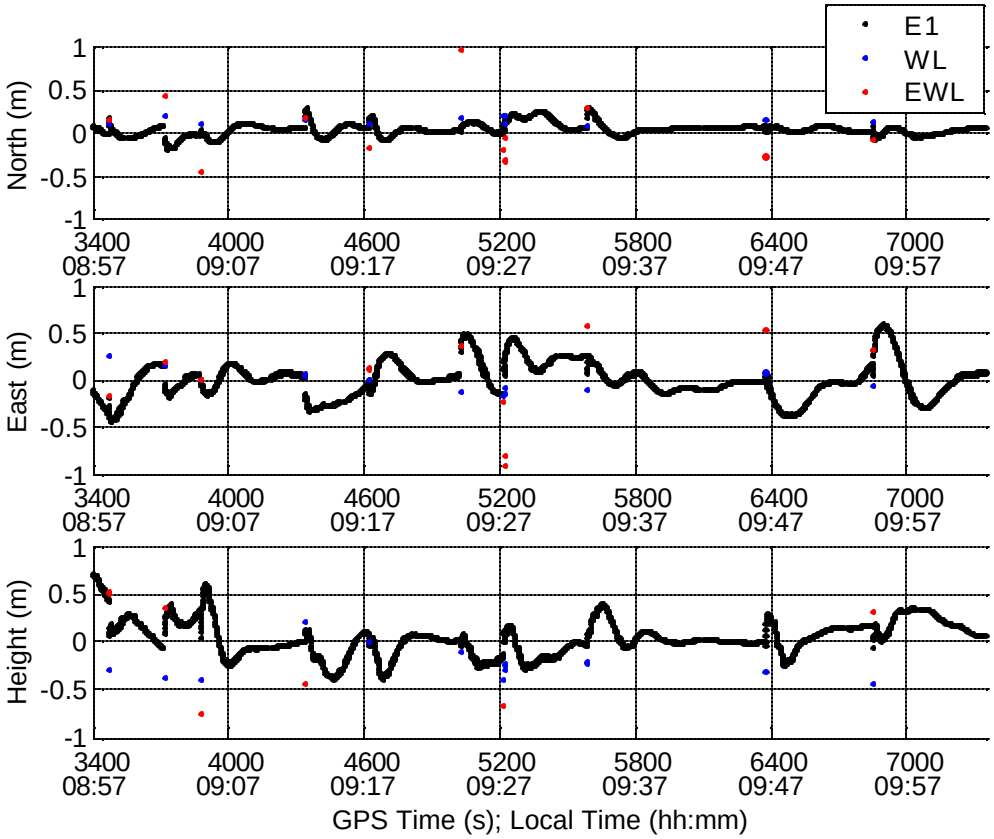

Figure 7.38 Illustration of Three-step Convergence Procedure when Implementing IF Model in the Last Step of CAR

8 CONCLUSIONS AND RECOMMENDATIONS

In this research, a significant amount of work focused on triple-frequency cascading ambiguity resolution. The general form of triple frequency phase linear combinations was studied for both GALILEO and modernized GPS, by using some combinations of cascading wavelengths. A method of cascading ambiguity resolution was then derived and comprehensively studied. Meanwhile, in order to deal with the residual ionospheric errors, both the ionosphere-free and stochastic ionospheric models were explored and implemented. Besides, the combination of modernized GPS and GALILEO was investigated, followed by the implementation of all the studied methods in a three-step cascading ambiguity resolution scheme. For both the individual and combined systems, tests were conducted on the scheme over short (1 ~ 20 km) to medium baselines (30 ~ 70 km), at medium and high ionospheric levels (3 and 6 ppm), in different multipath scenarios (MpSf: 0.25 ~ 0.50) through simulation.

From the results discussed in previous chapters, the following conclusions can be drawn:

(1) Cascading ambiguity resolution is a promising method, which makes best use of the characteristics of different phase linear combinations with cascading wavelengths that are enabled by both modernized GPS and GALILEO due to their frequency allocations. Generally speaking, the best combinations for both systems are (0, 1, -1), (1, -1, 0) and (1, 0, 0) according to the analyses and tests in previous chapters.

(2) Compared to the conventional ambiguity resolution method, the cascading ambiguity resolution method possesses higher computational efficiency, since the dimensional size of the filter in each step is only around one third of the filter compared to using a conventional method. Particularly in the combination of GPS and GALILEO, the filter's dimensional size becomes an implementation issue. The cascading ambiguity resolution therefore shows great advantages over the conventional method.

(3) Compared to the integer rounding, integrating the LAMBDA method to cascading ambiguity resolution is of great benefit in improving the percentage of correct fixes. According to Table 7.3 and Table 7.6, the PC improvements for three-frequency case over the 1 to 20 km baselines range from 2.29% to 11.1%; with two frequencies over the 1 km baseline, the improvement even amounts to 56.35%.

(4) For the basic CAR, the CAR integrating geometry-free model, ionosphere-free model, and stochastic ionospheric model, each has its own limitations. Under different conditions, to achieve the best ambiguity resolution performance, different models should be adopted.

Over very short baselines (1 ~ 10 km), since atmospheric errors are efficiently canceled in differencing, the measurement noise dominates the error sources. Among the aforementioned methods, the basic CAR suffers the least from measurement noise, so it performs the best under this condition. However, with the increase of baseline length or ionospheric level, the residual ionospheric error becomes the

dominant error source, so that the basic CAR no longer shows any advantage. In this case, the ionosphere-free model can be integrated in CAR for augmentation. But the ionosphere-free model has the limitations of enlarged measurement noise, so this model is beneficial only when the ionospheric residuals dominate the error sources. Stochastic ionospheric modeling is able to deal with the increased ionospheric residuals without enlarging the measurement noise. However, the stochastic ionospheric model is very sensitive to the variance tuning for the ionospheric measurements, and sufficient a priori knowledge of the ionospheric activities and proper tuning of the variance is the prerequisite for good performance. With a further increase of baseline length, the geometrical residuals are no longer negligible, so the geometry-free integer ambiguity model is of merit under the condition of an accurate ionospheric correction.

(5) Generally speaking, according to the MTTCF and PC in the test results, the combined GPS/GALILEO always performs the best, followed by the GALILEO system only, and then by the modernized GPS system only. Table 7.12 shows a clear contrast, in which the PC of combined GPS/GALILEO remains over 90% even on a 70 km baseline at the 6 ppm ionospheric level, however the PCs for GPS only and GALILEO only already degrade to few percentiles. Other results also show that the ambiguity resolution in each cascading step for GPS only seems the most susceptible to both ionospheric and multipath errors, while GALILEO only seems the most susceptible to measurement noise. Combined GPS/GALILEO shows the best insusceptibility in the presence of any errors.

(6) Under the assumption of the measurement noise adopted in this thesis, using triple frequencies, although very fast ambiguity resolution can be obtained, it is still difficult to achieve instantaneous ambiguity resolution for either GPS only or GALILEO. However, for combined GPS/GALILEO, at medium ionospheric level (3 ppm), over 98.85% or 97.7% of the time, ambiguities can be fixed instantaneously using triple or dual frequencies on 1 ~ 10 km baselines. For instantaneous ambiguity resolution over short baselines, the reduction of measurement noise through receiver technology is necessary, and in addition, external ionospheric corrections are also indispensable to extend the successful instantaneous ambiguity resolution to longer baselines.

(7) Generally speaking, triple frequency systems are much better than dual frequency systems. According to the results, the longer the baselines or the higher the error levels, the more significant advantages triple-frequency systems have over the dual-frequency systems. Over the short baselines (1 ~ 20 km), as the ionospheric level increases from 3 to 6 ppm, the maximum PC difference between triple and dual-frequency systems increases from 0.5% to 11.53% (Table 7.6 and Table 7.8). In the case that the two systems are combined, although the triple-frequency still shows advantage over the dual-frequency, the advantage is less impressive than for single system under the same conditions. As shown in Table 7.6, at 3 ppm ionospheric level, from the 1 to 20 km baselines, the MTTCF of triple-frequency system only might be up to 14 times faster than the dual-frequency system only, however, with

combined GPS/GALILEO, the triple-frequency only outperforms dual-frequency by 1.1 times at most.

(8) The cascading ambiguity resolution scheme also has its drawbacks especially in the case that one ambiguity resolution trial lasts too long before timing out. The worst result would be a failure due to insufficient measurements because the new satellites appearing in the last two cascading steps are always discarded. As shown in both Figure 7.36 and Figure 7.37, the straight slopes correspond to long trials of ambiguity resolution, most of which ended up with failures in ambiguity resolution.

Here are some recommendations for the future work on the cascading ambiguity resolution:

(1) For simplicity purposes, the measurements on different frequencies are assumed uncorrelated, and the measurement correlation among different satellites is neglected. In addition, for the stochastic ionospheric modeling, the elevation-dependent feature, temporal correlation and spatial correlation are not taken into account. From optimal point of view, all these factors should be carefully dealt with in future work.

(2) As the CAR still suffers from ionospheric influence after augmented with ionospheric modeling in the third step, it is necessary to apply ionospheric modeling to the first two cascading steps to better eliminate the ionospheric influence.

(3) It is necessary to switch the realization of CAR algorithm from sequential LSQ to Kalman filter to better handle random processes and dynamic applications.

(4) In case that real data is used, many simplifications or assumptions can no longer be made. The first is to deal with the different coordinate frames for the two systems. One system can be converted into another through published conversion parameters, so that combination of the two systems can be carried through. The second is to handle the two different time systems. It is expected that the parameters of time difference between the two systems will be available in either future GPS or GALILEO's real time broadcast ephemeris. In case that the parameter correction does not suffice the accuracy need, it would be necessary to add a new state for estimation.

(5) When real data becomes available, it is necessary to consider how to apply external differential corrections, in order to extend the application of the CAR to long baselines.

REFERENCES

Alves, P. (2001) The Effect of Galileo on Carrier Phase Ambiguity Resolution, *Proceedings of ION GPS-01*, 11-14 September, Salt Lake City, UT, pp. 933 - 944.

Alves, P., G. Lachapelle, M.E. Cannon, J. Park, and P. Park (2002) Use of Self-Contained Ionospheric Modeling to Enhance Long Baseline Multiple Reference Station RTK Positioning, *Proceedings of ION GPS-02*, 24-29 September Potland, OR, pp. 1388 – 1399.

ARINC, Inc. (1993) *Navstar GPS Space Segment/Navigation User Interfaces*, ICD-GPS-200, Fountain Valley, CA, April.

ARINC, Inc. (2001) *Navstar GPS Space Segment User Segment L5 Interfaces*, ICD-GPS-705, El Segundo, CA, GPS Navstar JPO SNC/CZ, 16 April.

Bossche, M., C. Bourga and B. Lobert (2004) GPS Galileo Time Offset: How it Affects Positioning Accuracy and How to Cope with It, *Proceedings of ION GNSS-04*, 21-24 September, Long Beach, CA, pp. 654-659.

B. W. Parkinson and J. J. Spilker, eds. (1996) *Global Positioning System*: *Theory and Application*. Washington, D.C.: AIAA.

Bonillo-Martinez, C., M. Toledo-Lopez and M. Romay-Merino (1999) The Benefits of the GPS Three Frequencies on the Ambiguity Resolution Techniques, *Proceedings of ION GPS-99*, 14-17 September, Nashville, TN, pp. 1737 - 1746.

Center for Orbit Determination in Europe (CODE) (2005) Global Ionosphere Maps Produced by CODE, Retrieved in February 2005, from http://www.aiub.unibe.ch/ionosphere.html

Collins, J.P. (2000) An overview of GPS inter-frequency carrier phase combinations, Online available at: http://gauss.gge.unb.ca/papers.pdf/L1L2combinations.collins.pdf

Dellago, R., E. Detoma and F.Luongo (2003) Galileo-GPS Interoperability and Compatibility: A Synergetic Viewpoint, *Proceedings of ION GPS/GNSS-03*, 9-12 September, Portland, OR, pp. 542-548.

de Jong, K. and P. Joosten (2001) Triple-frequency GPS and GALILEO Ambiguity Resolution, *Proceedings 8th GNSS Workshop – 2001 International Symposium on GPS/GNSS*, 7-9 November, Cheju Island, Korea, pp. 49 - 52.

D. McDonald, K. (2001) A Future GNSS Concern on the Modernization of GPS and the Evolution of Galileo, *Proceedings of the ION GPS-01*, 11-14 September, Salt Lake City, UT, pp. 2804 - 2809.

Eissfeller, B., C. Tiberius, T. Pany and G. Heinrichs (2001) Real-Time Kinematic in the Light of GPS Modernization and Galileo, *Proceedings of ION GPS-01*, 11-14 September, Salt Lake City, UT, pp. 650 - 662.

Ericson, S. (1999) A Study of Linear Phase Combinations in Considering Future Civil GPS Frequencies, *Proceedings of ION NTM-99*, 25-27, January, San Diego, CA, pp. 677 - 686.

European Commission (2002) GALILEO High Level Mission Definition Document, Ver. 3.0, 23.02.2002, Online available at: http://europa.eu.int/comm/dgs/energy_transport

European Commission (2003) The Galilei project: GALILEO Design Consolidation, Online available at: http://europa.eu.int/comm/dgs/energy_transport

Fontana, R.D., W. Cheung and T. Stansell (2001) The Modernized L2 Civil Signal, *GPS World*, September, Eugene, OR, pp. 28-34.

Forssell, B., M. Martin-Neira, and R. A. Harris (1997) Carrier Phase Ambiguity Resolution in GNSS-2, *Proceedings of ION GPS-97*, 16-19 September, Kansas City, MO, pp. 1727 - 1736.

Fyfe, P., K. Davis, I. Jeng, C. Kelley and C. Mosley (2002) GPS and Galileo – Interoperability for Civil Aviation Applications, *Proceedings of ION GPS-02*, 24-27 September, Portland, OR, pp. 289 - 302.

Ganguly, S., A. Jovancevic and J. Noronha (2004) Interoperability Study Between GPS and Galileo, *Proceedings of ION GNSS-04*, 21-24 September, Long Beach, CA, pp. 670-680.

GPS World (2004a) Global View: GALILEO Moves Ahead, Retrieved in December 2004, from http://www.gpsworld.com/gpsworld/article/articleDetail.jsp?id=105343

GPS World (2005a) Global View: New Presidential GPS Policy Elevates Executive Oversight, Security Issues, Retrieved in Jan 2005, from http://www.gpsworld.com/gpsworld/article/articleDetail.jsp?id=140801

GPS World (2005b) Global View: ESA Awards Key Galileo Contract, Retrieved on February 2005 from www.gpsworld.com/gpsworld/article/articleDetail.jsp?id=145033

GPS World (2005c) Global View: L2C, M-Code Signals Will Appear Soon, Retrieved in Feb 2005 from http://ww.gpsworld.com/gpsworld/article/articleDetail.jsp?id=148724

GPS World (2005d) Global View: Galileo Authority Chooses Director, Retrieved in June 2005 from http://www.gpsworld.com/gpsworld/article/articleDetail.jsp?id=163652

Han, S. and C. Rizos (1999) The Impact of Two Additional Civilian GPS Frequencies on Ambiguity Resolution Strategies, *Proceedings of ION 55th Annual Meeting*, 28-30 June 1999, Cambridge, MA, pp. 315 – 321.

Hatch, R. (1996) The Promise of a Third Frequency, GPS World, May 1996, pp. 55 - 58.

Hein, G.W., J. Godet, J.-L. Issler, J.-C. Martin, P. Erhard, R. Lucas-Rodriguez and T. Pratt (2001) The Galileo Frequency Structure and Signal Design, *Proceedings of ION GPS-01*, 11-14 September, Salt Lake City, UT, pp. 1273 - 1282.

Hein, G.W., J. Godet, J.-L. Issler, J.-C. Martin, P. Erhard, R. Lucas-Rodriguez and T. Pratt (2002), Status of Galileo Frequency and Signal Design, *Proceedings of ION GPS-02*, 24-27 September, Portland, OR, pp. 266 - 277.

Hoffmann-Wellenhof, B., H. Lichtenegger, and J. Collins (1994) *GPS Theory and Practice*, third edition, Springer-Verlag Wien, New York.

Internaltional GPS Service (IGS) (2005) IGS Product Table, Retrieved in February 2005, from http://igscb.jpl.nasa.gov/components/prods.html

Julien, O., P. Alves, M.E. Cannon and W. Zhang (2003) A Tightly Coupled GPS/GALILEO Combination for Improved Ambiguity Resolution, *Proceedings of ENC-GNSS 2003*, 22-25 April, Graz, Austria, CDROM, 14 pages.

Julien, O., P. Alves, M.E. Cannon and G. Lachapelle (2004) Improved Triple-Frequency GPS/GALILEO Carrier Phase Ambiguity Resolution Using a Stochastic Ionosphere Modeling, *Proceedings of ION NTM-04*, 26-28 January, San Diego, CA, pp. 441 -452.

Joosten, P., T. Pany and J. Winkel (2002) The Impact of unmodelled multipath on ambiguity resolution, *Proceedings of ION GPS-02*, 24-27 September, Portland, OR, pp. 953 - 959.

Joseph, P., Jr. (2000), Future GNSS Architecture: Interoperability or Compatibility Between Systems, What is the Prudent Course to Pursue, *Proceedings of ION GPS-00*, 19-22 September, Salt Lake City, UT, pp. 1332 - 1339.

Jung, J. (1999) High Integrity Carrier Phase Navigation for Future LAAS Using Multiple Civilian GPS Signals, *Proceedings of ION GPS-99*, 14-17 September, Nashville, TN, pp. 727 - 736.

Jung, J, P. Enge, and B. Pervan (2000) Optimization of Cascade Integer Resolution with Three Civil GPS Frequencies. *Proceedings of the ION GPS-00*, 19-22 September, Salt Lake City, UT, pp. 2191 - 2201.

Lachapelle, G., M.E. Cannon, K. O'Keefe and P. Alves (2001) *Technical Benefit Analysis of Galileo for Canada,* Technical Report for Canadian Space Agency, The Univeristy of Calgary.

Leonard, A. and I. Izquierdo (2002) GPS and GALILEO Interoperability and Synergies, *Proceedings of ION GPS-02*, 24-27 September, Portland, OR, pp. 330 - 341.

Liu, G.C. and G. Lachapelle (2002) Ionosphere Weighted GPS Cycle Ambiguity Resolution, *Proceedings of ION NTM-02*, 28-30 January, San Diego, CA, pp. 889 - 899.

Luo, N. (2000) *Precise Relative Positioning of Multiple Moving Platforms Using GPS Carrier Phase Observables*, UCGE Report, Number 20147, January, 2001, http://www.geomatics.ucalgary.ca/links/GradThesis.html

McDonald, K. (2001) A Future GNSS Concern on the Modernization of GPS and the Evolution of Galileo, *Proceedings of ION GPS-01*, 11-14 September, Salt Lake City, UT, pp. 2804-2809.

McDonald, K. (2002) The Modernization of GPS: Plans, New Capabilities and the Future Relationship to Galileo, *Journal of Global Positioning System*, Vol.1, No. 1: 1-17.

Miller, J. (2004) GPS &GALILEO: Evolution Towards GNSS, *Presentation at ION NTM-04*, 26-28 January, San Diego, CA, pp. 73-91.

M. Romay-Merino, M., A.J.G. Alarcon, I. J. Villares and E. H. Monseco (2001) An integrated GNSS concept, Galileo &GPS, benefits in terms of Accuracy, Integrity, Availability and Continuity, *Proceedings of the ION GPS-01*, 11-14 September, Salt Lake City, UT, pp 2114 - 2122.

Odijk, D. (2000) Weighted Ionospheric Correction to Improve Fast GPS Positioning Over Medium Distances, *Proceedings of ION NTM-00*, 19-22 September, Salt Lake City, UT, pp. 1113 - 1124.

O'Donnell, M. and T. Watson, J. Fisher and S. Simpson, G. Brodin et al. (2002) A Study of Galileo Performance – GPS Interoperability and Discriminators for Urban and Indoor Environments, *Proceedings of ION GPS-02*, 24-27 September, Portland, OR, pp. 2160 - 2172.

O'Keefe, K. (2001) Availability and Reliability Advantage of GPS/Galileo Integration, *Procceeding of ION GPS-01*, 11-14 September, Salt Lake City, UT, pp. 2096 - 2104.

Perz, C.M. (2004) GPS Modernization Update, Presentation at IEEE Plans, Session D4, 28 April, Monterey, CA.

Radovanovic, R.S., F. Georgia, and N. El-Sheimy (2001) On Optimizing Multi-Frequency Carrier Phase Combinations for Precise Positioning, *IAG Scientific Assembly*, 2-7 September, Budapest, Hungary, CDROM.

Richert, T. (2005) *The Impact of Future Global Navigation Satellite Systems on Precise Carrier Phase Positioning*, UCGE Report, Number 20218, May, 2005, http://www.geomatics.ucalgary.ca/links/GradThesis.html

Rodriguez, J., M. Irsigler, G. W. Hein and T. Pany (2004) Combined Galileo/GPS Frequency and Signal Performance Analysis, *Proceedings of ION GNSS-04, 21-24 September*, Long Beach, CA, pp. 632-649.

Rothacher, M. and G. Beutler (2002) Lecture Notes: Course 699.80 *Advanced Aspects of Satellite Positioning*, Summer 2002.

R.Weill, L. (2002), Multipath Mitigation Using Modernized GPS Signals: How Good Can it Get? *Proceedings of ION GPS-02*, 24-27 September, Portland, OR, pp. 493 - 502.

Sandhoo, K., D. Turner and M. Shaw (2000) Modernization of the Global Positioning System, *Proceedings of ION GPS-00*, 19-22 September, Salt Lake City, UT, pp. 2175 – 2183.

Schaer, S. (1997) *How to use CODE's Global Ionosphere Maps*. Astronomical Institute, University of Berne.

Sheridan, K., W. Ochieng, K. Sauer, P. Cross, J. Iliffe, S. Lannelongue, N. Ammour and K.Petit (2001), Performance Potential of a Combined Galileo/GPS Navigation System, *Proceedings of GNSS International Symposium 2001*, 8-11 May, Sevilla, Spain.

Sielski, H. (2000) The Impacts of GPS Modernization on DAG-TM. *DAG-TM Workshop CNS Breakout Session*, May 24.

Soualle, F. and T. Burger (2003) Impact of Galileo Spreading Code Selection and Data Rate onto Navigation Signal Inteference, *Proceedings of ION GPS/GNSS-03*, 9-12 September,Portland, OR, pp. 1035-1043.

Spiller, J., T. Tapsell and R. Peckham (2001) Galileo plus GPS – Opportunities, *Proceedings of ION GPS-01*, 11-14 September, Salt Lake City, UT, pp. 2059 - 2066.

Spilker, J.J., and A.J. Van Dierendonck (1999) Proposed New Civil GPS Signal at 1176.45 MHz, *Proceedings of ION GPS-99*, 14-17 September, Nashville, TN, pp. 1717 - 1725.

Swider, R. (2001) GPS Policy Update, Presentation at Civil GPS Service Interface Committee, Department of Defense, 9-11 September, Salt Lake City, UT.

Teunissen, P. (1993) Least-square estimation of the integer GPS ambiguities. In IAG General Meeting. Invited Lecture. Section IV Theory and Methodology, Beijing, China.

Teunissen, P. (1998) Success probability of integer GPS ambiguity rounding and bootstrapping, *Journal of Geodesy*, 72: pp. 606-612.

Teunissen, P., P. Joosten and C. Tiberius (2002) A Comparison of TCAR, CIR and LAMBDA GNSS Ambiguity Resolution, *Proceedings of ION GPS-02*, 24-27 September, Portland, OR, pp. 2799 - 2808.

U.S. Department of Transportation (DoT) (2003) *National Civilian GPS Services: GPS Augmentations &GPS Modernization*, Technical brochure. Online available at: http://www.igeb.gov/outreach/civil-gps-brochure.ppt

Verhagen, S. (2002) Performance Analysis of GPS, Galileo and Integrated GPS-Galileo, *Proceedings of ION GPS-02*, 24-27 September, Portland, OR, pp. 2208 - 2215.

Vollath, U., S. Birnbach and H. Landau (1998) Analysis of Three-Carrier Ambiguity Resolution (TCAR) Technique for Precise Relative Positioning in GNSS-2, *Proceedings of ION GPS-98*, 15-18 September, Nashville, TN, pp. 417 – 426.

Zandbergen, R., S.Dinwiddy, J.Hahn, E.Breeuwer and D.Blonski (2004) Galileo Orbit Selection, *Proceedings of ION GNSS-04*, 21-24 September, Long Beach, CA, pp. 616-623.

Zhang, W., M.E. Cannon, O. Julien, and P. Alves (2003), Investigation of Combined GPS/Galileo Cascading Ambiguity Resolution Schemes, *Proceedings of ION GPS-03*, 9-12 September, Portland, OR, pp. 2599-2610.